

Copyright
by
Courtney Brooke Woolsey

The Dissertation Committee for Courtney Brooke Woolsey certifies that this is the approved version of the following dissertation:

**POST-EXPOSURE TREATMENT OF MARBURG VIRUS ANGOLA
DISEASE IN NON-HUMAN PRIMATES USING RECOMBINANT
VESICULAR STOMATITIS VIRUS VECTORS**

Committee:

Thomas W. Geisbert, Ph.D.
Committee Chair

Chad E. Mire, Ph.D.

Tian Wang, Ph.D.

Chien-Te K. Tseng, Ph.D.

John Connor, Ph.D.

Dean, Graduate School

**POST-EXPOSURE TREATMENT OF MARBURG VIRUS ANGOLA
DISEASE IN NON-HUMAN PRIMATES USING RECOMBINANT
VESICULAR STOMATITIS VIRUS VECTORS**

by

Courtney Brooke Woolsey, Bachelor of Science

Dissertation

Presented to the Faculty of the Graduate School of

The University of Texas Medical Branch

in Partial Fulfillment

of the Requirements

for the Degree of

Doctor of Philosophy

The University of Texas Medical Branch

February 2018

Dedication

To my husband James, who inspires me daily and pardons my moonlight trysts with the BSL4 flow cytometer. You're the top.

Acknowledgments

My utmost thanks and appreciation go to my committee chair and advisor, Professor Thomas W. Geisbert, without whom this endeavor would not be possible. Tom is a living role model to me and always made time in his demanding schedule to be an excellent and supportive mentor. My good friend, Dr. Chad Mire, was a crucial committee member and provided invaluable support during my graduate school career; his good counsel is manifest in this dissertation. To additional committee members, thank you for devoting your precious time to the completion of this project and for your guidance and criticism: Dr. John Connor, Dr. Tian Wang, and Dr. Chien-Te Tseng. The bioinformatics work in this dissertation would not be possible without collaboration with Dr. Ilhem Messaoudi-Powers, Allen Jankeel, and Andrea Rivera at the University of California, Irvine. Dr. Messaoudi-Powers additionally acquainted me with flow cytometry and was kind enough to train me in her laboratory. I also wish to acknowledge Dr. John H. Eldridge, Dr. Demetrius Matassov, and Dr. Michael Egan at Profectus BioSciences, Inc., for allowing me to share the Vesiculovax post-exposure data. A hearty thanks to past and present members of the Geisbert lab for assistance with experiments, instruction, and encouragement: Dr. Karla Fenton, Daniel Deer, Dr. Viktoriya Borisevich, Dr. Robert W. Cross, Dr. Krista Versteeg, Natalie Dobias, Dr. Ben Satterfield, and Sergio Rodriguez. I especially wish to thank Joan Geisbert and Krystle Agans. Joan provided “industrial-strength” experimental assistance and technical expertise; Krystle taught me various molecular techniques and assays and made significant experimental contributions. Lastly, thank you to the following financial supporters: the James W. McLaughlin Foundation Predoctoral Scholarship, Robert E. Shope Endowed Scholarship, Harold T. Sanders Endowed Fellowship for Vaccine Development, and National Institutes of Health grant U19 AI109711.

POST-EXPOSURE TREATMENT OF MARBURG VIRUS ANGOLA DISEASE IN NON-HUMAN PRIMATES USING RECOMBINANT VESICULAR STOMATITIS VIRUS VECTORS

Publication No. _____

Courtney Brooke Woolsey

The University of Texas Medical Branch, 2018

Supervisor: Thomas W. Geisbert

No licensed vaccines or treatments exist for Marburg virus (MARV) disease. As a preventative vaccine, a recombinant vesicular stomatitis virus (rVSV) expressing the Musoke strain glycoprotein (GP) of MARV protects macaques against MARV Musoke and Angola variants, as well as Ravn virus. The vector is also effective as a post-exposure treatment against a high dose homologous MARV Musoke challenge. To determine post-exposure efficacy against the most pathogenic MARV isolate, Angola, we engineered rVSV vectors expressing homologous Angola GP for use as a potential therapeutic. In this study, rhesus monkeys were challenged with a high or low, uniformly lethal dose of MARV Angola and administered rVSV treatment thirty minutes after infection. Although treated macaques had a delayed time-to-death, the treatment was incompletely protective (25%) against a high dose challenge. For the low dose challenge, 60-89% survived and treated animals exhibited fewer signs of disease. To determine immune correlates associated with treatment protection or failure, we performed RNA sequencing and flow cytometry. Humoral responses were assessed via enzyme-linked immunosorbent assays and plaque-reduction neutralization tests. In survivors, we found upregulation of STAT4, an early transcription factor associated with T helper 1 (Th1) and T follicular helper differentiation, and genes mapping to antiviral responses and interferon signaling. In contrast, animals that succumbed had T helper 2 and regulatory T cell signatures; upregulation of genes associated with T-cell exhaustion; and delayed interferon signaling. Only survivor macaques formed MARV GP-specific IgM and IgG with low levels of neutralizing antibodies, and these animals had more antigen-specific Th1 (IFN-gamma and IL-2 positive) cells late in disease. These results suggest survival is correlated with antibody production and Th1-skewed immunity. The rapid disease progression of MARV Angola compared to other variants may account for the failure of rVSV treatment against the high dose challenge. For the low dose challenge, rVSV-mediated antiviral signaling likely reduces viral replication to delay disease progression until a protective adaptive response is formed. MARV Angola sets a high bar for achieving protection with vaccines and therapeutics in the rhesus macaque model. Combination therapy with Th1-skewing adjuvants might enhance post-exposure protection in non-responders.

TABLE OF CONTENTS

List of Tables	ix
List of Figures	xi
List of Abbreviations	xv
CHAPTER 1: BACKGROUND.....	1
Introduction to Rhabdo- and Filoviruses	1
Genomic Organization and Life Cycles of VSV and MARV.....	3
MARV Genome Structure and Proteins	4
MARV Life Cycle	7
VSV Genome Structure and Proteins	8
VSV Life Cycle	9
Clinical Features and Pathogenesis of Marburg Virus Disease	10
Activation and Evasion of Host Immune Responses by MARV and VSV	12
VSV Immune Activation and Evasion.....	14
MARV Immune Activation and Evasion.....	17
Prospective Vaccines and Therapeutics for MVD.....	21
Gaps in Knowledge of rVSV-Induced Immunity Against Filoviruses.....	30
Hypothesis.....	32
CHAPTER 2: POST-EXPOSURE EFFICACY OF RECOMBINANT VESICULAR STOMATITIS VIRUS VECTORS AGAINST HIGH AND LOW DOSES OF MARBURG ANGOLA VIRUS IN NONHUMAN PRIMATES	34
Introduction.....	34
Methods.....	35
Generation of rVSV Vectors.....	36
Challenge Virus	37
Animal Study Design.....	37

Blood Processing	38
Virus Titration	38
RNA Extraction and RT-qPCR	38
Hematology and Serum Biochemistry	39
Histopathology and Immunohistochemistry	39
Statistical analysis.....	40
Results.....	40
Conclusions.....	56
CHAPTER 3: IMMUNOLOGICAL CORRELATES OF RECOMBINANT VESICULAR STOMATITIS VIRUS-MEDIATED POST-EXPOSURE PROTECTION AGAINST MARBURG VIRUS	59
Methods.....	60
Animal Challenge	60
Blood Processing and PBMC Isolation	60
Bead-Based Multiplex Immunoassay	61
RNA Extraction	62
RNAseq Library Preparation	62
RNAseq Analysis and Functional Enrichment	62
Normalization of Samples	64
Flow Cytometry and Intracellular Cytokine Staining on Rhesus PBMC	64
Human Monocyte PDL-1 Assay.....	66
Anti-MARV GP IgM and IgG ELISAs	67
Plaque Reduction Neutralization Test (PRNT)	67
Statistical analysis.....	68
Results.....	68
Transcriptional Changes Were Greater in Fatal Cases at End-Stage Disease ..	69
rVSV-Treated Survivors Upregulate Antiviral and Interferon-Related Genes and Exhibit a Th1 (IFN-gamma) Gene Signature	70
Poor Prognosis is Associated with an Immunoregulatory and Th2 Phenotype	73

A Predominance of Th2 and CD8+ T-cell Transcripts, and Down-Regulation of B-cell Memory and Stimulated Monocytes Correlate with MARV Lethality	83
Survivor Responses are Th1-Skewed, Whereas Fatal Cases Exhibit an Unprotective Cytotoxic CD8+T-Cell and Immunosuppressive Phenotype	85
Fatal Cases are Associated with a Loss of Th and CTL IL-2 Expression, Concomitant with an Increase in Frequency of IL-10-secreting Treg (CD25+ FOXP3+) and CD25+ FOXP3- Cells	88
MARV-infected Primary Human Monocytes Express Low Levels of CD80 and CD86 and Upregulate PDL-1 to Facilitate Inhibitory PD-1 Signaling....	96
rVSV Post-Exposure Treatment Survival Is Dependent on Antibody Production	100
Minimal Titers of Neutralizing Antibodies Were Found in Treated Survivor Macaques	103
Conclusions.....	104
CHAPTER 5: PROPOSED MECHANISM OF RSVV-MEDIATED POST-EXPOSURE PROTECTION AGAINST MARBURG ANGOLA VIRUS	108
CHAPTER 6: FUTURE STUDIES	113
SUPPLEMENTARY FIGURES	123
REFERENCES.....	131

List of Tables

Table 1. A comparison of clinical findings and gross liver pathology of rhesus macaques challenged with 1000 PFU of MARV Musoke and Angola variants.	3
Table 2. Summary of vaccine studies for Marburg virus disease in the non-human primate model.	25
Table 3. Summary of post-exposure treatment studies for Marburg virus disease in the non-human primate model.	29
Table 4. Clinical findings in monkeys for the high dose experiment.	44
Table 5. Clinical findings in monkeys for the low dose experiment.	51
Table 6. List of antiviral and Th1-associated genes linked with early survivor signaling.	73
Table 7. Enrichment analysis of fatal group DEGs at terminal disease reveals a Th2 and tolerogenic gene signature.	76
Table 8. Upregulated DEGs associated with T-cell anergy and exhaustion in the fatal dataset at late disease.	83
Table 9. Neutralizing antibody titers.	104
Supplementary Table 1. Normalization of samples for RNAseq, flow cytometry, and cytokine analyses.	125

Supplementary Table 2. Antibodies used for flow cytometric analysis of immune cell subsets in rhesus monkeys (manufacturer and clone are indicated in parentheses).126

List of Figures

Figure 1. Genome organization and virion structure of MARV.....	5
Figure 2. Genome organization and bullet virion structure of VSV.....	9
Figure 3. Mechanisms of IFN antagonism by MARV VP35 and VP40 proteins.....	19
Figure 4. Generation of rVSV vectors and study design.	41
Figure 5. Postexposure treatment of macaques with rVSV Δ G/MARV-Angola-GP was incompletely protective against a 1000 PFU high dose challenge of MARV Angola.....	42
Figure 6. MARV viral loads in animals challenged with a high dose of MARV-Angola.....	45
Figure 7. Tissue viral loads in animals challenged with a high dose of MARV-Angola.....	46
Figure 8. Postexposure treatment of macaques with rVSV vectors was effective against a 50 PFU low dose challenge of MARV Angola.	48
Figure 9. MARV viral loads in animals challenged with a low dose of MARV-Angola.....	53
Figure 10. Tissue viral loads in animals challenged with a low dose of MARV-Angola.....	54
Figure 11. Immunolabeling of MARV antigen in the liver and spleen of rhesus macaques challenged with MARV Angola.	55

Figure 12. Venn diagram depicting overlap of DEGs within groups, and distribution of upregulated and downregulated DEGs in the fatal monkey dataset.	70
Figure 13. Heatmap comparison of the most highly upregulated and downregulated DEGS at mid-disease for each group.	72
Figure 14. Process network map illustrating direct interactions of DEGs upregulated in the fatal group late in disease that map to “Signal Transduction_TGF-beta, GDF and Activin signaling”	78
Figure 15. ImmQuant heatmap analysis of the relative contribution of immune cell subsets to differential gene expression within the fatal group.	84
Figure 16. CD8+/CD4+ T-cell ratio and percentage of degranulating CD8+ T-cells in PBMC.	85
Figure 17. Survivors had a lower percentage of Tregs and more IFN-gamma+ IL-2+ Th1 cells late in disease.	87
Figure 18. Comparison of concentrations of TGF-beta and IL-10 analytes in the serum of MARV-infected macaques.	88
Figure 19. Analysis of shifts in the regulatory T-cells (Treg) population over the course of infection in representative fatal and survivor macaques, and their contribution of IL-10 at late disease.	90
Figure 20. T helper (Th) cell phenotypes in survivors and fatals at mid- and late-disease.	94

Figure 21. CD8+ cytotoxic T-cell (CTL) phenotypes in survivors and fatals at mid- and late-disease.....	96
Figure 22. Expression of inhibitory PD-1 and PDL-1, and co-stimulatory CD80 and CD86, molecules in infected human primary monocytes.....	98
Figure 23. Reciprocal endpoint dilution titers of anti-MARV GP IgM and IgG in the serum of subjects challenged with a high dose MARV-Angola challenge.....	101
Figure 24. Reciprocal endpoint dilution titers of anti-MARV GP IgM and IgG in the serum of subjects subjected to a low dose MARV-Angola challenge..	102
Figure 25. Proposed mechanism for rVSV-mediated post-exposure protection.	112
Figure 26. Representative Amnis cytometer image demonstrating rVSVΔG/MARV-Angola-GP preferentially infects monocytes.....	115
Figure 27. RT-qPCR of VeroE6, Huh7, and HepG2 wells infected with rVSVΔG/MARV-Angola-GP and/or MARV.....	117
Figure 28. Immunofluorescence assay of VeroE6 and HepG2 wells infected with rVSVΔG/MARV-Angola-GP and/or MARV.....	119
Figure 29. In vitro screening of plasmids expressing selected shRNAs.....	121
Supplementary Figure 1. Confirmation of recovery of rVSVΔG/MARV-Angola-GP.	123
Supplementary Figure 2. PCA of survivor and fatal group individuals at baseline, mid-disease, and late-disease.....	124

Supplementary Figure 3. PBMC flow cytometry gating strategy.....	126
Supplementary Figure 4. Heatmap comparison of the most highly upregulated and downregulated DEGS at late-disease for each group.	127
Supplementary Figure 5. ImmQuant comparative view analysis of the relative contribution of immune cell subsets to differential gene expression within the control group.....	128
Supplementary Figure 6. Plasma levels of cytokines measured by Milliplex NHP 23- plex cytokine bead arrays.	130

List of Abbreviations

ΔG	The native VSV G_{IN} is absent
ACO1	Aconitase 1
ADCC	Antibody-dependent cell-mediated cytotoxicity
ALP	Alkaline phosphatase
ALT	Alanine aminotransferase
AP-1	Activator protein 1
AST	Aspartate aminotransferase
ANOVA	Analysis of variance
ANXA10	Annexin A10
AP1AR	Adaptor related protein complex 1 associated regulatory protein
APOBEC	Apolipoprotein B mRNA editing enzyme catalytic subunit 1
ARL14EP	ADP ribosylation factor like GTPase 14
BCAR3	Breast cancer anti-estrogen resistance 3
BCR	B-cell receptor
BHK	Baby hamster kidney cell line
BST2	Tetherin
BUN	Blood urea nitrogen
CARD (s)	Caspase recruitment domain (s)
CCDC47	Coiled-coil domain containing 47
CCL	Chemokine ligand
CCR	Chemokine receptor
CD	Cluster of differentiation
CD107a	Marker of degranulation
CDC	United States Center for Disease Control and Prevention
CDHR5	Cadherin related family member 5
CDX2	Caudal type homeobox 2
cDNA	Complementary DNA
CETP	Cholesteryl ester transfer protein
CFR	Case fatality rate
CLR (s)	C-type lectin receptor (s)
CM	Cynomolgus macaques
CMPK2	Cytidine/uridine monophosphate kinase 2
CRE	Creatinine
CRISPR	Clustered regularly interspaced short palindromic repeats
CRP	C-reactive protein
CRTH2	Chemoattractant receptor-homologous molecule expressed on Th2 cells
CT1	Truncated cytoplasmic tail of rVSV
CTL (s)	CD8+ cytotoxic T lymphocyte (s)
CTLA-4	Cytotoxic T lymphocyte antigen 4
CYP2W1	Cytochrome P450 family 2 subfamily W member 1
DAMP (s)	Damage-associated molecular pattern (s)
DC (s)	Dendritic cell (s)

DCQ	Digital cell quantification
DDX58	RIG-I gene
DEG (s)	Differentially expressed gene (s)
DIC	Disseminated intravascular coagulation
DMRTA2	Doublesex- and mab-3-related transcription factor
DMSO	Dimethyl sulfoxide
DRC	Democratic Republic of Congo
dsRNA	Double-stranded viral RNA
EBOV	Ebola virus
EDTA	Ethylenediaminetetraacetic acid
ELISA (s)	Enzyme-linked immunosorbent assay (s)
EMEM	Eagle's minimum essential medium
ER	Endoplasmic reticulum
ESCRT	Endosomal sorting complexes required for transport
EU	Endotoxin units
FAM	Carboxyfluorescein
FAM216B	Family with sequence similarity 216 member B
FBS	Fetal bovine serum
FDA	United States Food and Drug Administration
FDR	False discovery rate
FOXP3	Forkhead box P3, master regulator for Tregs
FSC	Forward scatter
G/GP	Glycoprotein
G-CSF	Granulocyte colony-stimulating factor
gag	Group-specific antigen (HIV protein)
GATA3	Master regulator for Th2 cells
GBP1	Guanylate binding protein 1
GDF6	Growth differentiation factor 6
GGT	Gamma-glutamyltransferase
G _{IN}	Native VSV Indiana glycoprotein gene
GLS	Glutaminase
GM-CSF	Granulocyte-macrophage colony-stimulating factor
GPΔTM	MARV GP without transmembrane region
GP1	Subunit 1 of GP
GP2	Subunit 2 of GP
GSBS	Graduate School of Biomedical Sciences
HAS1	Hyaluronan synthase 1
HECW2	NEDD4-like E3 ubiquitin-protein ligase 2
HERC6	HECT and RLD domain containing E3 ubiquitin protein ligase
HERPUD1	Homocysteine inducible ER protein with ubiquitin like domain
HF	Hemorrhagic fever
HIV	Human immunodeficiency virus
HRP	Horseradish peroxidase
HSPBAP1	Heat shock protein-associated protein 1
i.m.	Intramuscular
ICS	Intracellular cytokine staining

ICTV	International Committee on Taxonomy of Viruses
IDO	Indoleamine 2,3-dioxygenase-1
IFIH1	MDA-5 gene
IFIT	IFN-induced protein with tetratricopeptide repeats
IFITM	IFN-induced transmembrane protein
IFN (s)	Interferon (s)
IFNAR	IFN-alpha receptor complex
IFNG	IFN-gamma gene
IFNGR	Interferon gamma receptor
IgG	Immunoglobulin G
IgM	Immunoglobulin M
IHC	Immunohistochemistry
IL	Interleukin
ION	Ionomycin
IR	Intergenic regions
IRF	Interferon regulatory factor
IRS2	Insulin receptor substrate 2
ISG (s)	Interferon-stimulated gene (s)
ISRE (s)	Interferon-stimulated response element (s)
i.m.	Intramuscular
i.v.	Intravenous
JAK	Janus kinase
Keap1	Kelch-like ECH-associated protein 1
Ki67	Marker for proliferation
KLRF1	Killer cell lectin like receptor F1
L	Large protein
LAG-3	Lymphocyte-activation gene 3
LCMV	Lymphocytic choriomeningitis virus
LD ₅₀	Median lethal dose
LASV	Lassa virus
LGP2	Laboratory of genetics and physiology 2 protein
LIMS2	LIM zinc finger domain containing 2
LIPA	Lipase A
logFC	Log fold-change
LPS	Lipopolysaccharide
LTF	Lactotransferrin
LY6E	Lymphocyte antigen 6 family member E
M	Matrix protein
mAb (s)	Monoclonal antibody or antibodies
MARV	Marburg virus
MCP-1	Monocyte chemoattractant protein
MDA-5	Melanoma differentiation-associated protein 5
MFI	Mean fluorescence intensity
MHC	Major histocompatibility complex
ml	Milliliter
MOI	Multiplicity of infection

mRNA (s)	Messenger RNA (s)
MVB	Multi-vesicular bodies
MVD	Marburg virus disease
MX1	Myxoma resistance protein 1
N	Nucleoprotein (VSV)
N-RNA	Nucleocapsid-RNA structure
N.D.	Not determined
N2	The rVSV nucleoprotein is at position 2 in the genome
N4	The rVSV nucleoprotein is at position 4 in the genome
NCAPH2	Non-SMC condensin II Complex Subunit H2
NEDD4	Neural precursor cell expressed, developmentally down-regulated 4, E3 ubiquitin ligase
NFkB	Nuclear factor kappa-light-chain-enhancer of activated B cells
NHP (s)	Non-human primate (s)
NIAID	National Institute of Allergy and Infectious Diseases
NK	Natural killer
NLR (s)	NOD-like receptor (s)
NP	Nucleoprotein
NPC1	Niemann-Pick C1 protein
OAS	2'-5'-oligoadenylate synthetase
OPD	O-phenylenediamine
P	Phosphoprotein
PAMP (s)	Pathogen-associated molecular pattern (s)
PARP12	Poly (ADP-Ribose) polymerase family member 12
PARP9	Poly (ADP-Ribose) polymerase family member 9
PBMC	Peripheral blood mononuclear cells
PBS	Phosphate-buffered saline
PCA	Principal component analysis
PCR	Polymerase chain reaction
PD-1	Programmed death receptor 1
PDL-1	Programmed death ligand 1
PDL-2	Programmed death ligand 2
PFU	Plaque-forming units
PI	Post-infection
PKIB	CAMP-dependent protein kinase (PKA) inhibitor beta
PKR	Protein kinase R
PMA	Phorbol 12-myristate 13-acetate
PML	Promyelocytic leukemia protein
PMO (s)	Phosphorodiamidate morpholino oligomer (s)
Poly:IC	Polyinosinic-polycytidylic acid (dsRNA)
Poly:ICLC	A complex of carboxymethylcellulose, poly:IC, and poly-L-lysine
PRNT (s)	Plaque reduction neutralization test (s)
PRNT ₅₀	PRNT dilution that reduces 50% of plaques
PRR (s)	Pattern recognition receptor (s)
rAd5	Recombinant Adenovirus 5
RAVV	Ravn virus

RBC (s)	Red blood cell (s)
RdRP	RNA-dependent RNA polymerase
RIG-I	Retinoic acid inducible gene I
RIPK3	Receptor-interacting serine/threonine kinase 3
NFAT	Nuclear factor of activated T-cells
RLR (s)	RIG-I-like receptor (s)
RM	Rhesus macaques
RNAi	RNA interference
rNAPc2	Recombinant nematode anticoagulant protein c2
RNAseq	RNA sequencing
RNP	Ribonucleoprotein complex
RO	Isoform of CD45 expressed on memory T-cells
RPKM	Reads per kilobase of transcript per million reads
rRNA	Ribosomal RNA
RT	Room temperature
RT-qPCR	Quantitative reverse transcription PCR
rVSV (s)	Recombinant Vesicular stomatitis virus (es)
s.c.	Subcutaneous
shRNA (s)	Short hairpin RNA (s)
siRNA (s)	Short interfering RNA (s)
SLC9A9	Solute carrier family 9, subfamily A cation proton antiporter 9
SPICE	Simplified presentation of incredibly complex evaluations
RIPK3	Receptor interacting serine/threonine kinase 3
SNALP (s)	Stable nucleic acid lipid particle (s)
SOX17	SRX (sex determining region Y)-box 17
SSC	Side scatter
STAT	Signal transducer and activator of transcription
STAT4	Signal transducer and activator of transcription 4
TAMRA	Carboxytetramethylrhodamine
Tc	Transcription stop signal
TCR	T-cell receptor
TDC	Thesis and dissertation coordinator
Tfh	CD4+ T follicular helper lymphocyte
TGF-beta	Transforming growth factor-beta
Th	CD4+ T helper cells
Th0	Undifferentiated naïve CD4+ T-cells
Th1	CD4+ T helper 1 lymphocyte
Th2	CD4+ T helper 2 lymphocyte
Th17	CD4+ T helper 17 lymphocyte
TIM	T cell Ig mucin protein
TLR (s)	Toll-liked receptor (s)
TMPRS22	Transmembrane protease, serine 22
TNF	Tumor necrosis factor
TNFRSF17	Receptor for TNFSF13B/BLyS/BAFF and TNFSF13/APRIL
Treg (s)	CD4+ regulatory T-cell (s)
TSG101	Tumor susceptibility gene 101

UTMB	University of Texas Medical Branch
UTR (s)	Untranslated regions (s)
VEEV	Venezuelan equine encephalitis virus replicon
VLP (s)	Virus-like particle (s)
VP24	Viral protein 24
VP30	Viral protein 30
VP35	Viral protein 35
VP40	Viral protein 40
VSIG8	V-set and immunoglobulin domain containing 8
VSIV, VSV	Vesicular stomatitis Indiana virus
WBC (s)	White blood cell (s)
WNT6	Wingless-type MMTV integration site family, member 6
ZCRB1	Zinc finger CCHC-type and RNA binding motif containing 1

CHAPTER 1: BACKGROUND

Introduction to Rhabdo- and Filoviruses

The order, *Mononegavirales*, encompasses a large group of enveloped viruses with single-stranded, negative-sense, nonsegmented RNA genomes. According to the latest International Committee on Taxonomy of Viruses (ICTV) classification, eight virus families—*Rhabdoviridae*, *Filoviridae*, *Paramyxoviridae*, *Myxonaviridae*, *Nyamiviridae*, *Pneumoviridae*, *Sunviridae*, and *Bornaviridae*—comprise the order [1]. Members of these families share similar genomic structures and life cycles. In fact, taxonomists initially grouped *Rhabdoviridae* with *Filoviridae* based on their similar virion morphology; however, subsequent studies revealed distinct properties that warranted their placement in a separate family [2]. This dissertation focuses on these two virus families.

Seventeen genera represent the family *Rhabdoviridae*. Vesicular stomatitis Indiana virus (VSIV, henceforth referred to as VSV) is a zoonotic arbovirus within the genus *Vesiculovirus* (type species *Indiana vesiculovirus*) [1]. VSV is endemic to the Americas and is transmitted by arthropod vectors, such as sandflies, mites, and mosquitoes [3, 4, 5]. In livestock, the virus causes vesicular lesions of the tongue, gums, lips, teats, and hooves that are indistinguishable from foot-and-mouth disease [6]. In humans, infection is asymptomatic or results in a mild flu-like illness. VSV is often used as a prototype in biomedical research to study viral entry, replication, and transcription [7]. Other important uses include oncolytic therapies, pseudotyping of retrovirus and lentivirus vectors to enable transduction of genes of interest into a broad range of mammalian cells, and vaccine vectors against human pathogens, such as Human

immunodeficiency virus (HIV), influenza, Respiratory syncytial virus, Marburg virus (MARV), Ebola virus (EBOV), and Lassa virus (LASV) [8, 9, 10].

MARV and EBOV are in the family *Filoviridae*, which includes three genera: *Cuevavirus*, *Ebolavirus*, and *Marburgvirus* [7]. This family contains emerging viruses endemic to Africa that cause severe, and often lethal, hemorrhagic fever (HF) in humans and non-human primates (NHPs). While there are five species of *Ebolavirus*—*Zaire ebolavirus*, *Bundibugyo ebolavirus*, *Sudan ebolavirus*, *Tai Forest ebolavirus*, and *Reston ebolavirus*—only a single species of *Marburgvirus* exists: *Marburg marburgvirus* [1]. Bayesian phylogenetic analyses reveal two distinct evolutionary lineages within this sole species corresponding to MARV and Ravn virus (RAVV). Two clades further divide MARV. Clade A consists of 10 Ugandan isolates, a group of Kenyan isolates obtained in 1980, a single isolate from the 2000 Democratic Republic of Congo (DRC) outbreak, and isolates during the 2004–2005 Angola epidemic. Clade B includes a single 1975 isolate from Zimbabwe, the majority of isolates acquired during the 1998–2000 DRC outbreak, and several Ugandan isolates from 2007–2009. Analysis of MARV variants, including Musoke, Angola, Ozolin, Ci67, and Popp, reveal a median nucleotide difference of 6 substitutions per 100 sites. Genomic divergence of MARV compared to the more distant RAVV isolates is ~16.9% at the nucleotide level [11].

The two main MARV variants used for research are Musoke and Angola. MARV-Musoke was isolated in 1980 from a non-fatal case in Kenya [12]. A young male doctor contracted the virus after a failed attempt to resuscitate an infected patient. MARV-Angola is considered the most pathogenic variant since it was associated with the largest outbreak (252 cases) and highest case fatality rate (~90%) [13]. Moreover, NHPs infected with MARV-Angola tend to have severer hepatic injury and accelerated disease onset compared to MARV-Musoke or other variants (Table 1). For a 1000 plaque-forming unit

(PFU) intramuscular challenge, rhesus macaques infected with MARV-Angola have a terminal stage of 6-8 days versus 10-12 for MARV-Musoke, as well as earlier signs of clinical disease, e.g. viremia, fever, rash, and anorexia [14, 15, 16]. Inherited differences between variants should, therefore, be considered when evaluating vaccines and therapeutics, as they may lead to different outcomes in hosts.

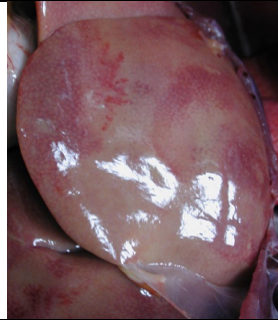
	<i>Days after challenge</i>	
	Musoke	Angola
Terminal Stage	10-12	6-8
Asymptomatic	0-4	0-3
Viremia	4-12	3-8
Fever	6-12	4-8
Rash	9-12	6-8
Dehydration	6-12	4-8
Depression	6-12	4-8
Anorexia	6-12	4-8
Liver pathology		

Table 1. A comparison of clinical findings and gross liver pathology of rhesus macaques challenged with 1000 PFU of MARV Musoke and Angola variants.

Angola causes a more rapid disease onset and progression compared to the Musoke variant. Angola-infected livers show severe reticulation and pale coloration. Numbers indicate days post-infection. PFU (plaque forming units). Photographs used with permission from Dr. Thomas W. Geisbert (UTMB).

Genomic Organization and Life Cycles of VSV and MARV

MARV GENOME STRUCTURE AND PROTEINS

MARV virions are highly pleomorphic with filamentous, shepherd's crook, "U", "6", or branched forms and a mean length of 892 nm x 91 nm [17, 18]. The negative-sense, single-stranded ~19.1kb RNA genome of MARV encodes seven monocistronic genes: NP-VP35-VP40-GP-VP30-VP24-L (Figure 1). Each gene contains a single open reading frame, 3' and 5' untranslated regions (UTRs) and a highly conserved UAAUU transcription start/stop signal. To enable transcription and replication, the viral RNA-dependent RNA polymerase (RdRP) recognizes *cis*-acting regulatory elements located at the 3' leader and 5' trailer ends of the genome [19]. The RdRP uses a stop-start mechanism to transcribe mRNAs sequentially; consequently, it produces more positive-sense mRNA transcripts at the 3' end of the genome than at the 5' end. Short intergenic regions segregate genes, except for an overlapping region at the VP30-VP24 gene junction. The abundance of particular viral proteins governs replication. The filovirus replication promoter has a bipartite structure similar to paramyxoviruses, although it does not abide by the "rule of six". The first element of the MARV replication promoter is at the 3' end of the genome and is predicted to adopt a secondary stem-loop structure; the second promoter element consists of a (UN₅) x 3 hexamer motif and is located within the 3' UTR of the NP gene. The 5' non-coding region of the genome contains the antigenomic replication promoter [20].

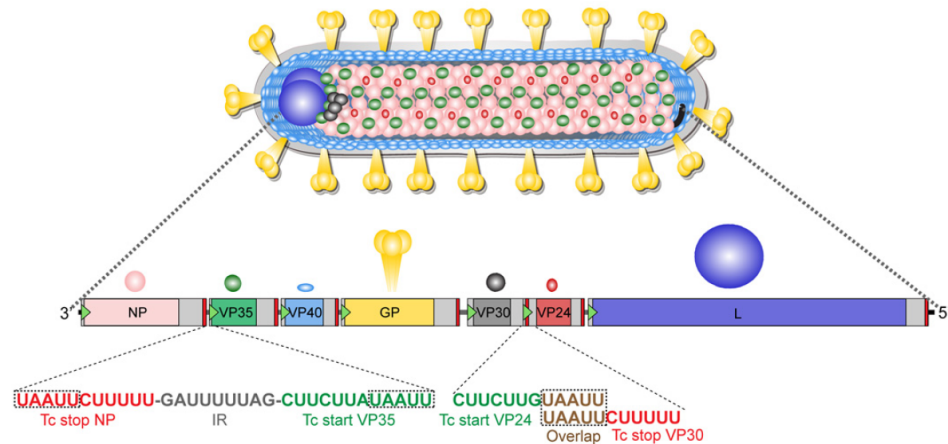


Figure 1. Genome organization and virion structure of MARV.

*Each gene color corresponds to the encoded viral protein. The following are used to denote specific regions: light grey boxes for untranslated regions; dark grey lines for intergenic regions (IR); green triangles for transcription start signals; red bars for transcription stop signals (Tc stop). Note the VP30-VP24 gene junction contains overlapping transcription signals. Brauburger, K. et al. "Forty-Five Years of Marburg Virus Research." *Viruses*. 4(10): 1878-1927. © 2012 by the authors; licensee MDPI, Basel, Switzerland. This figure is from an open-access article distributed under the terms and conditions of the Creative Commons Attribution License (<http://creativecommons.org/licenses/by/4.0/>) [21].*

MARV mRNA transcripts are translated into proteins that contribute to the structural integrity of the virion or serve a role in replication:

Nucleoprotein (NP): The highly phosphorylated NP encapsulates MARV genomes and antigenomes to protect RNA from being degraded by RNases or recognized by host pattern-recognition receptors. The abundance of NP determines the RdRP switch from transcription to replication [21]. NP also participates in budding by recruiting endosomal sorting complexes required for transport (ESCRT) protein, TSG101 [22].

Viral protein 35 (VP35): This polymerase cofactor is crucial for transcription and replication. VP35, along with the large protein (L) catalytic component forms the RNA-

dependent RNA polymerase (RdRP) [23]. VP35 assists in nucleocapsid formation by forming a strong association with NP to establish a bridge between NP and L [24].

Viral protein 40 (VP40): The VP40 matrix protein is the most abundant protein in the virion and is responsible for its filamentous morphology. Sole expression of VP40 in cells results in the release of virus-like particles (VLP) that bud from the cell membrane [25]. The primary roles of VP40 are negative regulation of replication and transcription, assembly and budding, and interferon (IFN) antagonism. VP40 recruits the glycoprotein (GP) to budding sites at the plasma membrane and forms a flexible, weak interaction with the nucleocapsid [26, 22]. A PPPY late domain motif in the VP40 N-terminus interacts with proteins of the host ESCRT machinery, namely tumor susceptibility gene 101 (TSG101) and neural precursor cell expressed, developmentally down-regulated 4, E3 ubiquitin ligase (NEDD4), to facilitate budding [28, 29, 30].

Glycoprotein (GP): MARV GP is expressed on the surface of virions as homotrimeric spikes and performs the following functions: attachment, entry, fusion, and immune evasion [21]. The precursor GP undergoes various posttranslational modifications in the endoplasmic reticulum (ER) including glycosylation, phosphorylation, and acylation [30, 31, 32, 33, 34]. It is then cleaved by a furin-like protease in the trans-Golgi network into two disulfide-linked subunits, GP1 and GP2 [35]. GP1 facilitates receptor binding, whereas the transmembrane subunit, GP2, mediates fusion [36,37].

Viral protein 30 (VP30): This protein tightly associates with the nucleocapsid via NP binding following phosphorylation [32]. Its role in viral transcription and replication is not fully understood, as it is not required for these functions in a minigenome system [39].

Viral protein VP24 (VP24): VP24 is a minor matrix protein and is involved in the maturation of nucleocapsids by functioning as an interface between nucleocapsids and budding sites. It also plays a role in the regulation of transcription and replication [40].

Large protein (L): The major and catalytic component of the MARV RdRP, L, is essential for both transcription and replication. MARV L carries out RNA synthesis, capping, and polyadenylation of viral mRNAs [41].

MARV LIFE CYCLE

The MARV life cycle begins when GP binds to lectins (e.g. DC-SIGN, L-SIGN, hMGL ASGP-R, LSECTin) on the surface of host cells [42, 43, 44]. Other putative attachment factors include the receptor tyrosine kinase Ax1, and T cell Ig mucin (TIM) proteins TIM-1 and TIM-3 [45, 46, 47]. The latter group of proteins is thought to interact with phosphatidylserine molecules on the viral envelope. Next, MARV virions enter cells by a macropinocytosis-like mechanism and compartmentalize in an endosome [48, 49]. The GP1 subunit is cleaved by an endosomal cysteine protease to remove heavily-glycosylated domains, allowing GP1 to bind the entry receptor, Niemann-Pick C1 (NPC1) [50]. Endosomal acidification causes the MARV GP2 subunit to undergo a pH-dependent conformational change releasing the fusogenic loop and permitting fusion of the viral and late endosomal membranes [51, 52]. Following nucleocapsid release into the cytosol, the genome is uncoated and mRNAs are sequentially transcribed, co-transcriptionally capped, and polyadenylated by the viral RdRP. Host cell machinery then translates these positive-sense mRNAs into viral proteins. The genome serves as a template to generate positive-sense antigenomes. Antigenomes then serve as templates to produce progeny genomes that can be packaged into virions or transcribed. Assembly and budding are induced by VP40 via recruitment of GP, VP24, and nucleocapsids from the

inclusion bodies to the plasma membrane with the aid of ESCRT machinery. The lipid envelope of the virion is host-derived and acquired from budding off the host cell membrane [52].

VSV GENOME STRUCTURE AND PROTEINS

VSV virions are bullet-shaped particles measuring 170 x 80 nm [53]. The ~11,161 nucleotide genome encodes five genes in the following order: N-P-M-G-L (Figure 2). The leader is situated at the 3' end and trailer at the 5' end. Similar to MARV, the RNA genome is encapsidated by the nucleoprotein (N) to resist nuclease activity. The viral RNA RdRP is primarily composed of a large protein (L) catalytic subunit and a phosphoprotein (P) cofactor (an equivalent of MARV VP35), which allows the polymerase to recognize the nucleocapsid-RNA structure (N-RNA). The RdRP, along with the N-RNA, form the ribonucleoprotein (RNP) complex. The RdRP recognizes cis-acting signals within the 3' end of the N-RNA template that govern replication and transcription. Stop-start sequences for transcription are (3'AUACUUUUUU5') for the end of the upstream gene, an untranscribed intergenic dinucleotide (G/CA), and a gene start sequence for the downstream gene (3'UUGUC5') [8]. The VSV matrix protein (M) assists in budding and surrounds the RNP complex to contribute to the structural integrity of the virion [54]. The lipid membrane of the virion is host-cell derived and studded with glycoprotein (G) to facilitate receptor binding and entry [55].

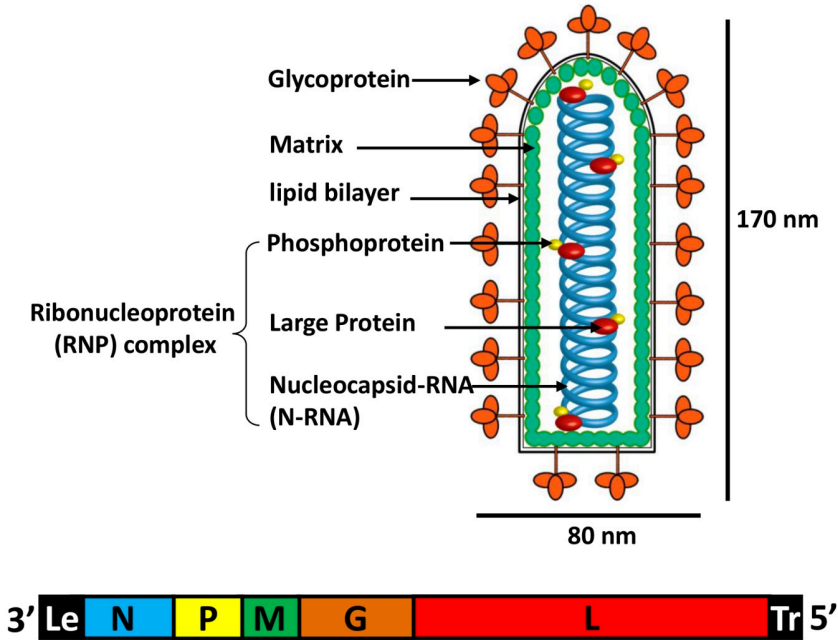


Figure 2. Genome organization and bullet virion structure of VSV.

Gene open reading frames match the respective translated viral proteins. Abbreviations: nucleoprotein (N); phosphoprotein (P); matrix protein (M); glycoprotein (G); large protein (L); leader (Le); and trailer (Tr). Jianrong Li and Yu Zhang. (2012). Messenger RNA Cap Methylation in Vesicular Stomatitis Virus, a Prototype of Non-Segmented Negative-Sense RNA Virus, Methylation - From DNA, RNA and Histones to Diseases and Treatment, Prof. Anica Dricu (Ed.), InTech, Available from <https://www.intechopen.com/books/methylation-from-dna-rna-and-histones-to-diseases-and-treatment/messenger-rna-cap-methylation-in-vesicular-stomatitis-virus-a-prototype-of-non-segmented-negative-se> [56].

VSV LIFE CYCLE

VSV enters host cells via the low-density lipoprotein receptor (or its family members) and undergoes clathrin-mediated endocytosis [55]. The host actin network and positive residues of the G interact with negatively-charged phospholipids of the cell membrane to aid in this process [57]. The low pH of the early endosome triggers G-mediated fusion and uncoating, allowing delivery of the RNP into the cytoplasm [58]. Following recognition and transcription of the N-RNA complex by the RdRP, mRNAs are polyadenylated at the 3' end and capped and methylated at the 5' end [59]. Host ribosomes next translate the mature mRNAs. Replication occurs at the 3' end of the

genome to synthesize a complementary antigenome template. The antigenome is then replicated to form full-length progeny genomes. Genomes are then loaded into virions following translation of viral proteins or they serve as a template for secondary transcription. Budding is enabled by the M and G proteins, as well interaction with host ESCRT or associated proteins, and occurs at the plasma membrane at lipid raft sites [8].

Clinical Features and Pathogenesis of Marburg Virus Disease

MARV is believed to persist in a fruit bat reservoir host, *Rousettus aegyptiacus*, and infect humans and NHPs during spillover events [60, 61]. Humans become infected by exposure to an infected animal or direct contact with body fluids, such as blood, saliva, sweat, tears, urine, stool, semen, and breast milk [62, 63]. Immunity and severity of disease is attributed to various factors, or a combination thereof, including 1) inherent differences of virus isolates 2) quality and availability of medical treatment 3) variance in host populations due to genetic susceptibility or diet 4) dose and route of transmission and 5) co-infections which exacerbate disease (especially HIV).

Marburg virus disease (MVD) symptoms in humans are primarily based upon clinical data acquired during outbreaks in Germany, Yugoslavia, the DRC, and Angola. There are four stages of disease: an incubation period, a generalization phase, an early organ phase, and late organ phase or convalescent period [64]. The incubation period ranges from 3-21 days with an average of 5-10 days, depending on the route of transmission and infectious dose. The generalization phase (day(s) 1-4) is characterized by fever, severe headache, malaise, myalgia, pharyngitis, and gastrointestinal symptoms (nausea, abdominal pain, diarrhea, anorexia). These symptoms may persist for the entire course of infection. By day 4-5, patients develop a maculopapular rash, the earliest

distinguishing feature indicating infection by a filovirus. Other common symptoms include thrombocytopenia, leukopenia, and lymphadenopathy. At days 5-13 (early organ phase), multiple organs are affected including the liver, kidney, and pancreas. Most patients show hemorrhagic manifestations at this point, such as petechiae, ecchymoses, bloody diarrhea, and mucosal bleeding. Infected individuals may appear irritable, aggressive, and confused. Patients may also experience dyspnea, increased vascular permeability, edema, or conjunctival infection. From day 13 on, victims enter the late organ phase characterized by preagonal symptoms such as severe disseminated intravascular coagulation (DIC), multiorgan failure, coma, shock, and eventually death. Alternatively, survivors enter an extensive convalescent period typified by partial amnesia, sweating, myalgia, exhaustion, sweating, and peeling at rash sites. [65, 66, 67]

Animal models have advanced the understanding of virus infection and dissemination. Filovirus pathogenesis studies have largely been conducted in rodents and NHPs. NHPs most accurately recapitulate human infection, as rodents do not typically exhibit some of the immunological aspects of the disease or hemorrhagic manifestations [7]. MARV particles enter the body through compromised skin or mucosal membranes and infect monocytes, macrophages and dendritic cells (DCs) [68]. These early target cells then migrate to regional lymph nodes and spread through the lymphatic system to major organs [69]. The liver and spleen are preferred sites of replication and contain high numbers of monocytes and macrophages [70]. In the late stages of disease, nearly every organ is affected [70, 71, 72, 73]. Monocytes and macrophages appear highly activated and secrete reactive oxygen species and proinflammatory cytokines/chemokines, such as TNF-alpha, IL-1-beta, IL-6, IL-8, and gro-alpha [74]. These soluble factors recruit other inflammatory cells and increase vascular permeability [75, 76]. The secretion of tissue factor by macrophages likely plays a role in coagulopathy and DIC. Consequences of DIC include widespread deposition of fibrin resulting in ischemia, hemolytic anemia, as

well as hemorrhagic diathesis due to consumption of platelets and clotting factors [77, 78, 79]. In culture, human primary macrophages slightly upregulate T-cell costimulatory molecules CD40 and CD80, fail to upregulate CD83, and only result in low expression of CD86 and major histocompatibility complexes (MHCs) [80, 81]. In contrast to monocytes and macrophages, MARV-infected dendritic cells (DCs) upregulate co-inhibitory molecules and fail to undergo maturation or elicit cytokine production [80, 81]. Costimulatory molecules of DCs are downregulated, and infected cells fail to induce proliferation of allogenic T-cells [81]. The lack of support from DCs is thought to contribute to lymphocyte apoptosis and an impaired adaptive response [7, 81]. Direct interaction with viral proteins or induction of Fas death receptor pathways may also contribute to filovirus-induced lymphocyte apoptosis [7, 82]. Due to extensive necrosis and apoptosis of lymphocytes in secondary lymphatic tissues, an appropriate adaptive immune response is delayed or not induced. Other cell types permissive to MARV infection include endothelial cells, fibroblasts, hepatocytes, and adrenal cortical and medullary cells [7, 14, 70, 71, 72, 73, 83]. Neutrophils and lymphocytes are spared. Infected endothelial cells are observed in low numbers in the NHP animal model suggesting vascular changes are caused by paracrine signaling [73]. This is likely exacerbated by the impaired synthesis of clotting factors in the liver, given the prominent pathology seen in this organ. MVD causes necrosis of the adrenal glands leading to decreased steroid synthesis [66]. Steroids help control blood pressure and thus infection with MARV may lead to hypovolemia. The systemic virus spread and replication, dysregulation of the immune response, coagulopathies, and hypotension ultimately result in shock and multiorgan failure.

Activation and Evasion of Host Immune Responses by MARV and VSV

The innate immune system orchestrates a broad and non-specific defense response to invading pathogens. Host pattern-recognition receptors (PRRs) play a pivotal part in mediating successful defense by sensing two classes of structures: pathogen-associated molecular patterns (PAMPs) and endogenous damage-associated molecular patterns (DAMPs). PAMPs are associated with microbial constituents such as bacterial carbohydrates, viral glycoproteins and bacterial or viral DNA/RNA, whereas DAMPs are molecules released following cell damage or death [84]. Some examples of DAMPs include heat-shock proteins, uric acid, and extracellular ATP. Specific PRRs become activated depending on the localization and type of molecular pattern. Expression of toll-like receptors (TLRs) and C-type lectin receptors (CLRs) occurs at cell/endosomal membranes; NOD-like receptors (NLRs) and retinoic acid inducible gene I (RIG-I)-like receptors (RLRs) are intracellular. Stimulation of these PRRs triggers signaling pathways leading to downstream transcription of genes involved in defense and release of immunostimulatory cytokines/chemokines, such as IFNs, TNF-alpha, and IL-12 [85].

Of particular importance in viral infections are IFNs [86]. Type I and II IFNs modulate the immune response in response to viral components, particularly nucleic acids. Type I IFNs—IFN-alpha, IFN-beta, IFN-epsilon, IFN-kappa, and IFN-omega—are produced by several cell types including monocytes, dendritic cells, macrophages, lymphocytes, and fibroblasts. Basically, all nucleated cells are capable of inducing IFN responses. IFNs also downregulate/inhibit the proliferation of host cells, a well-recognized function. These secreted proteins act in an autocrine or paracrine manner to induce an antiviral state [87]. Type I IFNs initially bind the IFN-alpha receptor (IFNAR) complex, activating the canonical Janus kinase (JAK)/STAT signaling pathway. This process causes binding and phosphorylation of JAK proteins and results in successive recruitment and phosphorylation of STAT1 and STAT2 transcription factors. Next, STAT molecules form heterodimers and associate with interferon regulatory factor (IRF)

9, to enable translocation of the STAT complex into the nucleus. There, the complex binds interferon-stimulated response elements (ISREs) within particular gene promoters, resulting in transcription of hundreds of interferon-stimulated genes (ISGs) that have potent antiviral and antiproliferative ability [88].

An additional role of IFNs is to upregulate major histocompatibility complex molecules, MHC-I and MHC-II [89]. Expression of MHC-I and MHC-II increases antigen presentation to CD8+ cytotoxic T lymphocytes (CTLs) and CD4+ T helper (Th) cells, respectively, thereby increasing the detection and killing of infected cells.

Signaling of the sole type II interferon, IFN-gamma, is restricted to Th1 cells, CTLs, innate lymphoid cells, and natural killer (NK) cells. IFN-gamma can inhibit viral replication directly or by promoting NK cell and macrophage activity, nitric oxide synthase production, leukocyte migration, and antigen presentation [90]. IFN-gamma is also the primary cytokine that defines Th1 cells. Interleukin (IL)-12 secretion by antigen-presenting cells binds to the interferon gamma receptor (IFNGR) to initiate Th1 development [91]. Th1 lymphocytes secrete IFN-gamma, which in turn causes more undifferentiated CD4+ cells (Th0 cells) to differentiate into Th1 cells [92]. The Th1 response elicits B-cell isotype switching to opsonizing IgG1 and IgG3 (IgG2a and IgG3 in mice) subclasses. These antibodies have increased Fc receptor affinity that makes them best suited for antibody-dependent cell-mediated cytotoxicity (ADCC) and complement-dependent cytotoxicity [92]. Thus, IFNs are not only crucial in innate defense, but they also bridge innate and adaptive arms of immunity.

VSV IMMUNE ACTIVATION AND EVASION

Multiple experimental approaches have revealed the importance of PRR and ISGs for the clearance of viruses within the order *Mononegavirales* [93, 94, 95]. RLRs are the essential PRRs for sensing VSV. This family consists of RIG-I, melanoma differentiation-associated protein 5 (MDA-5), and laboratory of genetics and physiology 2 protein (LGP2). Several RLR-associated genes have been shown to restrict VSV replication including interferon regulatory factor (IRF) 1, DDX58 (RIG-I gene), and IFIH1 (MDA-5 gene) [96]. RLRs interact with blunt-ended 5' terminal triphosphate (5'ppp) moieties of double-stranded viral RNA (dsRNA) resulting in IRF signaling and IFN activation. All three RLRs have a conserved Asp-Glu-Ala-Asp (DEAD-box) helicase domain that functions in RNA binding. Unlike LGP2, RIG-I and MDA-5 have two caspase recruitment domains (CARDs), interaction motifs involved in inflammation and apoptosis. RIG-I senses short (< 300 base pairs) paired strands while MDA-5 responds to long dsRNA [97]. LGP2 modulates RIG-I and MDA-5 activity. It serves as a negative regulator by competing with these proteins for RNA binding; LGP2 can also enhance recognition by RIG-I and MDA-5 by unwinding viral nucleoproteins that normally mask viral RNAs [98].

Less significant PRRs in recognition of VSV are TLRs. Many cells ubiquitously express RLRs, whereas TLRs are more widely expressed by immune cells [99]. Some examples include TLR3, TLR7, and TLR9 endosomal receptors, which sense dsRNA, ssRNA, and DNA, respectively. Triggering of TLRs activates IRF3/7 and nuclear factor kappa-light-chain-enhancer of activated B cells (NFkB), prompting synthesis of pro-inflammatory molecules and release of IFNs [100]. For VSV, activation of IRF7 by TLR7/9 stimulation promotes IFN-gamma production; however, stimulation of TLR7 alone does not seem sufficient to mount an antiviral response [101]. Similarly, TLR3^{-/-} mice infected with VSV do not have enhanced disease or susceptibility [102]. On the contrary, VSV G triggers TLR4 by interacting with the co-receptor CD14, leading to

downstream phosphorylation and activation of IRF3 and IRF7. CD14 or TLR4 mutations abrogated IFN production and survival of VSV-infected macrophages, suggesting some TLRs are important for VSV recognition [103].

Following viral sensing by PRR and activation of downstream signaling pathways, antiviral genes are transcribed that serve various functions. A functional screen revealed 34 interferon-related genes that impede VSV replication [96]. These included common viral response genes such as 2'-5'-oligoadenylate synthetase (OAS) genes, OAS 1 and OAS2, and myxoma resistance protein 1 (MX1). OAS proteins activate RNase L to degrade viral genomes and endogenous RNA, whereas MX genes encode for dynamin-like GTPases that sequester viral proteins and prevent genome replication and viral egress [104]. Other genes identified in the VSV antiviral screen included apolipoprotein B mRNA editing enzyme catalytic subunit 1 (APOBEC1), which causes cytidine deamination of the viral genome; interferon stimulated exonuclease gene 20 (ISG20), which hinders viral RNA synthesis via nuclease activity; and interferon induced transmembrane protein 3 (IFITM3), which is thought to interfere with the endocytic pathway [96]. Some selected interferon-induced proteins that exhibit the greatest antiviral activity against VSV include: promyelocytic leukemia protein (PML), which sequesters viral proteins in nuclear bodies; tetherin (BST2) [105], a type 2 integral membrane protein at lipid raft sites which restricts budding; and protein kinase R (PKR), which limits translation of viral mRNAs primarily by phosphorylating translation initiation factor eIF-2 [106].

The evolved mechanisms of pathogens to circumvent and combat host defense responses are as impressive as the innate immune system's ability to recognize and respond to them. Like many viruses, one strategy used by VSV to dismantle the host response is rapid cytolitic growth. The compact <12kb VSV genome structure enables

accelerated transcription of genes and viral replication [107]. Also, the VSV M protein can blockade global gene transcription [108]. VSV is highly sensitive to IFN and seldom overcomes host defenses if a robust response occurs [109].

MARV IMMUNE ACTIVATION AND EVASION

The antiviral activities of IFN and its downstream associated genes are more controversial for MARV. Most studies report MARV blocks the ability of cells to upregulate innate antiviral responses. MARV-infected immortalized human liver cells (Huh7) secrete low levels of IFN, and treatment of infected cells with polyinosinic-polycytidylic acid (poly I:C) or exogenous IFN does not lead to the expected transcription of classical ISGs [110]. If type I or II IFN is added to cultured cells prior to filovirus infection; however, viral replication is substantially reduced [111]. Accordingly, supplemental IFN-alpha or beta ameliorates disease in mice and prolongs survival, but does not prevent death in NHPs [112, 113, 114, 115]. These results suggest at least some ISGs restrict filovirus replication and that MARV has a decreased ability to suppress antiviral gene expression once a host initiates an innate response.

More is known about the mechanisms of immune evasion than the receptor interactions involved in recognition and inhibition of Marburg virus. Two proteins are considered the main players in MARV IFN antagonism: VP40 and VP35 (Figure 3). MARV VP40 blocks the tyrosine phosphorylation of JAK proteins to disrupt JAK/STAT signaling, whereas MARV VP35 prevents the induction of RIG-I and MDA-5 signaling [116, 117, 118]. During serial adaptation of MARV and RAVV to establish lethal mouse and guinea pig animal models (non-adapted virus does not cause disease in wild-type rodents), amino acid changes in the VP40 protein accumulated [119, 120, 121]. Mouse-adapted RAVV VP40 more efficiently blocked IFN responses than non-adapted protein in mouse cell lines [122]. These data imply VP40-mediated IFN antagonism is a

virulence determinant and may contribute to host tropism. Moreover, IFN-alpha/beta receptor knockout mice are susceptible to disease with non-adapted filovirus, suggesting antagonism of IFN plays an integral part in pathogenesis [123]. Recently, Guito et al. reported that MARV viral proteins downregulated several ISGs [124]. MARV VP40 strongly suppressed ISG54, ISRE, IRF1, and IFN-beta induction in cells stimulated with universal IFN or a potent and broad ISG-inducer, Sendai virus. MARV VP35 also attenuated expression of these genes, but to a much lesser extent compared to EBOV VP35. This difference is likely attributed to the different dsRNA binding moieties of each virus. MARV VP35 coats the backbone of dsRNA to inhibit RLR activation, whereas EBOV VP35 can also bind the blunt ends of dsRNA (end capping) [118, 125]. At a higher multiplicity of infection (MOI) of Sendai virus, MARV VP35 and VP40 were less effective IFN antagonists [124]. In summary, these studies demonstrate MARV proteins broadly interfere with ISG induction, but robust innate defense signaling can diminish some of the effects.

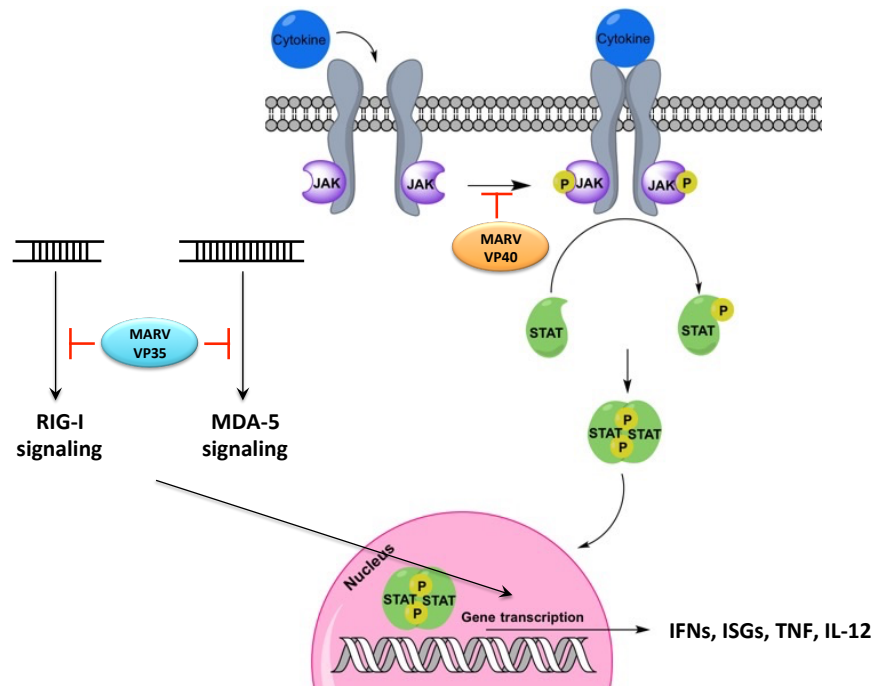


Figure 3. Mechanisms of IFN antagonism by MARV VP35 and VP40 proteins.

Binding of cytokines to the cell surface receptor activates the JAK/STAT pathway. This interaction increases the kinase activity of JAKs, promoting tyrosine phosphorylation of the receptor complex and mobilization of STAT proteins. STAT proteins then form hetero- or homodimers and translocate into the nucleus to induce transcription of antiviral genes. These genes include IFNs, ISGs, TNF, and IL-12. MARV VP40 blocks STAT signaling by preventing the phosphorylation activity of JAKs. In the cytoplasm, RIG-I and MDA-5 recognize short and long viral dsRNA, respectively. A complex of proteins then signals recruitment of interferon regulatory factor (IRF) proteins that migrate to the nucleus to stimulate the production of ISGs and IFN-beta. MARV VP35 prevents immune signaling by interfering with IRF proteins. This figure was modified to accommodate additional elements pertinent to this dissertation. The original image is a licensed file under the Creative Commons Attribution License domain (author: Pharmstudice 2016). Abbreviations: Janus kinase (JAK); signal transducer and activator of transcription (STAT); retinoic acid-inducible gene I protein (RIG-I); melanoma differentiation-associated protein 5 (MDA-5); interferons (IFNs); tumor necrosis factor (TNF); interleukin 12 (IL-12).

The MARV GP and VP24 proteins also dampen host immunity. MARV GP evades IFN-induced tetherin responses at lipid-raft sites to allow egress of viral particles from the cell surface [126]. In addition, the heavily glycosylated domains of GP sterically shield epitopes and host surface proteins of cells, e.g. MHC-I and integrins [127]. Presumably, this interferes with the formation of an appropriate adaptive response. MARV VP24 interacts with host Kelch-like E3-associated protein 1 (Keap1) to modulate cytoprotective antioxidant pathways and cell survival pathways. The VP24-Keap1 interaction may promote infection by upregulating anti-apoptotic pathways in target cells. Thus, MARV-mediated immune evasion is multifaceted [128].

As mentioned previously, most studies indicate Marburg virus infection suppresses innate immunity. More recent transcriptomics data challenge this dogma by demonstrating the virus leads to substantial immune activation. In a macrophage-like THP-1 cell line, MARV-Angola compared to EBOV was less capable of suppressing RIG-I/MDA-5-mediated activation of antiviral genes. This supposed impairment did not appear to attenuate virus growth and corresponded with the reduced capacity of MARV

VP35 to inhibit RLR signaling [125]. Temporal characterization of gene expression in MARV-Angola-infected cynomolgus macaques further supports this concept [129]. Upregulation of common innate response and pro-inflammatory genes in peripheral blood were observed early after infection (days 1-3) and sustained throughout the disease course. Many of these genes function in RLR and IFN signaling, for instance, MX1, RIG-I (DDX58), PARP14, STAT1, IRF3, IRF7, IRF9, IFITs, RNA helicases, and ISG15. However, increases in IFN-alpha and IFN-beta gene expression were not detected, nor were genes involved in other innate defense pathways, such as complement activation or antigen presentation. ISG upregulation did not appear to reduce viral load, or postpone death or clinical signs of disease in these animals, proving MARV-Angola tolerates a high level of IFN-mediated antiviral activity. It is possible the virus may weaken or overcome the effects of ISG activation by actuating alternative signaling pathways or modulating key proteins in these antiviral pathways. The authors of this same study also noted that infection in macaques led to early signaling of T helper 2 (Th2; humoral response)-associated genes, IL-4 and IL-5, and increasing plasma protein concentrations of immunosuppressive IL-10 [129]. No appreciable changes in T helper 1 (Th1; cell-mediated response) cytokines, such as IFN-gamma and TNF-alpha, were noted until late in the disease. These cytokines might be of importance since Stonier et al. recently demonstrated that survival from a 2012 MARV outbreak in Uganda was associated with a Th1 response [130]. IL-4 and IL-10 suppress Th1 production of IFN-gamma and IL-2 [131], so it is possible these cytokines may have exacerbated pathogenesis by skewing immunity towards a detrimental Th2 or immunoregulatory response.

While numerous studies point to antibody development as a key mediator of protection in humans and animal models, few studies describe the function of cellular immunity in clearance of MARV infection. More studies are needed to distinguish

protective from detrimental host responses against this virus, as it is still unclear whether IFN expression *in vivo* promotes or hinders the pathogenic cascade.

Prospective Vaccines and Therapeutics for MVD

Approximately 590 cases and 478 recorded deaths have been attributed to MVD, corresponding to a ~81% overall mortality rate [132, 133]. MARV is endemic to Africa, but imported cases have also occurred in Germany, the former Yugoslavia (presently Serbia), the Netherlands, and the United States [7]. The spread of this virus into non-endemic regions and future outbreaks are likely given MARV is continuously circulating, and the bat reservoir has a wide distribution ranging throughout Africa to the Middle East [134]. Additionally, Towner et al. surveyed a Ugandan cave associated with previous human spillover events and detected MARV RNA in ~5% of Egyptian fruit bats within a population exceeding 100,000. This species of bats migrates as much as 300 miles seasonally; therefore, the potential pool of vertebrate hosts includes up to tens of millions of bats [61]. This means there is a high risk of transmission for individuals that spend prolonged periods near these bat colonies. The bioweapon potential of filoviruses is another cause for concern. MARV was allegedly weaponized in the past according to the previous deputy chief of the former Soviet Union biological weapons Biopreparat program, indicating this is a bona fide possibility [135]. Together, these sobering realities emphasize the need for adequate countermeasures against this deadly virus. Scientists have made considerable progress in this arena over the past decade, yet no licensed vaccines or therapeutics currently exist. Lack of commercial interest and limited high containment facilities have hampered development.

Tables 2 and 3 provide an overview of prospective vaccines and therapeutics for MVD. Although rodent studies may yield proof-of-concept efficacy and inform dosing

regimens, protective immunity in these models may not translate to the NHP model. As the latter model most reliably reproduces the pathophysiology observed in humans [7], only NHP studies are discussed below.

Initially, researchers explored formalin-inactivated MARV particles as a vaccine. These failed to induce a protective immune response in rhesus macaques (Table 2) [136]. Next, Venezuelan equine encephalitis virus replicons expressing the Musoke variant GP, NP, or a combination of both antigens, were evaluated. This platform protected 67-100% of cynomolgus monkeys against a high dose (8000 PFU) subcutaneous (s.c.) Musoke challenge, but was not effective against RAVV [137, 138]. Virus-like particles (VLPs) fully protected NHPs and were cross-protective against Musoke and Ci67, as well as RAVV [139]. However, efficacy against the most pathogenic variant, Angola, was not reported.

The safety profile of DNA subunit vaccines makes them an attractive option for countermeasures against various pathogens, but these afforded only partial defense of cynomolgus macaques against MVD using MARV GP as a primary immunogen [140, 141]. Three doses of homologous vaccine resulted in 67% and 100% survival of monkeys against a 1000 PFU i.m. Musoke and Angola challenge, respectively. All of the animals became sick for the Musoke challenge and half for the Angola challenge, indicating lack of sterile immunity for this vaccine platform.

The most promising vaccines against MARV-Angola use a recombinant Adenovirus 5 (rAd5) or VSV (rVSV) vector to express the MARV GP. Both vaccines are safe, immunogenic, and require only a single injection to elicit complete protection against multiple MARV variants [141, 142, 143, 144, 145, 146]. The rVSV-based vaccine has the added benefits of defense against aerosols [145] and potential as a post-

exposure treatment [147, 148]. Vaccination with rAd5 or rVSV results in robust antibody production and cellular responses that are thought to elicit protection. Safety is a significant issue for any replication-competent vaccine, particularly in the immunocompromised. Yet, immunization with a rVSV expressing EBOV GP resulted in only transient viremia in simian/human immunodeficiency virus-infected macaques, and NHPs intrathalamically inoculated with MARV GP- or EBOV GP-expressing rVSVs were not neurovirulent [149, 150]. Another concern for the rVSV vaccine was that pre-existing immunity against the vector would influence protective efficacy. Marzi et al. disproved this claim by showing that previous vaccination in macaques with a Lassa virus GP-expressing vaccine did not abrogate immunity when NHP were sequentially immunized with an EBOV GP-expressing rVSV and challenged with EBOV [151]. Other advantages of rVSV are its high genetic stability, low seropositivity in the general population, ability to accommodate large or multiple gene inserts, and inability to integrate into host genomes or recombine [9, 146]. The rVSV vaccine is also durable, with protection lasting as long as 14 months after vaccination [152].

Vaccine	Animal Model	Immunogen (MARV variant)	MARV Variant	Doses	Survivors/ Total	Illness/ Total	Reference
Inactivated MARV	RM	Irradiated whole virus	200 LD ₅₀ Popp parenteral	1?	3/6	3/6	136
VEEV replicon	CM	GP (Musoke)	8000 PFU Musoke s.c.	3	3/3	0/3	137
VEEV replicon	CM	GP (Musoke)	RAVV	3	0/3	?	138
VEEV replicon	CM	NP (Musoke)	8000 PFU Musoke s.c.	3	2/3	3/3	137

VEEV replicon	CM	GP + NP (Musoke)	8000 PFU Musoke s.c.	3	3/3	0/3	137
VEEV replicon	CM	GP + NP (Musoke)	RAVV	3	0/3	?	138
VLPs	CM	GP + NP + VP40 (Musoke) QS-21 Adjuvant	1000 PFU Musoke s.c.	3	3/3	0/3	139
VLPs	CM	GP + NP + VP40 (Musoke) QS-21 Adjuvant	1000 PFU Ci67 s.c.	3	3/3	0/3	139
VLPs	CM	GP + NP + VP40 (Musoke) QS-21 Adjuvant	1000 PFU RAVV s.c.	3	3/3	1/3	139
DNA plasmid	CM	GP (Musoke)	1000 PFU Musoke s.c.	3	4/6	6/6	140
DNA plasmid	CM	GP (Angola)	1000 PFU Angola i.m.	4	4/4	2/4	141
DNA plasmid prime + rAd5 boost	CM	GP (Angola)	1000 PFU Angola i.m.	3+1	4/4	1/4	141
rAd5	CM	GP (Angola)	1000 PFU Angola i.m.	1	4/4	0/4	141
rAd5	CM	Blend GP (Z+S+Ci67+RAVV) + Z NP	1000 PFU Musoke Angola s.c.	2	5/5	0/5	142
rVSV	CM	GP (Musoke)	1000 PFU Musoke i.m.	1	4/4	0/4	143
rVSV	CM	GP (Musoke)	1000 PFU Musoke i.m.	1	1/1	0/1	144
rVSV	CM	GP (Musoke)	1000 PFU RAVV i.m.	1	3/3	0/3	144
rVSV	CM	GP (Musoke)	1000 PFU Angola i.m.	1	3/3	0/3	144

rVSV	CM	GP (Musoke)	1000 PFU Musoke aerosol	1	4/4	0/3	145
rVSV	CM	Blend GP (Z+S+Musoke)	1000 PFU Musoke i.m.	1	3/3	0/3	146

Table 2. Summary of vaccine studies for Marburg virus disease in the non-human primate model.

Abbreviations: MARV (Marburg virus); VEEV (Venezuelan equine encephalitis virus); VLPs (virus-like particles); rAd5 (recombinant Adenovirus 5); rVSV (recombinant Vesicular stomatitis virus); RM (rhesus macaques); CM (cynomolgus macaques); GP (glycoprotein); NP (nucleoprotein); VP40 (viral protein 40); Z (Zaire ebolavirus); S (Sudan ebolavirus); RAVV (Ravn virus); PFU (particle-forming units); s.c. (subcutaneous); i.m. (intramuscular). Illness is defined as an animal having fever, viremia, and/or exhibiting significant clinical signs of disease. A question mark (?) indicates the data was unclear or not provided in the literature.

Current treatment for MVD focuses on supportive care. Immunomodulatory treatment with IFN or an anticoagulant (recombinant nematode anticoagulant protein c2 (rNAPc2)) proved unsuccessful in the NHP model [153, 14]. Other interventions such as twice-daily delivery of a nucleoside analog (BCX4430), or daily administration of phosphorodiamidate morpholino oligomers (PMOs), protected 100% of NHPs up to 2 or 4 days, respectively. However, these antivirals did not prevent viremia and/or disease in the majority of animals [154, 155, 156].

Dye and others were the first group to highlight the usefulness of antibody therapy against MARV [157]. Three doses of convalescent purified IgG from the serum of immunized NHP survivors protected 100% of rhesus macaques from a lethal MARV-Ci67 challenge and prevented 67% from disease when given up to 48 hours post-infection. For this study, the efficacy of convalescent serum against MARV-Angola was not evaluated.

Currently, the most encouraging therapeutics against the Angola variant are stable nucleic acid-lipid particles (SNALPs) and MR191-N monoclonal antibodies [158, 159, 160]. These treatments are able to rescue NHPs from MVD after viremia and clinical signs have already developed. SNALPs use short interfering RNAs (siRNAs) that are recognized by host RNA interference (RNAi) machinery to target and degrade viral transcripts. Seven doses of SNALPs directed at the NP protected rhesus monkeys from a high dose 1000 PFU Angola challenge whenever treatment was delayed up to 5 days. Treatment with MR191-N antibodies had a similar therapeutic window, but only required two doses. MR191-N was isolated from a human survivor and is a neutralizing antibody that blocks receptor binding [161]. Intravenous (i.v.) administration of MR191-N protected macaques from advanced stages of disease with 100% survival when monkeys were treated on days 4 and 7, and 80% survival on days 5 and 8 [145].

Results from these studies are promising, but some inherent drawbacks exist for these drugs. siRNAs can have off-target effects [162], and minor changes in antigen epitope structure can affect the function of monoclonal antibodies [163]. Secondly, the availability of these treatments is limited, and the effect is of short duration. Additional resources and equipment are needed for i.v. infusions, as well as trained medical personnel, which may be difficult to convene in MARV-endemic regions.

The use of live attenuated vaccines for post-exposure prophylaxis has many advantages over conventional therapies, even though the treatment window is generally shorter. When propagated in mammalian cells, rVSV can achieve high titers, making the rapid production of ample stocks readily achievable in the event of an outbreak. Admittedly, release to human subjects would likely pose a challenge. Also, treatment does not require highly trained staff, and only a single intramuscular injection is needed instead of continuous therapy over the course of several days. Lastly, rVSV elicits a

broad and robust innate and adaptive response that makes immune evasion less likely [164, 165, 166, 167].

A rVSV construct expressing a Musoke variant GP was an effective post-exposure treatment against a high dose 1000 PFU homologous Musoke challenge. Efficacy was 100% when administered at 20-30 minutes, ~83% at 24 hours, and 33% at 48 hours [147, 148]. Unfortunately, the treatment failed to protect macaques subjected to a heterologous 1000 PFU MARV-Angola challenge when administered 20-30 minutes after infection [Thomas W. Geisbert communication]. Treated Angola-infected monkeys had a slightly delayed time-to-death possibly due to activation of the innate immune system, but failed to form a vaccine-mediated adaptive response. The same rVSV vaccine was able to cross-protect against RAVV and the Angola variant preventatively [144]. Thus, slight amino acid variation (<10%) of the surface GPs between these viruses [13] might be of greater importance in the post-exposure context. For this reason, rVSVs expressing homologous MARV-Angola-GP would likely yield a better result against the Angola variant. This dual vaccine and treatment could be administered to individuals that have come into contact with an infected person(s) during outbreaks, similar to the ring vaccination strategy used during the West African EBOV epidemic. Alternatively, it could be used in the event of laboratory and healthcare worker exposures or a bioterrorism attack.

Treatment	Animal Model	Time Post-Exposure	Doses	MARV Variant	Survivors/ Total	Illness/ Total	Viremic/ Total	Reference
IFN-beta	RM	1 hr	15	1000 PFU Musoke i.m.	1/3	3/3	3/3	153
rNAPc2	RM	10 min	15	1000 PFU Angola i.m.	1/6	6/6	6/6	14

BCX4430	CM	1 hr	30	1275 PFU Musoke s.c.	5/6	1/6?	6/6	154
BCX4430	CM	24 hr	28	1275 PFU Musoke s.c.	6/6	2/6?	6/6	154
BCX4430	CM	48 hr	26	1275 PFU Musoke s.c.	6/6	0/6?	6/6	154
PMOplus (pool)	RM	30-60 min	14	1000 PFU Musoke s.c.	4/4	4/4	4/4	155
PMOplus (NP)	CM	1 hr	14	1000 PFU Musoke i.m.	5/6	6/6	6/6	156
PMOplus (NP)	CM	24 hr	14	1000 PFU Musoke i.m.	5/6	6/6	6/6	156
PMOplus (NP)	CM	48 hr	14	1000 PFU Musoke i.m.	6/6	6/6	6/6	156
PMOplus (NP)	CM	4 d	14	1000 PFU Musoke i.m.	5/6	6/6	5/6	156
Convalescent IgG (purified)	RM	15-30 min	3	1000 PFU Ci67 i.m.	3/3	0/3	0/3	157
Convalescent IgG (purified)	RM	48 hr	3	1000 PFU Ci67 i.m.	3/3	1/3	1/3	157
siRNA SNALPs	RM	30-45 min	7	1775 PFU Angola i.m.	4/4	2/4	2/6	158
siRNA SNALPs	RM	24 hr	7	1250 PFU Angola i.m.	4/4	1/4	0/6	158
siRNA SNALPs	RM	48 hr	7	1100 PFU Angola i.m.	4/4	2/4	0/6	158
siRNA SNALPs	RM	3 d	7	1000 PFU Angola i.m.	4/4	2/4	1/6	158

siRNA SNALPs	RM	4 d	7	1063 PFU Angola i.m.	4/4	4/4	3/4	159
siRNA SNALPs	RM	5 d	7	1138 PFU Angola i.m.	2/4	4/4	4/4	159
siRNA SNALPs	RM	3 d	7	1125 PFU RAVV i.m.	4/4	1/4	1/4	159
siRNA SNALPs	RM	6 d	7	1163 PFU RAVV i.m.	4/4	4/4	4/4	159
MR191-N mAbs	RM	4 d	2	1050 PFU Angola i.m.	3/3	3/3	3/3	160
MR191-N mAbs	RM	5 d	2	1240 PFU Angola i.m.	4/5	4/5	5/5	160
MR191-N mAbs	RM	5 d	2	1100 PFU RAVV i.m.	5/5	3/5	5/5	160
rVSV	RM	20-30 min	1	1000 PFU Musoke i.m.	5/5	3/5	0/5	147
rVSV	RM	24 hr	1	1000 PFU Musoke i.m.	5/6	1/6	0/6	148
rVSV	RM	48 hr	1	1000 PFU Musoke i.m.	2/6	4/6	5/6	148

Table 3. Summary of post-exposure treatment studies for Marburg virus disease in the non-human primate model.

Abbreviations: IFN (interferon); rNAPc2 (recombinant nematode anticoagulant protein c2); PMO (phosphorodiamidate morpholino oligomers); NP (Marburg virus nucleoprotein); IgG (immunoglobulin G); siRNA (short interfering RNAs); SNALPs (stable nucleic acid lipid particles); mAbs (monoclonal antibodies); rVSV (recombinant Vesicular stomatitis virus); RM (rhesus macaques); CM (cynomolgus macaques); PFU (plaque-forming units); MARV (Marburg virus); RAVV (Ravn virus); i.m. (intramuscular); s.c. (subcutaneous). Illness is defined as an animal having fever and/or showing significant clinical signs of disease.

Gaps in Knowledge of rVSV-Induced Immunity Against Filoviruses

Wild-type VSV infection is commonly known to elicit Th1 and Th2 immunity, with a predominant Th1 response. Activation of Th1 effector cells results in IFN-gamma secretion and isotype switching of antibodies to opsonizing subtypes. The polarization towards this response likely reflects secretion of IL-12 by antigen-presenting cells, as depletion of macrophages and DCs eliminates this response. Th2 immunity is preserved, suggesting another class of cells initiate this cascade [168].

Few studies describe mechanisms of rVSV-mediated immunity against filoviruses, particularly in the post-exposure context. Antibody levels against the GP are reliable predictors of protection; yet, neutralizing activity is not required [143, 144, 147, 152]. In contrast, cellular responses are poor correlates of rVSV defense against MVD according to the few NHP studies that exist [143, 144, 145, 147, 169]. Interestingly, rhesus monkeys that were given two doses of a rVSV-based MARV vaccine at 1 and 24 hours post-infection demonstrated partial protection against a lethal EBOV-Makona challenge, implying a non-specific innate response drives post-exposure protection [169]. This contradicts our historical findings, which proved an irrelevant rVSV vector expressing an EBOV or Lassa virus GP did not enhance survival against a MARV challenge [147, 148]. The number of doses (2) might explain this difference. Alternatively, these animals may have survived without treatment, as EBOV is not uniformly lethal in the rhesus macaque model [170, 171].

For EBOV, a study in cynomolgus macaques revealed CD4⁺ T-cell depletion during rVSV vaccination rescinded protection, and these animals failed to form GP-specific IgG [172]. To differentiate between effector versus B-cell helper function for the CD4⁺ T cell group, the authors of this study performed an additional depletion experiment during challenge with EBOV. All animals in this group survived and

developed antibodies, suggesting a higher participation of CD4+ T-cells in mediating B-cell maturation and antibody isotype class switching. Depletion of CD20+ B-cells during vaccination was attempted to verify the importance of humoral immunity. These macaques developed EBOV GP-specific antibodies and survived, signifying depletion was not successful in lymphatic tissues (our laboratory yielded comparable results with a B-cell CD19 depletion experiment). CD8+ T-cells were dispensable against EBOV during rVSV vaccination, indicating cellular responses are less essential mediators of immunity. Only low levels of cellular responses in CD4+-depleted and undepleted groups were detected, further supporting this claim. Paradoxically, a transcriptomic analysis revealed a previously unrecognized role of CD8+ T-cell immunity in vaccine protection against EBOV [166]. Moreover, reports from phase I clinical trials proved immunization with rVSV elicited EBOV GP-specific Th cells and CTLs in human subjects, with IFN-gamma (the prototypical Th1 cytokine) being the most abundant analyte secreted [165, 167]. Another study emphasized the contribution of follicular T-helper cells to vaccine protection in humans [167].

The results of these data are seemingly contradictory. More experiments are needed to tease out mechanisms of rVSV immunity. Protection is probably multifactorial, including elements such as inherent differences in host immunity, vaccine dose or choice, challenge inoculum or virus species/variant, and time of vaccination or treatment. Immune mediators might also differ for post-exposure treatment compared to vaccine protection, as the host immune system may adapt to overcome cell deficits following a challenge if a memory T-cell or antibody response is pre-formed.

In this dissertation, I will test the ability of rVSVs expressing MARV-Angola-GP to provide post-exposure protection against the most pathogenic variant of MARV, Angola in the rhesus monkey model. If the treatment is successful, I hope to identify key

immune pathways that mediate host protection, so that these can be exploited to create better vaccines and therapeutics.

Hypothesis

rVSVs expressing a homologous MARV-Angola-GP can serve as a post-exposure treatment against MARV-Angola.

Aim 1: Evaluate the efficacy of rVSV post-exposure therapy against MARV-Angola in the rhesus macaque model.

I will first generate a rVSV expressing MARV-Angola-GP (rVSV Δ G/MARV-Angola-GP) via reverse genetics to test its therapeutic potential in NHPs. Animals will be challenged with a high (1000 PFU) or low dose (50 PFU) of MARV-Angola and treated with a rVSV vector 20-30 minutes after exposure. Animals will be monitored daily for signs of disease. Temporal blood samples and terminal tissues from major organs will be taken to evaluate viral load and disease status. Aim 1 hypothesis: rVSV treatment will elicit partial defense of monkeys against a MARV-Angola challenge by reducing viral replication to delay the onset of disease.

Aim 2: Identify rVSV-induced immune correlates that mediate post-exposure protection.

RNA sequencing (RNAseq), cytokine bead arrays, and flow cytometry will be used to assess differences in the immune response of rVSV-treated survivors compared to non-survivors. Humoral responses will be measured using MARV GP-specific IgM and IgG enzyme-linked immunosorbent assays (ELISAs) and plaque reduction neutralization tests

(PRNTs). Hypothesis: rVSV will activate host innate and adaptive immunity to mediate protection against MARV-Angola in the NHP animal model.

**CHAPTER 2: POST-EXPOSURE EFFICACY OF RECOMBINANT VESICULAR
STOMATITIS VIRUS VECTORS AGAINST HIGH AND LOW DOSES OF MARBURG
ANGOLA VIRUS IN NONHUMAN PRIMATES**

Introduction

MARV is an NIAID Category A Priority Pathogen and CDC Tier 1 select agent due to its high lethality, bioweapon potential, and the lack of FDA-approved vaccines and therapeutics. Sporadic, reoccurring outbreaks of MARV (including a recent episode in Uganda and Kenya), the vast geographic range of the bat reservoir, as well as imported cases into Europe and the United States, highlight the need for the advancement of effective treatments and vaccines [173]. Preferably, a vaccine could serve as a prophylactic and an emergency post-exposure treatment.

One of the most effective filovirus vaccine candidates uses a rVSV platform. Results from phase II and III human clinical trials for an EBOV-based rVSV showed favorable safety and immunogenicity profiles [174, 175]. For a ring vaccination trial in Guinea, vaccine efficacy was 100%, and no cases of EBOV were recorded in individuals ten days or more after immunization [174]. The rapid immunostimulatory properties of the vaccine emphasize the utility of rVSV vectors for emergency interventions. A similar strategy could be implemented during MARV outbreaks.

Guinea pigs and NHPs are the most widely used animals for rVSV vaccination and therapeutic studies, as these models most reliably reflect MARV infection in humans [9, 15]. Against a highly lethal 1000 PFU challenge of MARV-Musoke, a single

intramuscular (i.m.) injection of rVSV vaccine expressing the Musoke variant glycoprotein of MARV (rVSV Δ G/MARV-Musoke-GP) protected 100% of cynomolgus macaques [143]. The vector elicited robust humoral responses and provided cross-protection against MARV Angola, as well as the closely related RAVV [143, 144]. Interestingly, the vaccine administered 20-30 minutes post-infection also protected macaques against a 1000 PFU MARV-Musoke challenge [147]. Whenever the initial treatment time was extended to 24 and 48 hours, 83% and 33% survived, respectively [148]. These results are encouraging, though the effectiveness of rVSV post-exposure treatment against the most pathogenic variant, Angola, warrants evaluation. MARV-Angola was responsible for one of the worst viral hemorrhagic fever epidemics. In 2004-2005, this deadly outbreak occurred in the Uige province of Angola and resulted in 90% fatality of the 252 confirmed human cases [13]. In animal models, a challenge with the Angola variant causes earlier and worse clinical signs of disease in outbred guinea pigs and NHPs compared to RAVV and other MARV variants [14, 176, 177]. Additionally, histopathological analysis of livers from Angola-infected macaques reveals more advanced hepatocyte degeneration and extensive necrosis compared to other variants [14].

To assess the treatment potential of rVSV against MARV-Angola, we generated three rVSV vectors expressing the Angola GP of MARV. In order of the degree of attenuation, these are rVSV Δ G/MARV-Angola-GP, rVSVN2CT1-MARV-Angola-GP, and rVSVN4CT1-MARV-Angola-GP. A non-specific vector control expressing an HIV gag gene was also included. Treated monkeys were subjected to a high or low dose MARV-Angola challenge and compared to untreated animals or a vector control to determine post-exposure efficacy.

Methods

GENERATION OF RSV VECTORS

rVSVs were produced from infectious clones as described in the previous literature [179]. To generate the vectors used in this study, an expression cassette encoding the full-length Angola glycoprotein (MARV-Angola-GP, accession number: DQ447653) was cloned into plasmids containing the entire VSV genome. To create rVSV Δ G/MARV-Angola-GP (the “ Δ G” vector), a PCR-amplified Angola GP gene was cloned into the Mlu I/Nhe I gene site in place of the native G gene. The resulting plasmid was then transfected into a BHK-21 (CCL-10 ATCC) cell line. These cells were previously transfected with VSV G and infected with a Vaccinia virus that constitutively expresses T7 polymerase. The plasmid contained T7 polymerase promoter and terminator sequences at the 3’ and 5’ ends of the rVSV genome to drive gene expression. NP, VP30, VP35, and L helper plasmids were co-transfected into the infected cells to promote recovery. Recovered virus supernatants were subsequently filtered to remove contaminating Vaccinia virus and passaged on Vero cells. The amplified virus was then plaque-purified and passaged a second time. Supernatants were then centrifuged on a sucrose-TN cushion and pellets were suspended in a phosphate-buffered saline (PBS) solution containing a stabilizer. Virus stocks were aliquoted and frozen in an ethanol and dry ice bath and stored at -80°C . Angola GP gene insertion, protein expression, and infectivity were confirmed by PCR, western blot, and immunofluorescence assay, respectively (Supplementary Figure 1). The remaining vectors were engineered at Profectus BioSciences, Inc. To attenuate rVSVN4CT1-MARV-Angola-GP (the “N4” vector) and rVSVN4CT1-HIVgag (the “vector control”), the VSV N gene was translocated from the first to the fourth (N4) genomic position and the VSV G cytoplasmic tail (CT1) was truncated. The VSV G cytoplasmic tail helps drive budding; therefore, rVSVs with a truncated version have slower growth rates, reduced peak titers, and are less pathogenic in mice [180, 181, 182]. To produce rVSVN2CT1-MARV-

Angola-GP (the “N2” vector), the VSV N was instead shuffled from the first to the second (N2) genomic position. The N2 and N4 vectors express the Angola GP (or an HIV gag) gene at the first position to effectively drive antigen expression. The abundance of each protein depends on the distance of the encoded gene from the 3' end, as ~20-30% of transcriptase complexes fail to resume transcription at each gene junction. Thus, the N4 vector is more attenuated than the N2 vector. Rescue of these viruses is described elsewhere [183].

CHALLENGE VIRUS

The MARV Angola seed stock originates from the 2005 Uige, Angola outbreak. The source material is serum isolated from an 8-month old female fatal case (virus isolate 200501379). The study challenge material was created by passaging the original isolate twice in Vero E6 cells (titer 1.5×10^7 PFU/ml). Endotoxin content was < 0.5 EU/mL and mycoplasma was not detected in stocks following PCR testing.

ANIMAL STUDY DESIGN

Twenty-eight adult (19 females and 11 males) rhesus monkeys (*Macaca mulatta*), weighing ~3.6 to 7.2 kg, were randomly assigned to two experiments. For the high dose experiment, macaques were i.m. challenged with a target dose of 1000 PFU of MARV Angola (N=5). Four of 5 animals were treated with rVSV Δ G/MARV-Angola-GP. To assess the statistical significance of survival, two historical controls were used for the high dose experiment. For the low dose experiment, two additional treatment groups were added and a vector control. Macaques (N=23) in this experiment were i.m. challenged with a low uniformly lethal target dose of 50 PFU of MARV Angola and received Δ G (N=9), N4 (N=5), or N2 (N=5), vector treatment, or a non-specific vector control (N=1). Three were left untreated. Each rVSV vector was i.m. injected in the left quadriceps near the challenge site and also in the right quadriceps (the dose was equally divided between

the two sites). A single dose of 10 million PFU for each post-exposure treatment was delivered approximately 20-30 minutes after MARV Angola exposure. Actual MARV Angola doses were determined to be 1237 PFU for the high dose experiment and 45-80 PFU for the low dose experiment. An internal scoring protocol was implemented daily to monitor signs of disease in monkeys, such as posture/activity level, appetite, behavior, respiration, and hemorrhagic manifestations. Euthanasia protocols were executed after any animal reached a clinical score of ≥ 9 . Blood was collected at terminal timepoints, as well as days 0, 3, 6, 10, 14, and 21 post-challenge. Tissues were taken at the study endpoint for histopathology and immunohistochemistry.

BLOOD PROCESSING

Blood was collected by femoral venipuncture into EDTA and clot activating vacutainer tubes (BD Biosciences, San Jose, CA). For RT-qPCR, aliquots of EDTA-treated whole blood were inactivated with AVL buffer (Qiagen, Hilden, Germany) prior to centrifugation. Tubes were centrifuged at $\sim 800 \times g$ for 10 minutes; afterward, the plasma or sera upper layer was collected.

VIRUS TITRATION

MARV viremia was titrated by plaque assay on Vero E6 cells (CRL-1586 ATCC). Briefly, increasing ten-fold dilutions of plasma samples were adsorbed to monolayers in duplicate, overlaid with 0.8% agarose/2x EMEM, and incubated for six days at 37 °C in 5% CO₂. Neutral red stain was added and plaques were counted after a 48-hour incubation. The limit of detection for this assay is 25 PFU per ml.

RNA EXTRACTION AND RT-QPCR

For RT-qPCR, RNA from whole blood was extracted according to manufacturer recommendations (1:6 ratio) using a Qiagen Viral RNA Mini kit (Qiagen Mississauga,

ON, Canada). One-Step Probe qRT-PCR kits (Qiagen) and CFX96 system/software (BioRad) were used to determine viral copies in samples. To detect MARV RNA, we targeted the MARV NP gene with primer pairs and a 6-carboxyfluorescein (6FAM)–5'-CCCATAAGGTCACCCTCTT-3'–6 carboxytetramethylrhodamine (TAMRA) probe, as described previously [145]. Thermocycler run settings were 50°C for 10 min; 95°C for 10 s; and 40 cycles of 95°C for 10 s plus 59°C for 30s. Integrated DNA Technologies synthesized all primers and Life Technologies customized probes. Representative MARV genomes were calculated using a genome equivalent standard. The limit of detection for this assay is 1000 copies per ml.

HEMATOLOGY AND SERUM BIOCHEMISTRY

EDTA-treated blood was analyzed using a laser-based hematologic analyzer (Beckman Coulter) to determine total white blood cell counts, white blood cell differentials, red blood cell counts, platelet counts, hematocrit values, total hemoglobin concentrations, mean cell volumes, mean corpuscular volumes, and mean corpuscular hemoglobin concentrations. A Piccolo point-of-care analyzer and Biochemistry Panel Plus analyzer discs (Abaxis) were used to test for serum concentrations of albumin, amylase, alanine aminotransferase (ALT), aspartate aminotransferase (AST), alkaline phosphatase (ALP), gamma-glutamyltransferase (GGT), glucose, cholesterol, total protein, blood urea nitrogen (BUN), creatinine (CRE), uric acid, and C-reactive protein (CRP).

HISTOPATHOLOGY AND IMMUNOHISTOCHEMISTRY

Major organs from macaque subjects were collected during necropsy for histopathology and immunohistochemistry. Tissues were immersion-fixed in 10% neutral buffered formalin and processed as formerly outlined [159]. For immunohistochemistry of spleen and liver sections, slides were stained with a Dako Autostainer (Dako, Glostrup,

Denmark) using a 1:4000 dilution of polyclonal anti-MARV VP40 protein rabbit primary antibody (Integrated BioTherapeutics, Inc., Rockville, MD) or a non-immune rabbit IgG negative control. Biotinylated goat anti-rabbit IgG (1:200 dilution; Vector Laboratories, Burlingame, CA) served as a secondary antibody, followed by Dako LSAB2 streptavidin–horseradish peroxidase (Dako) for detection. Slides were developed with Dako diaminobenzidine chromagen substrate (Dako) and counterstained with hematoxylin stain.

STATISTICAL ANALYSIS

GraphPad Prism software was used to conduct statistical analyses (version 7.0). Log-rank tests were used to compare survival between treated and control groups.

Results

Based on the positive results from previous rVSV-MARV-Musoke GP post-exposure studies against MARV Musoke, we speculated whether similar protection was achievable against a highly pathogenic variant of MARV, Angola. Although there is limited amino acid divergence among the glycoproteins of MARV variants (<10%) [13], we thought the use of a homologous GP would more likely elicit protection. Consequently, we cloned an Angola variant GP into each rVSV vector for use in this study. Monkeys were challenged with a high (1000 PFU) or low (50 PFU) dose of MARV-Angola and treated with rVSV (107 PFU) approximately 20-30 minutes later. Our vector and study design are presented in Figure 4. Temporal blood samples were taken over the course of the study to assess clinical signs of disease and measure viral load. Liver and spleen tissues were collected terminally or at the study endpoint (day 28) for immunohistochemistry.

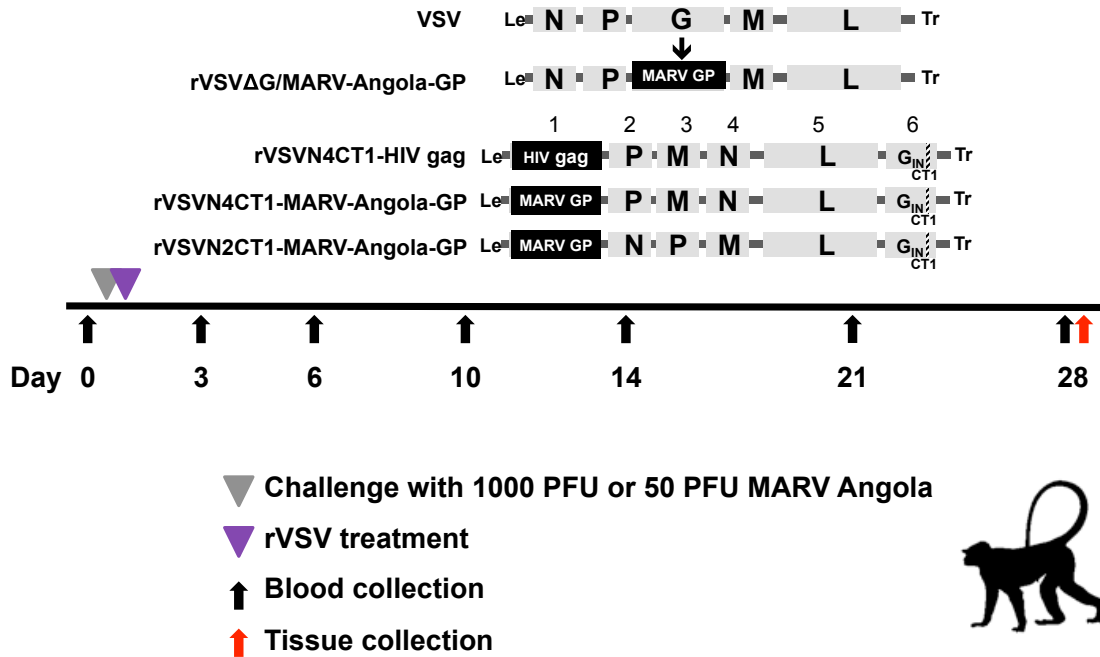


Figure 4. Generation of rVSV vectors and study design.

rVSVΔG/MARV-Angola-GP (ΔG) was created by swapping the native VSV Indiana glycoprotein gene (G_{IN}) with an Angola glycoprotein gene (MARV GP) via restriction enzyme integration. To maximize antigen expression, the MARV-Angola-GP or HIV gag gene was cloned into the first genomic position of *rVSVN4CT1-MARV-Angola-GP (N4)*, *rVSVN2CT1-MARV-Angola-GP (N2)*, or the *rVSVN4CT1-HIVgag* vector control. The latter vectors were attenuated by shuffling the VSV nucleoprotein (N) gene to the second or fourth position and truncating the G_{IN} cytoplasmic tail (genome position 6) from 29 to 1 amino acids (C_{T1}). The black and white-striped region within the G_{IN} gene denotes the amino acid substitution site. Animals were challenged with MARV Angola (gray nabla) and treated with rVSV (purple nabla) shortly after. Blood (black arrow) and tissues (red arrow) were taken at the indicated timepoints. Abbreviations: rVSV (recombinant Vesicular stomatitis virus); VSV (Vesicular stomatitis virus); N (VSV nucleoprotein); P, (VSV phosphoprotein); M (VSV matrix protein); G_{IN} (VSV serotype Indiana glycoprotein); C_{T1} (the native VSV glycoprotein with a truncated cytoplasmic tail); L, (VSV polymerase); Le (leader); Tr (trailer); ΔG (the native VSV G_{IN} is absent); N4 (the rVSV nucleoprotein (N) is at position 4 in the genome); HIV (human immunodeficiency virus); gag (group-specific antigen); MARV (Marburg virus); GP (glycoprotein); PFU, (plaque-forming units); MARV GP (Marburg virus Angola glycoprotein).

For the high dose challenge experiment, 4 of 7 subjects (including 2 historical controls) received a single treatment of *rVSVΔG/MARV-Angola-GP (ΔG)*. Treatment resulted in incomplete (25%) protection of monkeys but delayed the time-to-death

(Figure 5). Non-surviving treated macaques succumbed on days 9-11, whereas untreated controls succumbed on days 7-8.

- Control (N=1)
- Historical controls (N=2)
- Treated with rVSV Δ G/MARV-Angola-GP (N=4)

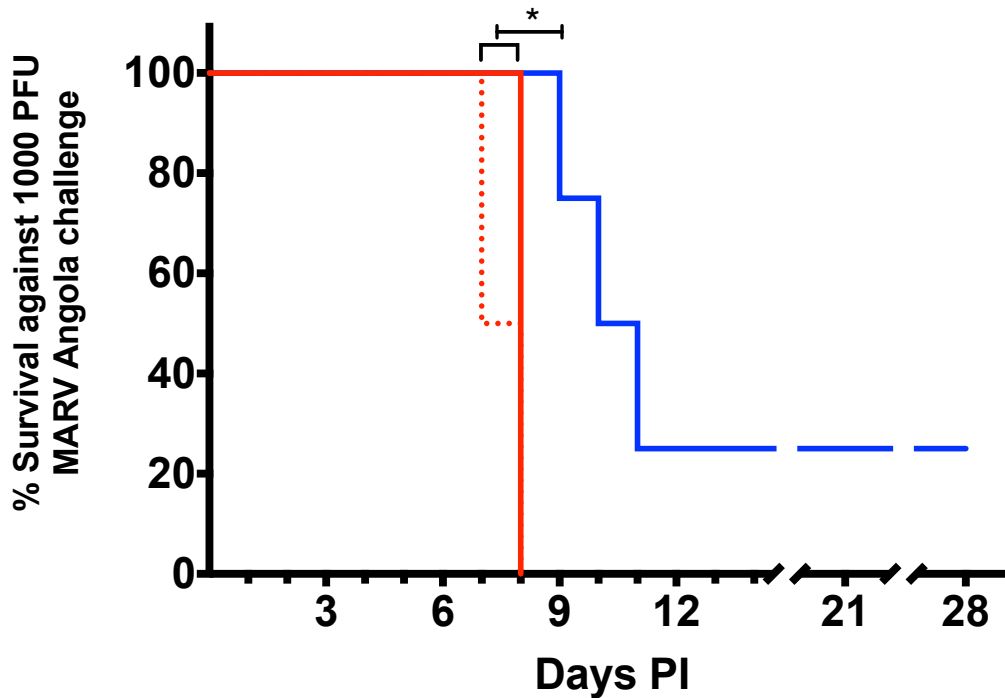


Figure 5. Postexposure treatment of macaques with rVSV Δ G/MARV-Angola-GP was incompletely protective against a 1000 PFU high dose challenge of MARV Angola.

*Kaplan-Meier survival curves of Δ G-treated subjects (solid blue line), compared to untreated historical controls (segmented red line) and an untreated control (solid red line). PFU (plaque-forming units); PI (post-infection). * $p \leq 0.05$ statistical significance for the treated group (N=4) compared to the controls (N=3).*

Both untreated and treated monkeys in this experiment developed a fever (Table 4) 3-6 days post-infection. The treated group developed clinical signs such as depression and petechial rash later than controls, and these animals had delayed increases in serum

concentrations of C-reactive protein; kidney products BUN and CRE; and liver enzymes ALT, AST, ALP, and GGT. Only the treated survivor did not form a petechial rash. Less prominent findings were mild dyspnea in Control 2 and edema in Treated Fatal 1. Leukocytosis, granulocytosis, and lymphopenia or lymphocytosis, were commonly observed at end-stage disease.

Animal	Challenge Dose	Treatment	Clinical Observations	Final Disposition
Control 1	High	None	Fever (6), depression (6-8), mild to moderate petechial rash (6-8), leukocytosis (8), monocytosis (3), monocytopenia (6), BUN +++ (8), CRE +++ (8), ALT +++ (6,8), AST +++ (6) > (8), ALP + (6), GGT ++ (8), CRP increase (6,8)	Succumbed on day 8
Control 2 (historical)	High	None	Fever (3,6,7), depression (6-7), anorexia (6-7), mild to moderate petechial rash (7), mild dyspnea (7), leukocytosis (7), lymphocytosis (7), granulocytosis (7), monocytopenia (6), BUN ++ (7), CRE + (7), ALT +++ (6) > (7), AST +++ (6) > (7), ALP ++ (6) +++ (7), GGT ++ (6) +++ (7), CRP increase (6,7)	Succumbed on day 7
Control 3 (historical)	High	None	Fever (4,6), depression (6-8), anorexia (7-8), mild to moderate petechial rash (7-8), leukocytosis (8), lymphopenia (3,6), monocytosis (6), CRE ++ (8), ALT +++ (6) > (8), AST +++ (6) > (8), ALP ++ (6) +++ (8), GGT ++ (8), CRP increase (6,8)	Succumbed on day 8
Treated Fatal 1	High	rVSVΔG/MARV-Angola-GP	Fever (6,10), depression (9-11), anorexia (10-11), mild to moderate petechial rash (10), moderate to severe petechial rash (11), edema (11), leukocytosis (10,11), lymphopenia (6), lymphocytosis (11), granulocytosis (10,11), monocytosis (3,10,11), thrombocytopenia (10,11), BUN + (10) +++ (11), CRE + (10) +++ (11), ALT +++ (10,11), AST > (10,11), GGT + (10,11), CRP increase (6,10,11)	Succumbed on day 11
Treated Fatal 2	High	rVSVΔG/MARV-Angola-GP	Fever (6), depression (8-9), moderate petechial rash (8-9), lymphopenia (6), AST + (6), CRP increase (6)	Succumbed on day 10
Treated Fatal 3	High	rVSVΔG/MARV-Angola-GP	Fever (6), depression (7-8), mild to moderate petechial rash (8), leukocytosis (6), granulocytosis (6), CRP increase (3,6)	Succumbed on day 9
Treated Survivor	High	rVSVΔG/MARV-Angola-GP	Fever (6), mild depression (11), anorexia (13), leukocytosis (6,14,21,28), lymphocytosis (14,28), granulocytosis (3,6,14,21), monocytosis (6,10,14,28), thrombocytopenia (10,14), ALT +++ (10) ++ (14), AST+++ (10), ALP + (3,6, 28) ++ (10,21) +++ (14), GGT + (10,11), CRP increase (3,6,10,14)	Survived to day 28

Table 4. Clinical findings in monkeys for the high dose experiment.

Blood was collected prior to challenge, terminally, and 3, 6, 10, 14, and 21 days post-challenge to perform serum biochemistry and hematology cell counts. Clinical signs, such as fever, depression, anorexia, and hemorrhagic manifestations were monitored daily. The day after challenge is in parentheses. Fever is defined as a temperature greater than 2.5 °F above baseline, at least 1.5 °F above baseline and ≥ 103.5 °F, or 1.1 °F above baseline and ≥ 104 °F. Lymphopenia, monocytopenia, and thrombocytopenia are defined by a respective $\geq 35\%$ drop in numbers of lymphocytes, monocytes, and platelets. Leukocytosis, lymphocytosis, monocytosis, and granulocytosis are defined as a respective \geq two-fold increase in leukocytes, lymphocytes, monocytes, and granulocytes respectively. Abbreviations: MARV (Marburg virus); rVSV (recombinant Vesicular stomatitis virus); MARV-Angola-GP (Marburg virus Angola glycoprotein); ΔG (the native VSV G is absent, referring to individual monkey treated with rVSV ΔG /MARV-Angola-GP); BUN (blood urea nitrogen); CRE (creatinine); ALT (alanine aminotransferase); AST (aspartate aminotransferase); ALP (alkaline phosphatase); GGT (gamma-glutamyltransferase); CRP (c-reactive protein). Crosses indicate increases in liver enzymes (ALT, AST, ALP, GGT) or renal function test values (BUN, CRE): 2- to 3-fold increase: +; >3- up to 5-fold increase, ++; >5 fold increase, and +++; out of range, >.

Viral load corresponded to time-to-death in fatal cases. Infectious MARV titers in untreated controls were detected three days before treated animals (Figure 6). Controls had high titers of infectious virus in plasma (~8 logs) and ~11 logs of MARV RNA copies/mL in whole blood at the terminal stage. Comparatively, viremia was 2-7 logs less in treated animals at this time point. For the sole survivor, viremia was not detected until day 6 and titers remained low (<3 logs). Viral load in this animal was cleared by day 21 or was below the detection limit of our plaque and RT-qPCR assays.

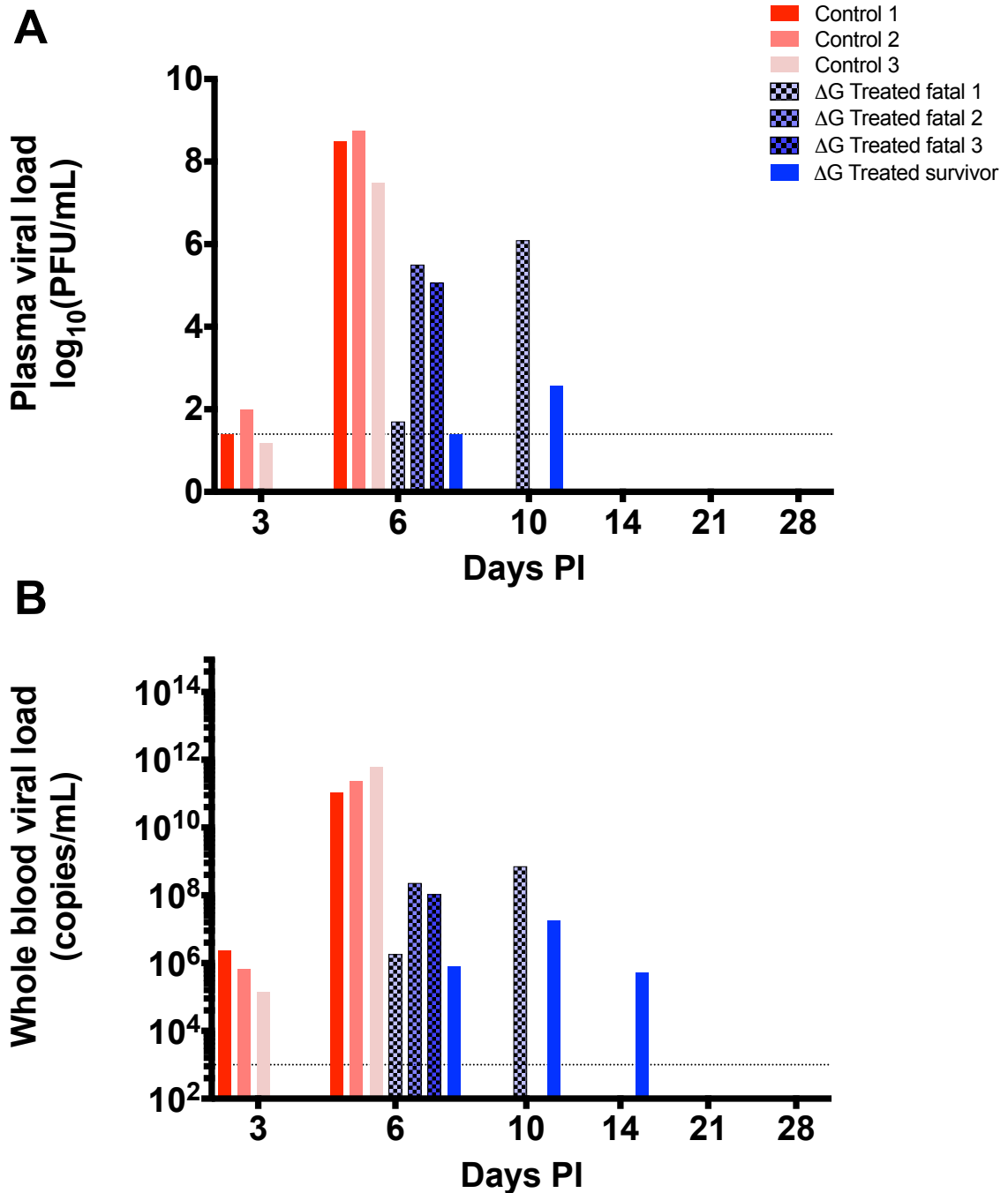


Figure 6. MARV viral loads in animals challenged with a high dose of MARV-Angola.

Viral load was assessed by plaque assay (A) and RT-qPCR (B). Each bar represents a single macaque at each time point. The three controls are represented by red to pink bars and individually *rVSV Δ G/MARV-Angola-GP* (Δ G)-treated macaques are represented by light to dark blue bars (treated fatal animals are checkered). The limit of detection for the plaque assay is 25 PFU/mL and 1000 copies/mL for the RT-qPCR assay (dotted line).

At the terminal time point, we additionally measured viral load in tissues. MARV RNA was only detected in axillary lymph nodes and the spleen of the treated survivor (Figure 7). In contrast, the untreated control subject and treated fatal animals were PCR-positive for all analyzed tissues (axillary lymph nodes, inguinal lymph nodes, liver spleen, kidney, adrenal glands, and the lung). Titers ranged from 8-11 logs and similar titers were observed in untreated and treated non-survivors.

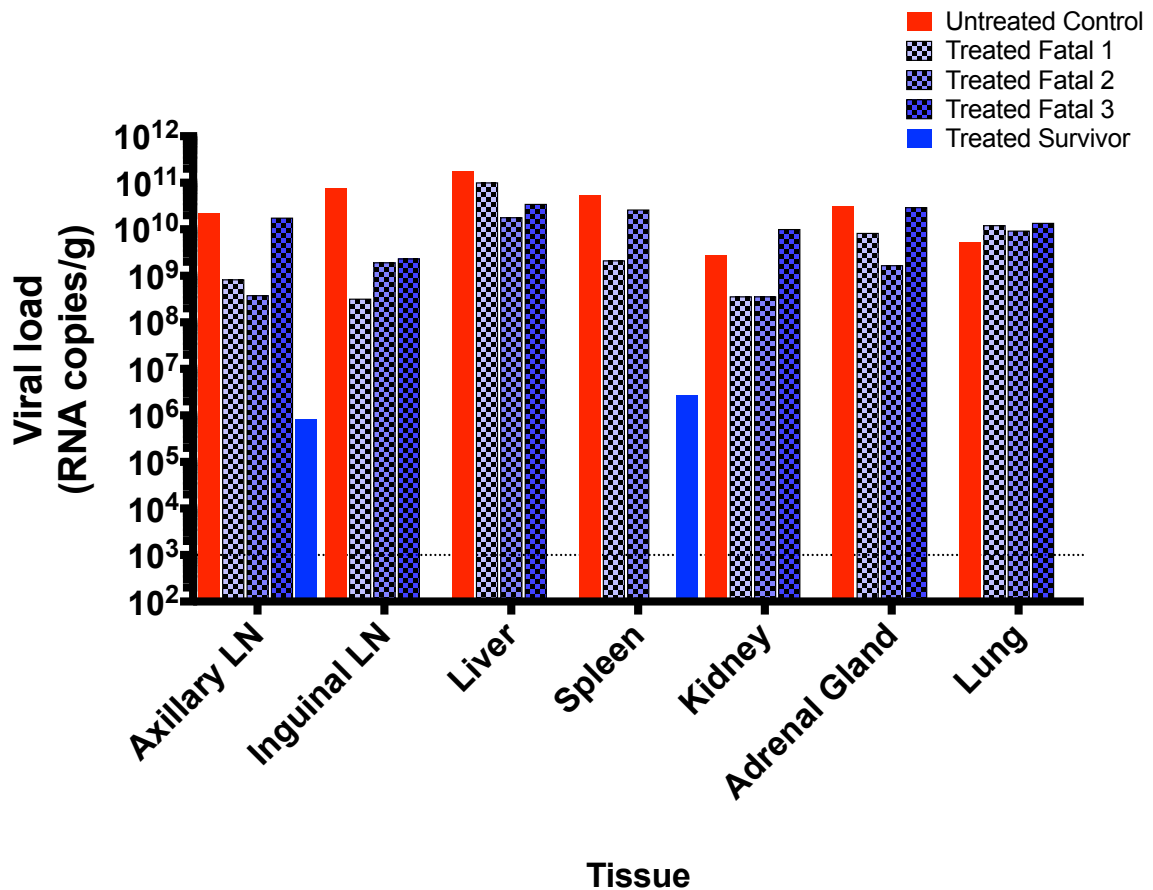


Figure 7. Tissue viral loads in animals challenged with a high dose of MARV-Angola. Viral load was assessed by RT-qPCR. Each bar represents a single macaque at each time point. The control animal is represented by a red bar and individually rVSVΔG/MARV-Angola-GP (ΔG)-treated macaques are represented by light to dark blue bars (treated fatal animals are checkered). The limit of detection for this assay is 1000 copies/mL (dotted line). Abbreviation: LN (lymph nodes).

Given the treatment was only 25% effective, we speculated whether the rapid disease course of Angola versus Musoke in NHPs might account for our failure to achieve protection against the high challenge dose. In the rhesus macaque model, the terminal stage of disease for a high dose (1000 PFU) MARV challenge is 10-12 days for the Musoke variant and 6-8 days for Angola. Lower challenge doses of MARV are known to extend the time-to-death in macaques by 1-4 days depending on the variant, dose, and route [177]. With this in mind, we challenged monkeys with a low 50 PFU of MARV-Angola to presumably delay the onset of disease. We hypothesized this would allow more time for the immune system in treated subjects to mount a protective response.

Animals in the low dose experiment were challenged and treated similarly as described for the high dose, except three additional treatment groups were included. Twenty-three macaques were challenged with 50 PFU of MARV Angola and 9 subjects received rVSV Δ G/MARV-Angola-GP (Δ G), 5 subjects received rVSVN4CT1-MARV-Angola-GP (N4), and 5 additional subjects received rVSVN2CT1-MARV-Angola-GP (N2) treatment. A single vector control was treated with rVSVN4CT1-HIV gag (vector control) to account for irrelevant, non-specific effects. The untreated control animals succumbed 8 to 10 days post-infection (Figure 8). Hence, the time-to-death is shorter for rhesus macaques in response to a low dose Angola compared to a high dose 1000 PFU Musoke challenge, in which the latter typically succumb 10-12 days post-infection (Table 1). The vector control was euthanized on day 12. Survival rates were 89% for Δ G-treated macaques, 80% for those receiving N4 treatment, and 66% for the N2 treatment group. Treated animals that succumbed to MARV disease had a delayed time-to-death of 10, 11, and 14 days for the N4 (N=2), Δ G (N=1), and N2 (N=1) groups, respectively. Treatment efficacies of the Angola-expressing rVSV groups compared to the untreated control

group were statistically significant; however, no differences were noted between the three treated groups.

- Controls (N=3)
- Vector control (N=1)
- Treated with rVSV Δ G/MARV-Angola GP (Δ G; N=9)
- Treated with rVSVN2CT1-MARV-Angola GP (N2; N=5)
- Treated with rVSVN4CT1-MARV-Angola GP (N4; N=5)

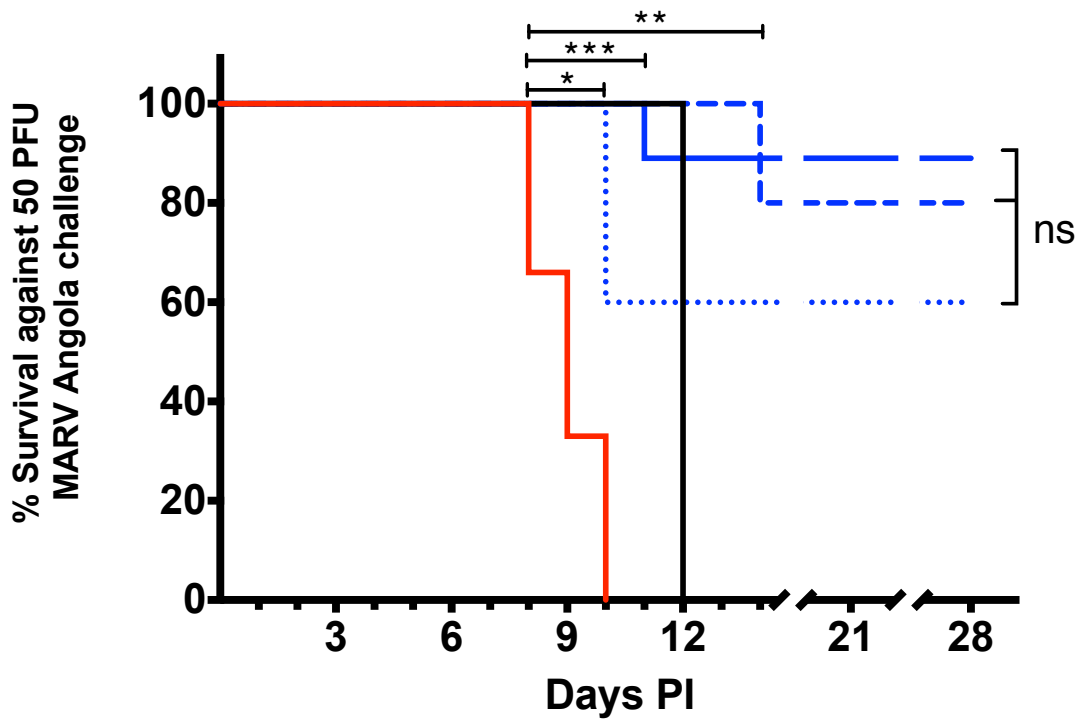


Figure 8. Postexposure treatment of macaques with rVSV vectors was effective against a 50 PFU low dose challenge of MARV Angola.

*Kaplan-Meier survival curves of animals treated with rVSV Δ G/MARV-Angola-GP (Δ G; solid blue line; N=9), rVSVN2CT1-MARV-Angola-GP (N2; segmented blue line; N=5), rVSVN4CT1-MARV-Angola-GP (N4; perforated blue line; N=5), and rVSVN4CT1-HIV gag (vector control; black line; N=1). Groups treated with rVSV vectors expressing Angola GP were significantly different than the untreated control group (red line; N=3). Statistical significance was not calculated against the vector control due to a lack of biological replicates, though we would expect a similar delay in death if additional animals were added based on previous studies. * $p \leq 0.05$, ** $p \leq 0.01$, *** $p \leq 0.001$.*

Survival for the low dose experiment was associated with fewer clinical indications of disease (Table 5). The controls exhibited signs consistent with MVD, such as fever, depression, anorexia, and a petechial rash. Elevated concentrations of C-reactive protein and liver enzymes were detected at mid disease and continued to increase up to death. BUN and/or CRE were also elevated in the untreated and vector control groups, indicating potential kidney damage. Of the 15 treated animals that survived, only one displayed major clinical signs: ΔG Survivor 5. The remaining survivors remained generally healthy. Only two N2-treated and two N4-treated macaques had temporary spikes in liver enzymes; this indicates rVSV treatment was able to protect most animals against detectable liver damage. Unexpectedly, 12 of the 15 survivors developed granulocytopenia during the course of the study. The significance of this finding is unclear but warrants further investigation as we often see the opposite in fatal cases (granulocytosis).

Animal	Challenge Dose	Treatment	Clinical Observations	Final Disposition
Control 1	Low	None	Fever (6), depression (6-8), anorexia (7-8), leukopenia (6), lymphopenia (3,6), ALT +++ (6), AST +++ (6) > (8), ALP + (6), GGT + (6), CRP increase (3,6)	Succumbed on day 8
Control 2	Low	None	Fever (6), depression (8-9), anorexia (7-9), mild to moderate petechial rash (8-9), lymphocytosis (9), monocytopenia (6), BUN ++ (9), CRE + (9), ALT ++ (6) +++ (9), AST +++ (6,9), ALP ++ (9), GGT +++ (9), CRP increase (9)	Succumbed on day 9
Control 3	Low	None	Fever (6), depression (10), anorexia (8,10), mild to moderate petechial rash (10), emesis (8), leukocytosis (6,10), granulocytosis (3,6), monocytosis (6), CRE + (10), ALT +++ (10), AST + (6) +++ (10), ALP +++ (10), GGT +++ (10), CRP increase (6,10)	Succumbed on day 10
Vector Control	Low	rVSVN4CT1-HIV gag	Fever (10), depression (12), anorexia (10-12), mild petechial rash (10-12), lymphocytosis (10,12), granulocytopenia (12), BUN + (12), CRE ++ (12), ALT +++ (10,12), AST +++ (10,12), ALP ++ (10,12), GGT +++ (10,12), CRP increase (10,12)	Succumbed on day 12

Δ G Treated Fatal	Low	rVSV Δ G/MARV-Angola-GP	Fever (6), depression (10,11), anorexia (8,9,11), mild to moderate petechial rash (10), ecchymotic rash (11), leukocytosis (11), lymphopenia (6,10), lymphocytosis (11), granulocytosis (3,6,10,11), monocytosis (11), thrombocytopenia (10), BUN + (10) +++ (11), CRE +++ (11), ALT > (10,11), AST > (10,11), ALP ++ (10,11), GGT +++ (10,11), CRP increase (6,10,11)	Succumbed on day 11
Δ G Survivor 1	Low	rVSV Δ G/MARV-Angola-GP	Lymphocytosis (14), granulocytopenia (14), granulocytosis (21)	Survived to day 28
Δ G Survivor 2	Low	rVSV Δ G/MARV-Angola-GP	Granulocytopenia (10), monocytopenia (6)	Survived to day 28
Δ G Survivor 3	Low	rVSV Δ G/MARV-Angola-GP	Granulocytopenia (3,10)	Survived to day 28
Δ G Survivor 4	Low	rVSV Δ G/MARV-Angola-GP	Leukopenia (3,6,10,14,21,28), granulocytopenia (3,6,10,14,21,28), monocytopenia (3,6,10,14,21,28)	Survived to day 28
Δ G Survivor 5	Low	rVSV Δ G/MARV-Angola-GP	Fever (6), mild depression (8,9), mild to moderate petechial rash (8,9,10,11), leukopenia (3,6), lymphopenia (6), lymphocytosis (10,14,28), granulocytopenia (3,6,10,14,21,28), monocytopenia (3,21), thrombocytosis (21), ALT + (21) +++ (10,14), AST + (14) +++ (10), ALP ++ (10), GGT + (14,21) +++ (10), CRP increase (10)	Survived to day 28
Δ G Survivor 6	Low	rVSV Δ G/MARV-Angola-GP	Lymphocytosis (10,28), granulocytopenia (28), monocytopenia (21), thrombocytopenia (28),	Survived to day 28
Δ G Survivor 7	Low	rVSV Δ G/MARV-Angola-GP	Monocytopenia (14,21)	Survived to day 28
Δ G Survivor 8	Low	rVSV Δ G/MARV-Angola-GP	Fever (21), leukopenia (6,10,14,21,28), granulocytopenia (3,6,10,14,21,28), monocytopenia (3,10,21), CRP increase (3)	Survived to day 28
N4 Fatal 1	Low	rVSVN4CT1-MARV-Angola GP	Fever (6), depression (10), anorexia (9-10), mild to moderate petechial rash (10), mild dyspnea (10), leukopenia (6), leukocytosis (10), lymphopenia (6), lymphocytosis (10), granulocytopenia (3,6), granulocytosis (10), monocytosis (10), BUN +++ (10), CRE +++ (10), ALT +++ (10), AST ++ (10), ALP ++ (10), GGT +++ (10), CRP increase (10)	Succumbed on day 10
N4 Fatal 2	Low	rVSVN4CT1-MARV-Angola GP	Fever (6), depression (10), anorexia (9-10), mild to moderate petechial rash (10), mild dyspnea (10), leukocytosis (10), lymphocytosis (10), granulocytosis (6), monocytosis (6), BUN +++ (10), CRE +++ (10), ALT +++ (10), AST ++ (10), ALP ++ (10), GGT ++ (10), CRP increase (6,10)	Succumbed on day 10
N4 Survivor 1	Low	rVSVN4CT1-MARV-Angola GP	Monocytosis (10)	Survived to day 28

N4 Survivor 2	Low	rVSVN4CT1- MARV-Angola GP	Leukopenia (6), lymphocytosis (10), granulocytopenia (3,6), monocytosis (10), ALT + (10,14)	Survived to day 28
N4 Survivor 3	Low	rVSVN4CT1- MARV-Angola GP	Fever (6), leukocytosis (14), lymphocytosis (14), granulocytosis (6), monocytosis (6,14), ALT ++ (10), AST +++ (10)	Survived to day 28
N2 Fatal	Low	rVSVN2CT1- MARV-Angola GP	Depression (12,13,14), anorexia (12), mild to moderate petechial rash (13,14), mild dyspnea (14), lymphopenia (10), granulocytosis (10,14), monocytosis (14), thrombocytopenia (10,14), BUN ++ (14), CRE + (14), ALT + (10) +++ (14), AST ++ (10) +++ (14), ALP ++ (14), GGT + (14), CRP increase (10,14)	Succumbed on day 14
N2 Survivor 1	Low	rVSVN2CT1- MARV-Angola GP	Fever (6), lymphocytosis (10,14), granulocytopenia (10,28), monocytopenia (14), monocytosis (6)	Survived to day 28
N2 Survivor 2	Low	rVSVN2CT1- MARV-Angola GP	Granulocytopenia (3), monocytopenia (6,14,21), ALT + (6,10,14)	Survived to day 28
N2 Survivor 3	Low	rVSVN2CT1- MARV-Angola GP	Fever (3,21), leukopenia (6), granulocytopenia (3,6,14,21,28), monocytopenia (3,10,14,21,28)	Survived to day 28
N2 Survivor 4	Low	rVSVN2CT1- MARV-Angola GP	Lymphopenia (6), granulocytopenia (3,10,14,28), monocytosis (21), ALT ++ (10)	Survived to day 28

Table 5. Clinical findings in monkeys for the low dose experiment.

The day after challenge is in parentheses. Fever: a temperature greater than 2.5 °F above baseline, at least 1.5 °F above baseline and ≥ 103.5 °F, or 1.1 °F above baseline and ≥ 104°F. Leukopenia, monocytopenia, lymphopenia, granulocytopenia, and thrombocytopenia: ≥ 35% drop in numbers of leukocytes, monocytes, lymphocytes, granulocytes, and platelets respectively. Leukocytosis, monocytosis, lymphocytosis, and granulocytosis: ≥ two-fold increase in leukocytes, monocytes, lymphocytes, and granulocytes respectively. Abbreviations: MARV (Marburg virus); rVSV (recombinant Vesicular stomatitis virus); MARV-Angola-GP (Marburg virus Angola glycoprotein); N4, (the rVSV nucleoprotein (N) is at position 4 in the genome); N2 (the rVSV nucleoprotein (N) is at position 2 in the genome); CT1 (the native rVSV glycoprotein (G) has a truncated cytoplasmic tail); ΔG (the native VSV G is absent); HIV (human immunodeficiency virus); gag (group-specific antigen); BUN (blood urea nitrogen); CRE (creatinine); ALT (alanine aminotransferase); AST (aspartate aminotransferase); ALP, (alkaline phosphatase); GGT (gamma-glutamyltransferase); CRP (c-reactive protein); ΔG (referring to individual monkey treated with rVSVΔG/MARV-Angola-GP); N4 (referring to individual monkey treated with rVSVN4CT1-MARV-Angola GP); and N2 (referring to individual monkey treated with rVSVN2CT1-MARV-Angola GP). Crosses indicate increases in liver enzymes (ALT, AST, ALP, GGT) and renal function test values (BUN, CRE): 2- to 3-fold increase, +; >3- up to 5-fold increase, ++; >5 fold increase, and +++; out of range, >.

As expected, treated survivors in the low dose experiment had decreased viral load (Figure 9). Only low, transient viremia was detected in a single survivor (ΔG Survivor 1) at day 10. Treatment with rVSV diminished viral replication in fatal cases, as evidenced by the decreased titers at mid- and terminal disease. At day 6 post-challenge, ~6 to 8 logs of infectious MARV was observed in the untreated control group. Comparatively, viral titers were 4-7 logs less for the treated non-survivors and ~3-5 logs less for the vector control at this time point. By day 10, the vector and remaining untreated control reached ~8 logs of MARV in the plasma, whereas treated animals that did not survive ranged from ~4 to 6 logs. A similar pattern was observed for RT-qPCR. Untreated controls and the vector control reached 11-12 logs of RNA copies/mL in whole blood at end-stage disease. In contrast, terminal titers in treated fatal cases were ~1 to 3 logs less. Transient MARV RNA was noted in roughly half of the treated survivors throughout the course of the study but never exceeded 7 logs.

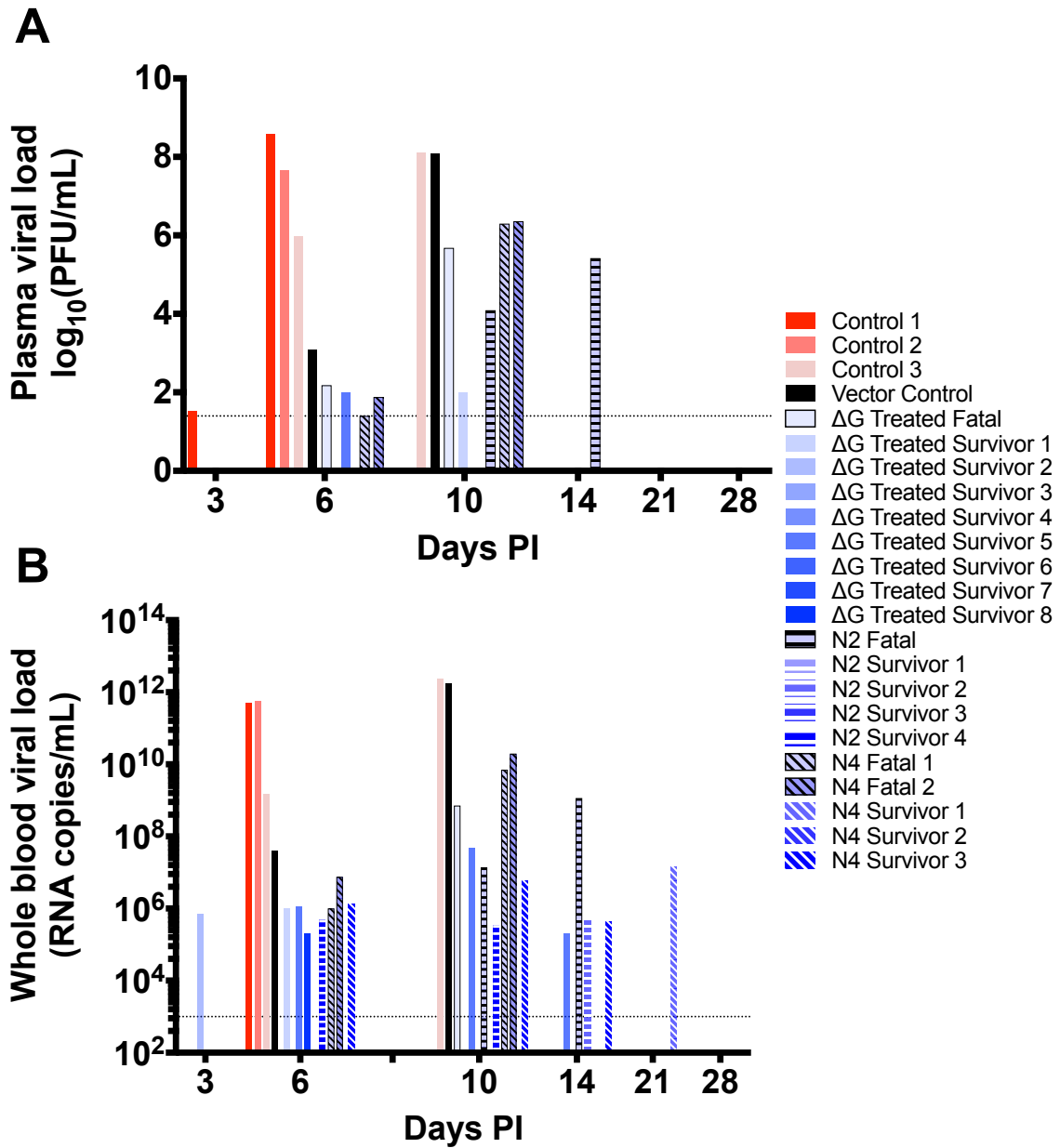


Figure 9. MARV viral loads in animals challenged with a low dose of MARV-Angola.

Plasma and whole blood MARV viral loads on days 3, 6, 10, 14, 21, and 28 after challenge as determined via plaque assay (A) and RT-qPCR (B). Shown are individual untreated (red-pink bars), rVSV Δ G/MARV-Angola-GP-treated (Δ G; solid blue gradient bars), rVSVN2CT1-MARV-Angola-GP-treated (N2; horizontal stripe blue gradient bars), and rVSVN4CT1-MARV-Angola-GP-treated (N4; diagonal stripe blue gradient bars) subjects, as well as the single vector control (black bar). The limit of detection is 25 PFU/mL for the plaque assay and 1000 copies/ml for RT-qPCR (dotted line).

Next, we examined viral titers in all major tissues for the low dose-challenged monkeys (Figure 10). The untreated controls, vector control, and treated fatal monkeys reached high titers of ~8-11 logs in all tissues tested. MARV RNA was also detected in treated survivors, indicating a lack of sterile immunity. However, PCR titers were reduced in these animals and ranged from ~5-7 logs.

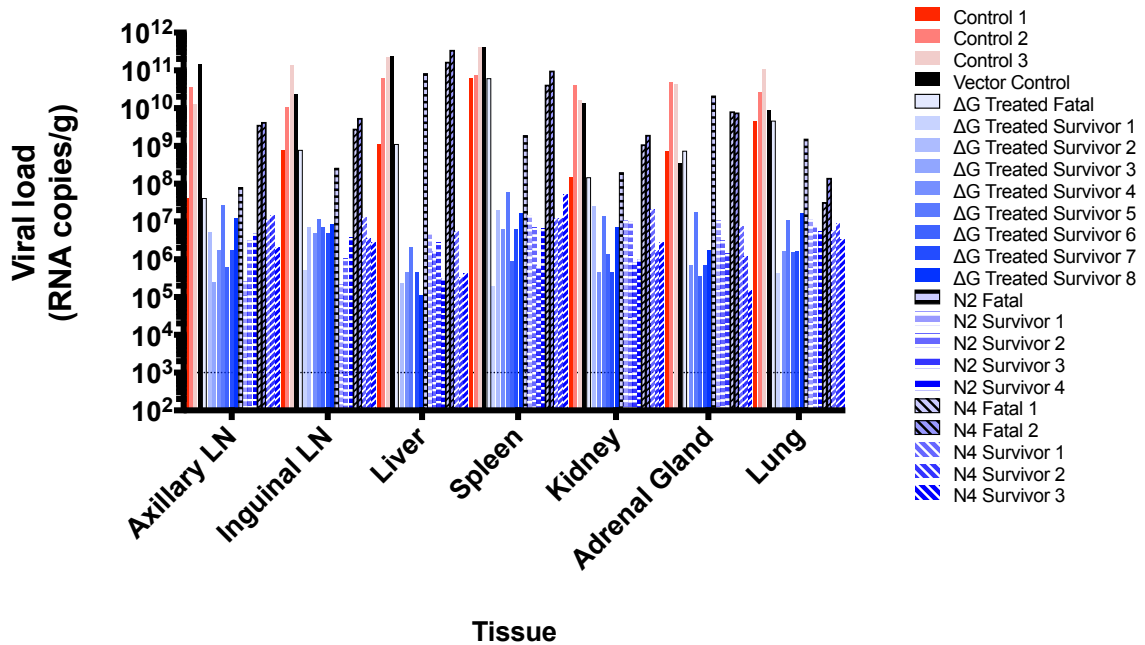


Figure 10. Tissue viral loads in animals challenged with a low dose of MARV-Angola.

Viral load was assessed by RT-qPCR. Each bar represents a single macaque at the time of euthanasia. Shown are individual untreated (red-pink bars), rVSVΔG/MARV-Angola-GP-treated (ΔG; solid blue gradient bars), rVSVN2CT1-MARV-Angola-GP-treated (N2; horizontal stripe blue gradient bars), and rVSVN4CT1-MARV-Angola-GP-treated (N4; diagonal stripe blue gradient bars) subjects, as well as the single vector control (black bar). The limit of detection for this assay is 1000 copies/mL (dotted line). Abbreviation: LN (lymph nodes).

Necropsies in fatal cases, in conjunction with histopathology and IHC, were consistent with MARV disease. Examination of liver and spleen tissue sections by IHC in controls and treated non-survivors showed abundant MARV antigen (red), extensive necrosis, hemorrhaging, cellular degeneration, and fibrin deposition (Figure 11). Due to

lymphocyte depletion in untreated and treated non-survivors, the splenic white pulp architecture was severely disturbed and the marginal zone was largely absent. No significant lesions or immunoreactivity were noted in tissues of treated survivors.

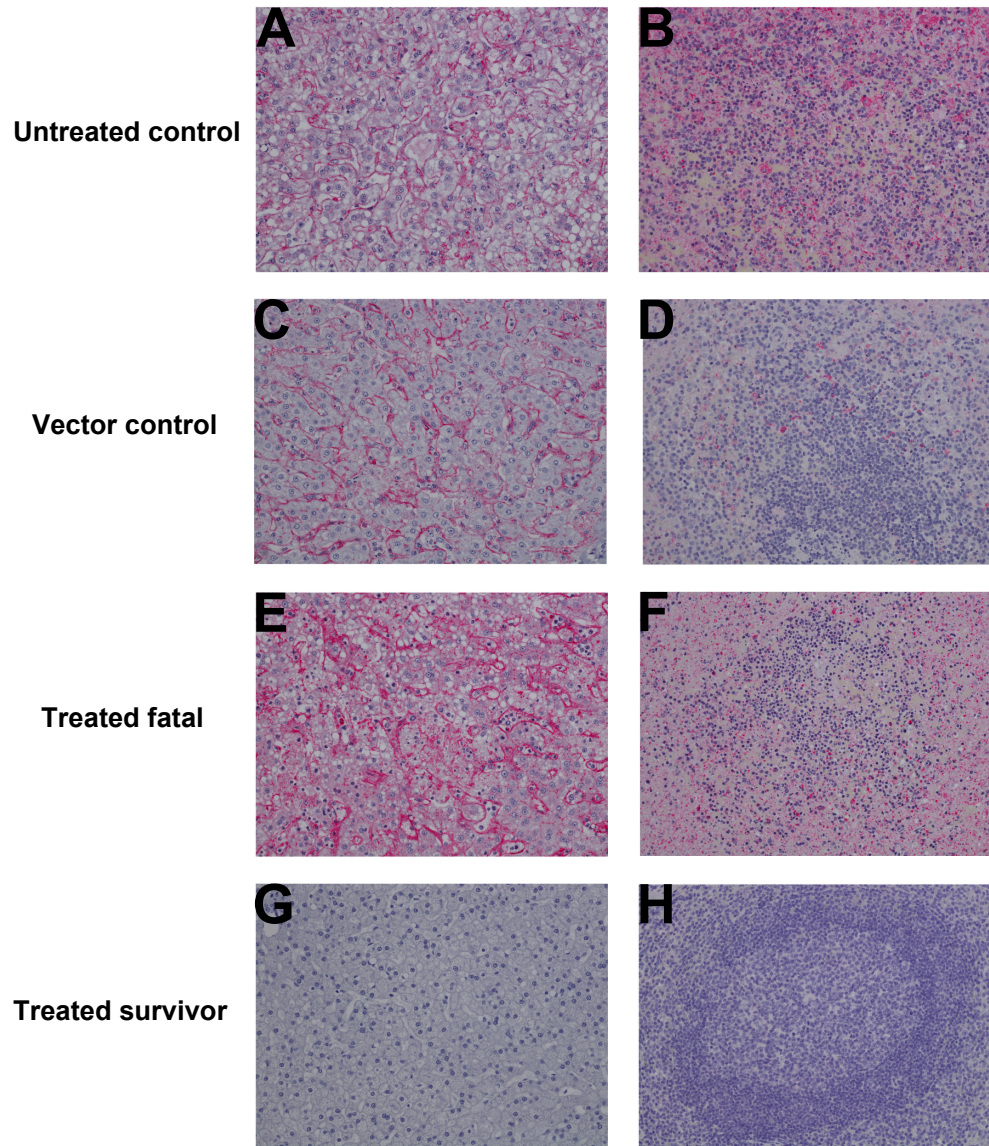


Figure 11. Immunolabeling of MARV antigen in the liver and spleen of rhesus macaques challenged with MARV Angola.

Comparison of MARV antigen in a representative untreated control (A, B), vector control (C, D), treated fatal (E, F), and treated survivor macaque (G, H). A, C, E) Livers of non-survivor macaques show diffuse, cytoplasmic immunolabeling (red) of sinusoidal lining

cells. B, D, F) Diffuse cytoplasmic immunolabeling of dendriform mononuclear cells in the red and white pulp was noted in non-survivor spleens. G, H) No immunolabeling was observed in the liver or spleen of a representative treated survivor.

Conclusions

Although rVSVs remain potent prophylactic vaccines for MVD, post-exposure treatment with these vectors has only limited efficacy against the most virulent variant, Angola. Only 25% of rhesus monkeys treated with rVSV Δ G/MARV-Angola-GP survived the high dose challenge. Conversely, the lower challenge dose likely delayed the disease course sufficiently for rVSV treatment to elicit protection in this model (the median time-to-death for untreated controls was 9 days versus 10.5 days for the treated fatal cases; p-value= 0.0499). Post-exposure treatment efficacies seemed to vary by the degree of attenuation of the vector, with 89% protection for monkeys treated with rVSV Δ G/MARV-Angola-GP, 80% for those treated with rVSVN2CT1-MARV-Angola-GP, and 60% for those treated with rVSVN4CT1-MARV-Angola-GP. However, survival-rate differences between these treatment groups were not statistically significant.

Given the susceptibility of MARV to a strong IFN response, VSV likely led to early immune signaling that decreased viral replication. Consequently, treated animals experienced later disease onset [107, 111, 112, 113, 114, 115, 124]. Treatment with IFN after MARV infection is not generally beneficial [110], but may be advantageous if VSV is able to prime initial target cells to prevent MARV entry or egress. VSV grows rapidly and is known to upregulate ISGs as early as 2-6 hours after infection in macrophage-like primary cells or immortalized cell lines [184, 185]. MARV-Angola replicates at a slower rate and is unable to activate many of these innate antiviral genes until 24 hours post-infection [125]. Additionally, rVSV may have precipitated the formation of protective antibodies by inducing an earlier innate immune response.

The terminal stage for a MARV-Angola challenge in rhesus monkeys ranges from 6-8 days for a high dose versus 8-10 days post-infection for a low dose challenge (Table 1). The humoral response to a rVSV vector normally overlaps with this time frame with concurrent development of MARV GP-specific IgM and IgG within 6-10 days post-vaccination [143, 144, 147, 148]. Therefore, a lower challenge dose may allow sufficient time for protective antibody responses to be mounted against these rVSV vectors. This hypothesis is supported by the fact that in previous post-exposure studies survivors produced GP-specific antibodies, whereas in fatal cases they did not [147, 148]. Monkeys treated with a non-specific vector in this and past studies did not survive [147, 148], so it is unlikely viral interference or stimulation of innate immunity alone confers protection.

In summary, rVSV treatment slows or prevents MVD. In a worst-case scenario, individuals exposed to high doses of this virus, such as a needlestick, would likely benefit from more effective therapies, for instance, monoclonal antibodies or SNALPs if these treatments are available [159, 160]. Combination therapy with adjuvants, antivirals, or SNALPs might enhance rVSV-mediated protection against a high dose exposure. Given reduced viral titers are associated with survival, SNALPs would likely provide the best benefit as these effectively inhibit MARV replication and alone confer complete survival of NHPs when treatment is delayed up to four days post-exposure. Natural exposures to MARV are probably lower than 1000 PFU, and for these routes of infection, the virus has to overcome additional mucosal barriers [186]. Post-exposure treatment with rVSV vectors might be of greater utility for ring immunization during outbreaks since stocks could be quickly produced. Live attenuated vaccines are also generally more economical and provide durable immunity.

More research is needed to define the mechanisms by which rVSV vectors mediate protective responses, particularly in the post-exposure context. We could then exploit these mechanisms to enhance host resistance to this deadly virus.

CHAPTER 3: IMMUNOLOGICAL CORRELATES OF RECOMBINANT VESICULAR STOMATITIS VIRUS-MEDIATED POST-EXPOSURE PROTECTION AGAINST MARBURG VIRUS

Few studies have analyzed mechanisms of rVSV-mediated immunity. Basic research and recent clinical studies have added to the growing body of evidence that supports antibody production as a chief contributor to protection. Human subjects and NHPs immunized with rVSV also produce antigen-specific T-cells that are thought to bolster immunity by secreting antiviral cytokines IFN-gamma, TNF-alpha, and IL-2 [165, 167]. Cell depletion studies in monkeys for the rVSV EBOV platform suggest CD4+ T-cells and antibodies are vital for vaccine protection, whereas CD8+ T cells are expendable [172].

Correlates of post-exposure immunity for the rVSV platform are mostly undefined. There is some speculation that viral interference or stimulation of innate immunity confers protection. These hypotheses are appealing given the rapid replication of the vector and its ability to induce a strong innate response. However, monkeys treated with non-specific rVSVs do not survive a lethal MARV challenge (although, treatment in some cases delays time-to-death), which indicates there are other contributing factors [147, 148]. Instead, protection is associated with the formation of GP-specific IgM and IgG antibodies with low levels of neutralization in survivor NHPs [143, 144, 147, 152]. Another group reported that monkeys administered post-exposure therapy with an irrelevant MARV GP-expressing rVSV exhibited partial protection against a lethal EBOV Makona challenge, and these animals developed anti-EBOV humoral responses [169]. Hence, the mechanisms of protection for these two viruses might differ. The role

of cell-mediated immunity in rVSV post-exposure treatment against MVD is unclear since T-cell responses were neither evaluated nor detected in these studies.

In a previous experiment, we challenged rhesus monkeys with a low or high lethal dose challenge of the most lethal variant of MARV, Angola, and inoculated them with rVSV vectors shortly after exposure. To identify immune signatures associated with post-exposure protection, we performed RNA sequencing on whole blood samples and flow cytometry on peripheral blood mononuclear cells (PBMC) from Δ G- and N2-treated monkeys (therapeutic efficacies were 89% and 80%, respectively). To monitor antibody responses in sera, we performed antigen-specific IgM and IgG ELISAs and a neutralization assay on sera from these animals. This is the most comprehensive study thus far to define rVSV-mediated correlates of post-exposure protection.

Methods

ANIMAL CHALLENGE

The *in vivo* experimental design is thoroughly described in the "Methods" section of Chapter 2 of this dissertation. Briefly, eighteen rhesus monkeys were challenged with a low, but uniformly lethal, 50 PFU dose of MARV-Angola and administered rVSV vectors 20-30 minutes after exposure. Three controls were left untreated, nine subjects received rVSV Δ G/AMARV GP treatment, five subjects received rVSV-N2CT1-AMARV GP treatment, and one subject received a vector control. Other than the ELISAs and PRNT assays, the five subjects administered rVSV-N4CT1-AMARV GP treatment were not included in these immune correlate studies (N=5).

BLOOD PROCESSING AND PBMC ISOLATION

Plasma and sera collection for cytokine-bead arrays, ELISAs and plaque reduction neutralization tests are also detailed in Chapter 2. Aliquots of EDTA-treated whole blood were inactivated with AVL buffer (Qiagen, Hilden, Germany) for RNA extraction. To isolate PBMC, we diluted heparin-treated blood and the remaining spun EDTA pellet with PBS, carefully layered the combined blood onto a Histopaque cushion in Accuspin tubes (Sigma, St. Louis, MO), and centrifuged the tubes at $\sim 800 \times g$ room temperature (RT) for 15 minutes. The resulting buffy coat was collected and washed once in R10 (RPMI media (Gibco, Gaithersburg, MD) supplemented with 10% fetal bovine serum (FBS), 100U/ml penicillin, 100g/ml streptomycin solution, and 1% L-glutamine). Cells were treated briefly with ACK lysing buffer (Gibco, Gaithersburg, MD) to rid PBMC of any contaminating erythrocytes. PBMC were then centrifuged at $\sim 250 \times g$ for 10 minutes to reduce residual platelets, washed twice with R10 media, and enumerated on a TC20 Automated Cell Counter (Bio-Rad, Hercules, CA). Cells were cryopreserved in 10% dimethyl sulfoxide (DMSO) in FBS. Before performing flow cytometry, cryopreserved PBMC were thawed rapidly in a 37°C water bath and washed in BD Staining Buffer (BD Biosciences, San Jose, CA).

BEAD-BASED MULTIPLEX IMMUNOASSAY

Concentrations of cytokines and other analytes were assayed using bead-based multiplex technology. Irradiated plasmas were incubated with magnetic beads from Milliplex NHP Cytokine Premixed 23-plex Panel (EMD Millipore, Billerica, MA) or ProcartaPlex NHP TGF-beta 1 simplex (eBioscience, Vienna, Austria) kits, according to the manufacturer protocols. The following concentrations in each plasma sample were measured using a Bioplex-200 array system (BioRad, Hercules, CA): granulocyte colony-stimulating factor (G-CSF); granulocyte-macrophage colony-stimulating factor (GM-CSF); IFN-gamma; interleukin 1 receptor agonist (IL-1ra); interleukin 1 beta (IL-1-beta); interleukin 2 (IL-2); interleukin 4 (IL-4); interleukin 5 (IL-5); interleukin 6 (IL-6);

interleukin 8 (IL-8); interleukin 10 (IL-10); interleukin IL-12/23 protein 40 (IL-12/23 p40); interleukin 13 (IL-13); interleukin 15 (IL-15); interleukin 17 (IL-17); interleukin 18 (IL-18); monocyte chemoattractant protein 1 (MCP-1); macrophage inflammatory protein 1-alpha (MIP-1-alpha); macrophage inflammatory protein 1-beta (MIP-1-beta); soluble CD40 ligand (sCD40L); transforming growth factor alpha (TGF-alpha); tumor necrosis factor alpha (TNF-alpha); and vascular endothelial growth factor (VEGF).

RNA EXTRACTION

RNA was extracted using Qiagen Viral Blood RNA Mini (Qiagen Mississauga, ON, Canada) and Zymo Direct-zol RNA MiniPrep kits. Prior to isolation, AVL-treated cells in whole blood were lysed using Qiagen Qias shredder tubes to liberate intracellular RNA.

RNASEQ LIBRARY PREPARATION

RNA concentration and quality were first determined using Agilent RNA 6000 chips and an Agilent 2100 Bioanalyzer. Next, we purified RNA samples with Agencourt RNAClean XP beads. Illumina TruSeq Stranded Total RNA LT kits were used to deplete ribosomal RNA (rRNA) and construct cDNA libraries. RNA was fragmented, converted to double-stranded cDNA, and adapters ligated to each strand. The resulting ~300 base-pair sheared cDNA fragments were then amplified by PCR and purified using AMPureXP Beads. Each library was prepared with a unique indexed adapter for multiplexing. Libraries were validated for size, concentration, and integrity with a bioanalyzer. After confirming the samples were of high quality, multiplexed libraries were subjected to single-end 75 base pair sequencing using the Illumina NextSeq500 V2 platform. On average, we retrieved 20 million reads per sample and ~90% aligned to the rhesus monkey genome.

RNASEQ ANALYSIS AND FUNCTIONAL ENRICHMENT

The RNA-seq workflow module of Bioconductor's systemPipeR open source software was used to perform the bioinformatic analysis. Demultiplexing and quality control of sequences were accomplished using the FastQC function. Trim Galore was used to trim three base pairs from the 5' end and two bases from the 3' end. Only RNAseq reads with a phred score ≥ 30 and a 50 base pair minimum length were included in these studies. The *Macaca mulatta* genome sequence (Macaca_mulatta.MMUL_1.dna.toplevel.fa) and corresponding annotation file from Ensembl (Macaca_mulatta.MMUL_1.78.gtf) were implemented for alignment purposes. To determine the level of rVSV transcription, the genome of a recombinant Vesicular stomatitis Indiana virus that expresses a fused C-terminal enhanced green fluorescent protein (rVSV-G/GFP; strain UNKNOWN-FJ478454; Accession ID FJ478454) was obtained from Virus Pathogen Resource and concatenated to the *Macaca mulatta* reference genome. VSV open reading frames, leader and trailer sequences, and IR were defined by the VSV genome annotation GTF file: leader (1-63), N (64-1332), IGR N_P (1333-1395), P (1396-2193), IGR P_M (2194-2249), M (2250-2939), M_G (2940-3077), G_L (6917-7026), L (7027-13356), and trailer (13357-13455). The G/GFP fusion gene was excluded from analyses because the rVSV vectors in this study lack this gene. Bowtie2/Tophat2 was used to align cleaned and trimmed RNA-Seq reads to the viral and macaque reference genomes. The summarizeOverlapsfunction generated raw read counts that mapped to overlapping exon regions of genes and discarded reads that mapped to ambiguous exon regions. The edgeR function was executed to normalize differentially expressed genes (DEGs) against a pre-challenge baseline (day 0) and perform the necessary statistical analyses. DEGs were further scrutinized by establishing a false discovery rate (FDR) corrected p-value threshold of ≤ 0.05 . Simply put, a p-value of 0.05 means that 5% of *all* tests will result in false positives. If there are 20,000 genes, 1,000 of these genes are then considered false positives. An FDR-adjusted p-value of 0.05 implies that 5% of *statistically significantly* tests will result in false positives. Thus, an FDR

value is a more conservative approach to defining statistical significance and results in fewer false positives. Only genes encoding proteins with human homologs and an average of 5 reads per kilobase of transcript per million reads (RPKM) were evaluated. Figures were generated with R tools and Adobe Illustrator. Heatmaps were created with gplot; Venn diagrams were created with the VennDiagram function. We used MetaCore™ (Thomson Reuters, New York, NY) to identify functionally related gene groups mapping to specific biological pathways. Interferon-stimulated genes (ISGs) were discovered using the Interferome v2.0 database [187]. Cell-type quantity matrix and comparative viewer images were created using ImmQuant software and the IRIS algorithm [188, 189].

NORMALIZATION OF SAMPLES

Principal component analyses (PCA) revealed a similar clustering of untreated, vector control-treated, and treated fatal samples (Supplementary Figure 2); therefore, these animals were combined into a single "Fatals" group for our RNAseq, flow cytometry, and cytokine analyses (except for the "Control" ImmQuant cell-type quantity supplementary analysis). The Δ G- and N2-treated survivors were pooled into a separate "Survivors" group, as they also clustered similarly. Due to the delayed onset of disease for the vector control and treated fatals versus untreated subjects, samples were normalized according to the first detectable viremia in these animals (mid-disease) (see Supplementary Table 1 for individual monkeys). The next bleed timepoint was termed late-disease in this group and corresponded to 0-2 days before the animal succumbed to MVD. The median timepoint for mid-disease in the "Fatal" group was 6 days and was used to define this disease stage in treated survivors.

FLOW CYTOMETRY AND INTRACELLULAR CYTOKINE STAINING ON RHESUS PBMC

PBMC were stained in the dark at 4°C with fluorochrome-conjugated antibodies in round-bottom 96-well plates (268200 ThermoScientific, Roskilde, Denmark). To delineate the various cell subsets for the monocyte HLA-DR MFI panel, the following markers were used: CD3, CD20, CD14, CD16, CD123, CD11c, and HLA-DR. Surface fixation was accomplished with a 4% paraformaldehyde solution. Approximately 200,000 events were collected on a FACS Canto II cytometer (BD Biosciences, San Jose, CA) using BD FACS Diva software, and analyzed using FlowJo (Tree Star, Ashland, OR) and Prism 7 (GraphPad Software Inc., La Jolla, CA). Compensation was calculated using BD CompBeads (BD). Live cells were distinguished from dead cells by forward scatter (FSC) and side-scatter (SSC) properties.

To examine polyfunctionality and frequency of antigen-specific Th1 and CTL populations, we performed intracellular cytokine staining (ICS) of CD4+ and CD8+ T-cells. Cells were stained with CD3, CD4, CD8b, IL-2, IFN-gamma, and CD107a (a degranulation marker) fluorochrome-conjugated antibodies. PBMC were stimulated with a DMSO negative control, or 2µg/ml of a high-quality (~95% purity), overlapping MARV GP peptide pool (15-mers overlapping by 11 amino acids, custom-made at GenScript, Piscataway, NJ), for 6 hours in the presence of CD28, CD49d, and CD107. For the regulatory T-cell (Treg) panel, we stimulated PBMC for 6 hours or overnight with a media-only control, or 50ng/ml phorbol 12-myristate 13 acetate (PMA) (P8139, Sigma, St. Louis, MO) and 1µg/ml ionomycin (ION) calcium salt from *Streptomyces cinglobatus* (I0634, Sigma, St. Louis, MO). PBMC were stained for surface markers (CD3, CD4, CD25, FOXP3, IL-10) in the dark for 30 minutes at 4°C in the presence of DNase (D4513, Sigma, St. Louis, MO) and rhesus Fc receptor binding inhibitor (eBioscience, San Diego, CA) to reduce clumping and non-specific binding. Cells were washed twice after staining in BD staining buffer, inactivated for 30 minutes using FOXP3/Transcription Factor Fix/Perm, and washed twice in FOXP3/Transcription Factor

Perm Buffer. Brefeldin A (B6542, Sigma, St. Louis, MO) protein transport inhibitor was added to all panels two hours before performing intracellular staining. After staining, we washed and suspended PBMC in FOXP3/Transcription Factor Perm Buffer. Roughly 200,000 events were collected on a BD FACS Canto II cytometer and analyzed using FACS Diva, FlowJo, Prism 7, and SPICE (Simplified Presentation of Incredibly Complex Evaluations, NIAID) software. Live versus dead cells were distinguished by BV510 fixable viability dye (BD).

Our panels and gating strategies are displayed in Supplementary Table 2 and Supplementary Figure 3, respectively.

HUMAN MONOCYTE PDL-1 ASSAY

Buffy coats from three healthy donors were acquired from the UTMB blood bank with informed consent. PBMC were isolated by density gradient centrifugation using Histopaque. Miltenyi CD14 magnetic beads and the fully automated Miltenyi AutoMacs Separator were used for positive selection of monocytes, according to the vendor's recommended protocols (Miltenyi Biotec, Inc., Auburn, CA). Purity was confirmed at >90% by flow cytometry. Purified monocytes were infected in 5ml culture tubes on ice at an MOI of 3 for each virus. Cells were either co-infected, or only infected with MARV or rVSV Δ G/MARV-Angola-GP. We included uninfected and lipopolysaccharide (LPS) controls for comparison. After a one-hour adsorption period in a 100 μ l volume, tubes were spun and inoculum was removed. Monocytes were transferred to 6-well plates and cultured in fresh R10 media at 37°C in 5% CO₂. After 24 and 48 hours, monocytes were blocked with Human TruStain FcX Fc Receptor Blocking Solution (BioLegend) and stained with the following antibodies for flow cytometry: CD14 APC (BioLegend, M5E2), CD16 BV480 (BD, 3G8) CD80 PE/Cy7 (BioLegend, 2D10), PD-1 PerCP/Cy5.5 (BioLegend, EH12.2H7), PDL-1 PE (BioLegend, 29E.2A3), CD86 BV421 (BD, FUN-1) and HLA-DR APC/Cy7 (BioLegend, L243).

ANTI-MARV GP IGM AND IGG ELISAS

Sera collected at the indicated time points were tested for MARV GP-specific immunoglobulin M (IgM) and immunoglobulin G (IgG) antibodies by ELISA. We coated MaxiSorp clear flat-bottom 96-well plates (44204 ThermoFisher, Rochester, NY) overnight with 15 ng/well (0.15ml) of recombinant MARV-Angola GP Δ TM (Δ TM: transmembrane region absent; Integrated Biotherapeutics, Gaithersburg, MD) in a sodium carbonate/bicarbonate solution (pH 9.6). Antigen-adsorbed wells were subsequently blocked with 4% bovine serum antigen (BSA) in 1 x PBS for at least two hours. Sera was initially diluted 1:100 and then two-fold through 1:12800 in ELISA diluent (1% BSA in 1x PBS, and 0.2% Tween-20). After a one-hour incubation, cells were washed six times with wash buffer (1 x PBS with 0.2% Tween-20) and incubated for an hour with a 1:2500 dilution of horseradish peroxidase (HRP)-conjugated anti-rhesus IgM or IgG antibody (Fitzgerald Industries International, Acton, MA). RT SigmaFast O-phenylenediamine (OPD) substrate (P9187, Sigma, St. Louis, MO) was added to the wells after six additional washes to develop the colorimetric reaction. The reaction was stopped with 3M sulfuric acid 10-15 minutes after OPD addition and absorbance values were measured at a wavelength of 492nm on a spectrophotometer (Molecular Devices Emax system, Sunnyvale, CA). Absorbance values were normalized by subtracting uncoated from antigen-coated wells at the corresponding serum dilution. End-point titers were defined as the reciprocal of the last adjusted serum dilution with a value ≥ 0.16 .

PLAQUE REDUCTION NEUTRALIZATION TEST (PRNT)

Neutralization titers were calculated by determining the dilution of serum that reduced 50% of plaques (PRNT₅₀). We incubated a standard 100 PFU amount of MARV with two-fold serial dilutions of serum samples for one hour. The virus-serum mixture was then used to inoculate Vero E6 cells for 60 minutes. Cells were overlaid with 2x

EMEM agar medium, incubated for 6 days, and plaques were counted after 24 hours of 5% neutral red staining.

STATISTICAL ANALYSIS

GraphPad Prism (version 7.0) was used to conduct statistical analyses. For the *in vitro* human monocyte infection experiment, a one-way ANOVA was used to detect differences between groups, followed by a Tukey's multiple comparisons test. Mann-Whitney non-parametric tests were used for other statistical analyses.

Results

To compare the host immune response in rVSV-treated survivors to monkeys that succumbed to a low dose MARV-Angola challenge, we sorted samples into two datasets: "survivors" and "fatals". The survivors group (N=12) included animals treated with rVSV Δ G/MARV-Angola-GP and rVSVN2CT1-MARV-Angola-GP, and the fatals group (N=6) comprised untreated controls, a vector control, and rVSV-treated animals that did not survive (N=6). As viral load is a strong predictor of MARV disease progression, this parameter was used to further separate samples into mid- and late-disease stages. Mid-disease was defined as the day post-exposure that viremia was first detected and late-disease corresponded to 0-2 days before death (see Supplementary Table 1 for individual animals). The median time points for mid- and late-disease in fatal cases were 6 and 10 days post-exposure, respectively, and were used to define survivor disease stages. Sample normalization was implemented for RNAseq, flow cytometry, and plasma cytokine analyses. PCA analysis revealed clustering of the fatal group at these stages, suggesting disease manifests similarly in rVSV-treated fatals as it does for the

untreated and vector controls (Supplementary Figure 2). For humoral responses, samples from both high and low dose challenge groups were evaluated on the days indicated.

TRANSCRIPTIONAL CHANGES WERE GREATER IN FATAL CASES AT END-STAGE DISEASE

Protective correlates elicited by rVSV vectors were determined by comparing whole blood transcriptomes of survivor and fatal samples. Only genes with a minimum RPKM value of 5 and an FDR-adjusted p-value of ≤ 0.05 were included. At mid-disease, 31 DEGs were identified in survivors and 10 in fatals, with no genes in common (Figure 12A). All DEGs were upregulated in the heatmap datasets, except for a gene encoding breast cancer anti-estrogen resistance 3 (BCAR3) in survivors. BCAR3 is involved in cancer cell proliferation [190]. At late-disease, robust gene expression was observed in fatal cases (6,334 DEGs) (Figure 12B). Of the 4,783 DEGs that mapped to human homologs, 4,478 were upregulated and 305 were downregulated (Figure 12C). In comparison, only ten distinct DEGs were detected in survivors at this disease phase, and three mutually expressed genes with fatals: SLC9A9 (solute carrier family 9 member A9), RIPK3 (receptor-interacting serine/threonine kinase 3), and HECW2 (NEDD4-like E3 ubiquitin-protein ligase 2) (Supplementary Figure 4). SLC9A9 participates in late endosomal recycling [191], and RIPK3 is a component of the TNF-receptor signaling complex and is vital for necroptosis (programmed cell death in response to TNF family members) [192]. Gene ontology (GO) annotations of HECW2 include ubiquitin transferase and ligase activities. The transcriptional response following immunization with a MARV GP-expressing rVSV has yet to be reported following a MARV challenge. For EBOV, Menicucci et al. showed that vaccination of cynomolgus monkeys with an EBOV GP-expressing rVSV led to transient expression of genes involved in innate immunity that peaked 7 days post-immunization, and vector control or CD4-depleted animals that succumbed to a challenge had a greater abundance of DEGs compared to

survivors prior to death [166]. Similarly, we observed larger transcriptional changes in fatal cases at the terminal stage.

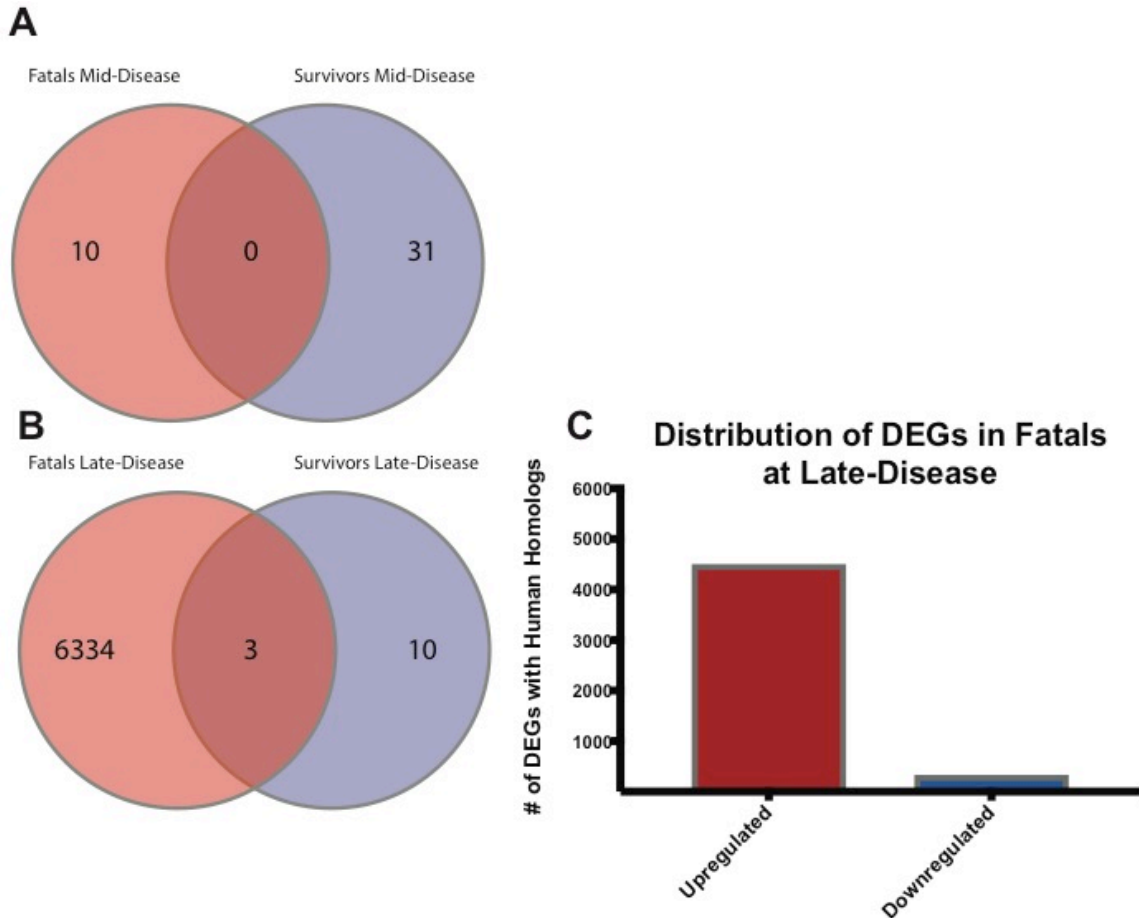


Figure 12. Venn diagram depicting overlap of DEGs within groups, and distribution of upregulated and downregulated DEGs in the fatal monkey dataset.

Whole blood transcriptomes from survivors and non-survivors had little to no overlap of differentially expressed genes (DEGs) at mid- (A) and late-disease (B). C) DEGs were predominantly upregulated in non-survivors at the terminal stage.

RVSV-TREATED SURVIVORS UPREGULATE ANTIVIRAL AND INTERFERON-RELATED GENES AND EXHIBIT A TH1 (IFN-GAMMA) GENE SIGNATURE

At mid-disease, nearly half of survivor DEGs were involved in IFN signaling (Figure 13A). Many of these genes have demonstrated antiviral activity against VSV *in vitro*, including cytidine/uridine monophosphate kinase (CMPK2), which may contribute

to terminal differentiation of monocytes and is part of the nucleotide synthesis salvage pathway [193, 194]; lymphocyte antigen 6 family member E (LY6E), which is affiliated with T-cell development [96, 195]; HECT and RLD domain containing E3 ubiquitin protein ligase family member 6 (HERC6), which encodes a ubiquitin-protein ligase functionally related to MHC-I class-mediated antigen processing and presentation [196, 197]; and IFN-gamma-induced guanylate binding protein 1 (GBP1), which promotes oxidative killing and delivery of antimicrobial peptides to phagolysosomes [198, 199]. Few rVSV reads were detected in these animals, indicating the vector was cleared by this stage.

Using the Interferome version 2.1 database [187], survivor ISGs were further examined to ascertain the dominant IFN subtype. Although there were limited DEGs detected, the majority mapped to type II IFN signaling (IFN-gamma) or were mutually shared with type I and III signaling (Figure 13B). This was an interesting finding in light of the fact that signal transducer and activator of transcription 4 (STAT4) was also induced in survivors. STAT4 is an early transcription factor that regulates the differentiation of Th1 and T follicular helper (Tfh) cells [200, 201]. Th1 cells secrete IFN-gamma and IL-2 and mediate responses to IL-12 in lymphocytes. These cells also stimulate antigen presentation and cellular immunity (macrophage and NK cell activity), and induce production of IgG opsonizing antibodies [200, 92]. In response to antigenic stimulation, Tfh cells secrete IL-21, upregulate the chemokine receptor CXCR5, and migrate into B-cell follicles to provide cognate help to germinal center B-cells. Tfh cells are therefore essential for clonal selection and affinity maturation, as well as class switching and the development of memory B-cells [201].

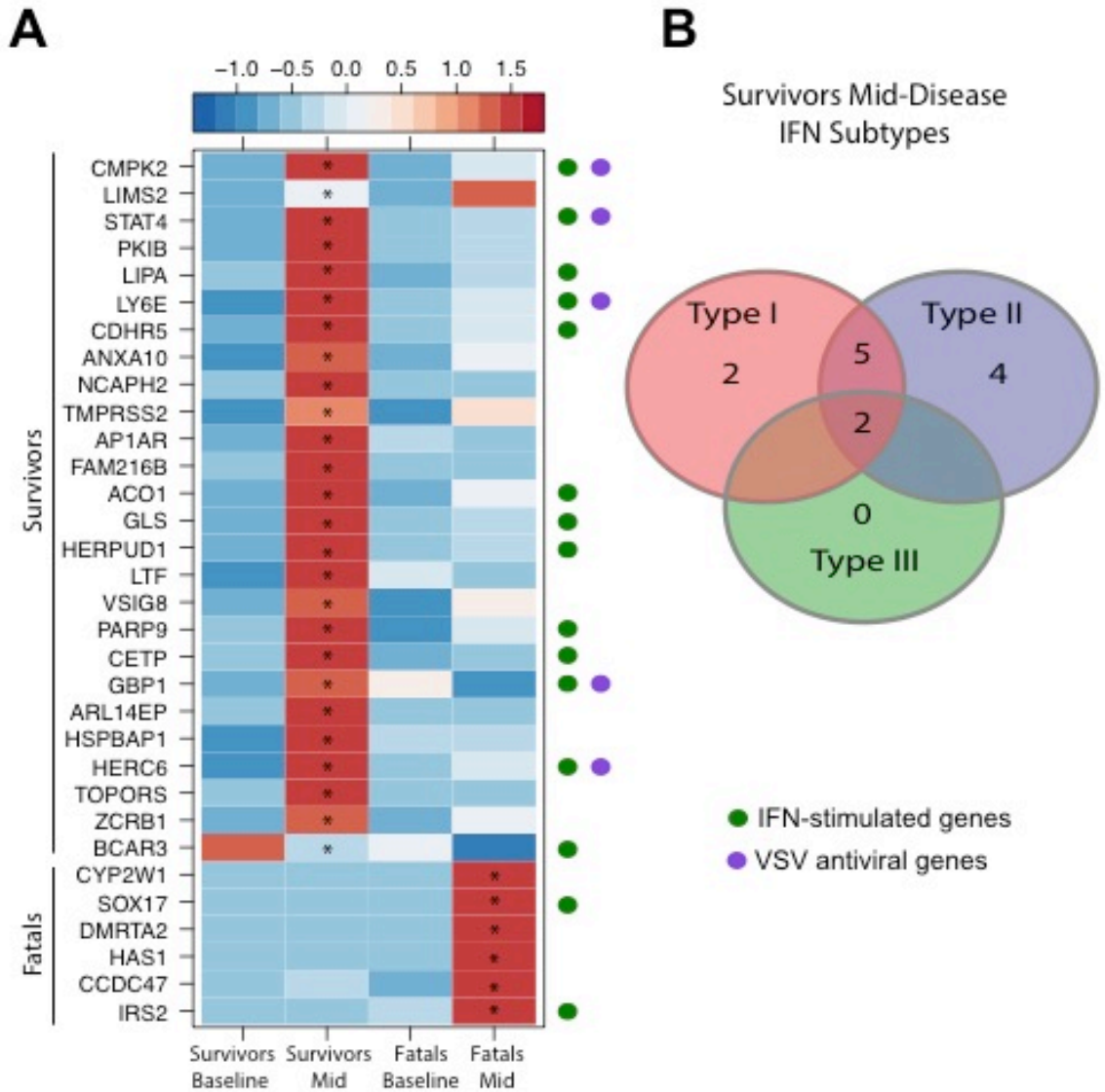


Figure 13. Heatmap comparison of the most highly upregulated and downregulated DEGs at mid-disease for each group.

A) Treatment with rVSV led to upregulation of interferon-related genes and Th1- and Tfh-associated *STAT4*. DEGs were calculated using EdgeR against a pre-challenge baseline to establish the most highly expressed genes based on log fold-change. This heatmap was based on scaled RPKM values within that set of genes (red represents increased expression while blue represents decreased expression); each column represents the median RPKM values for each time point. Genes were queried using the Interferome v2.01 database. Only human homologs and protein-coding genes were analyzed. *: statistically significant, FDR-corrected p-value of ≤ 0.05 B) Venn diagram showing the number of genes regulated by Type I, II, or III IFN for survivor ISGs. The image was generated using the Interferome v2.01 "IFN Type" tool.

Several additional DEGs associated with RLR and JAK/STAT signaling were upregulated in treated survivors, but failed to meet the FDR threshold. These included IFIT3, IFIT1, MDA-5, and IFIT5 genes (descriptions and statistics are in Table 6). The IFNGR1 gene encodes the ligand-binding chain of the IFN-gamma receptor. IL23A encodes a subunit of IL-23, and shares a subunit with IL-12. IL-12 and IL-23 share numerous functions, including activation of STAT4 and IFN-gamma production; however, IL-23 stimulates memory rather than naive T cells [202]. A former study indicated IL-23A was down-modulated in MARV-Angola infected monkeys [129], suggesting this cytokine might assist in protection. Collectively, these data indicate survival is associated with early innate immune signaling and a Th1 (IFN-gamma) gene profile.

Gene	logFC	P-value	FDR	Description
IFIT3	3.15	9.23E-05	5.97E-02	Interferon-induced protein with tetratricopeptide repeats 3
LGP2	2.76	2.50E-03	5.33E-01	Putative ATP-dependent RNA helicase (DHX58)
IFIT5	2.52	2.50E-03	5.33E-01	Interferon-induced protein with tetratricopeptide repeats 5
IFNGR1	2.18	9.00E-04	3.05E-01	Interferon gamma receptor 1
MDA-5	1.94	1.00E-03	3.23E-01	<i>Macaca mulatta</i> interferon induced with helicase C domain 1 (IFIH1)
IFIT1	1.90	1.00E-04	6.73E-02	Interferon-induced protein with tetratricopeptide repeats 1
IL23A	1.70	1.00E-04	6.59E-02	Interleukin-23 subunit alpha

Table 6. List of antiviral and Th1-associated genes linked with early survivor signaling.

These genes had a log-fold change (logFC) > 1.5 and a significant p-value, but did not meet the stringent false discovery rate (FDR) restriction. DEGs were calculated using EdgeR against a pre-challenge baseline.

POOR PROGNOSIS IS ASSOCIATED WITH AN IMMUNOREGULATORY AND TH2 PHENOTYPE

In fatals, fewer transcriptional variations were observed at mid-disease (Figure 12A). Some upregulated genes encoded for sex determining region Y-box 17 (SOX17), a transcriptional regulator associated with Wnt signaling-specific cell fate specification and

differentiation [203]; insulin receptor substrate 2 (IRS2), a signaling molecule that mediates the effects of insulin and may control cellular processes [204]; and hyaluronan synthase 1 (HAS1), which is implicated in TGF-beta signaling and wound healing. This protein indirectly enhances binding of SMAD3 by interacting with the leukocyte receptor CD44 [205, 206]. Binding of CD44 to the LGALS9 receptor promotes FOXP3 expression and Treg suppressive function [207]. Although SOX17 and IRS2 are constituents of the interferome, these genes are typically downregulated in the IFN response [187]. These results hint at delayed or suppressed activation of the innate immune response in non-survivor monkeys at mid-infection.

Due to the abundance of DEGs at terminal disease for the fatal dataset, gene enrichment was performed using MetaCore™ to identify key modulated pathways (Table 7). A heatmap of the most highly upregulated and downregulated DEGs is illustrated in Supplementary Figure 4. While many comprehensive network analysis tools exist for OMICS data including the popular Ingenuity Pathway Analysis and Panther programs, MetaCore™ has the most comprehensive curated database with >1.7 million molecular interactions, >1600 pathway maps, and >230,000 gene-disease associations. Therefore, we thought this software would be more capable of identifying potential biomarkers and immune pathways associated with poor outcome to MARV-Angola disease.

Selected down-modulated pathways and GO associations in fatal cases included dendritic cell migration, TLR, NFkB, IL-12 signaling, and CXCR4 signaling (Table 7). CXCR4 is potent chemokine for lymphocytes [208]. Expression of transcripts mapping to April and Baff signal transduction were also decreased. The proteins April and Baff promote differentiation and proliferation of B cells and augment immunoglobulin production [209]. Consequently, downregulation of these pathways may have interfered with T-cell chemotaxis and antibody production in these animals. Downregulation of IL-

12 signaling was an interesting finding as this cytokine drives Th1 differentiation, and we did not detect prototypical Th1 cytokine IL-2 or IFN-gamma reads in non-survivors at late disease.

Enrichment Pathway	Up/Down-Regulation	Metacore Enrichment Type	P-value	FDR
dendritic cell migration	Down	GO Processes	1.66E-04	5.51E-03
TRIF-dependent toll-like receptor signaling pathway	Down	GO Processes	2.69E-04	7.75E-03
MyD88-dependent toll-like receptor signaling pathway	Down	GO Processes	4.98E-04	1.14E-02
positive regulation of innate immune response	Down	GO Processes	5.55E-04	1.24E-02
interleukin-12-mediated signaling pathway	Down	GO Processes	1.21E-03	1.93E-02
cellular response to interleukin-12	Down	GO Processes	1.21E-03	1.93E-02
response to interleukin-12	Down	GO Processes	1.33E-03	2.06E-02
Apoptosis and survival_APRIL and BAFF signaling	Down	Pathway Maps	1.09E-04	2.56E-02
Signal transduction_NF-kB activation pathways	Down	Pathway Maps	3.13E-04	3.29E-02
Immune response_HSP60 and HSP70/TLR signaling pathway	Down	Pathway Maps	3.90E-04	3.29E-02
Immune_response_TLR2_and_TLR4 signaling pathways	Down	Pathway Maps	9.92E-04	4.42E-02
Chemotaxis_CXCR4 signaling pathway	Down	Pathway Maps	1.33E-03	4.88E-02
apoptotic process	Up	GO Processes	4.89E-17	1.97E-15
cell death	Up	GO Processes	1.62E-16	6.29E-15
Signal transduction_WNT signaling	Up	Pathway Maps	1.68E-10	8.89E-09
response to wounding	Up	GO Processes	1.21E-09	2.30E-08
response to transforming growth factor beta	Up	GO Processes	3.63E-09	6.57E-08
calcium-mediated signaling	Up	GO Processes	7.40E-08	1.09E-06
NF-AT signaling in cardiac hypertrophy	Up	Pathway Maps	6.13E-08	1.46E-05
Protein folding and maturation_POMC processing	Up	Pathway Maps	6.63E-08	1.46E-05
transforming growth factor beta receptor signaling pathway	Up	GO Processes	7.81E-06	7.84E-05
Ca(2+)-dependent NF-AT signaling in cardiac hypertrophy	Up	Pathway Maps	4.43E-06	2.07E-04
Chemotaxis_Inhibitory action of lipoxins on IL-8- and Leukotriene B4-induced neutrophil migration	Up	Pathway Maps	4.46E-06	2.07E-04
Development_TGF-beta-dependent induction of EMT via SMADs	Up	Pathway Maps	6.93E-06	2.78E-04
Development_WNT5A signaling	Up	Pathway Maps	8.96E-06	3.16E-06
Immune response_Function of MEF2 in T lymphocytes	Up	Pathway Maps	3.54E-05	9.54E-04
Immune response_IL-6 signaling pathway via JAK/STAT	Up	Pathway Maps	9.34E-05	1.68E-03

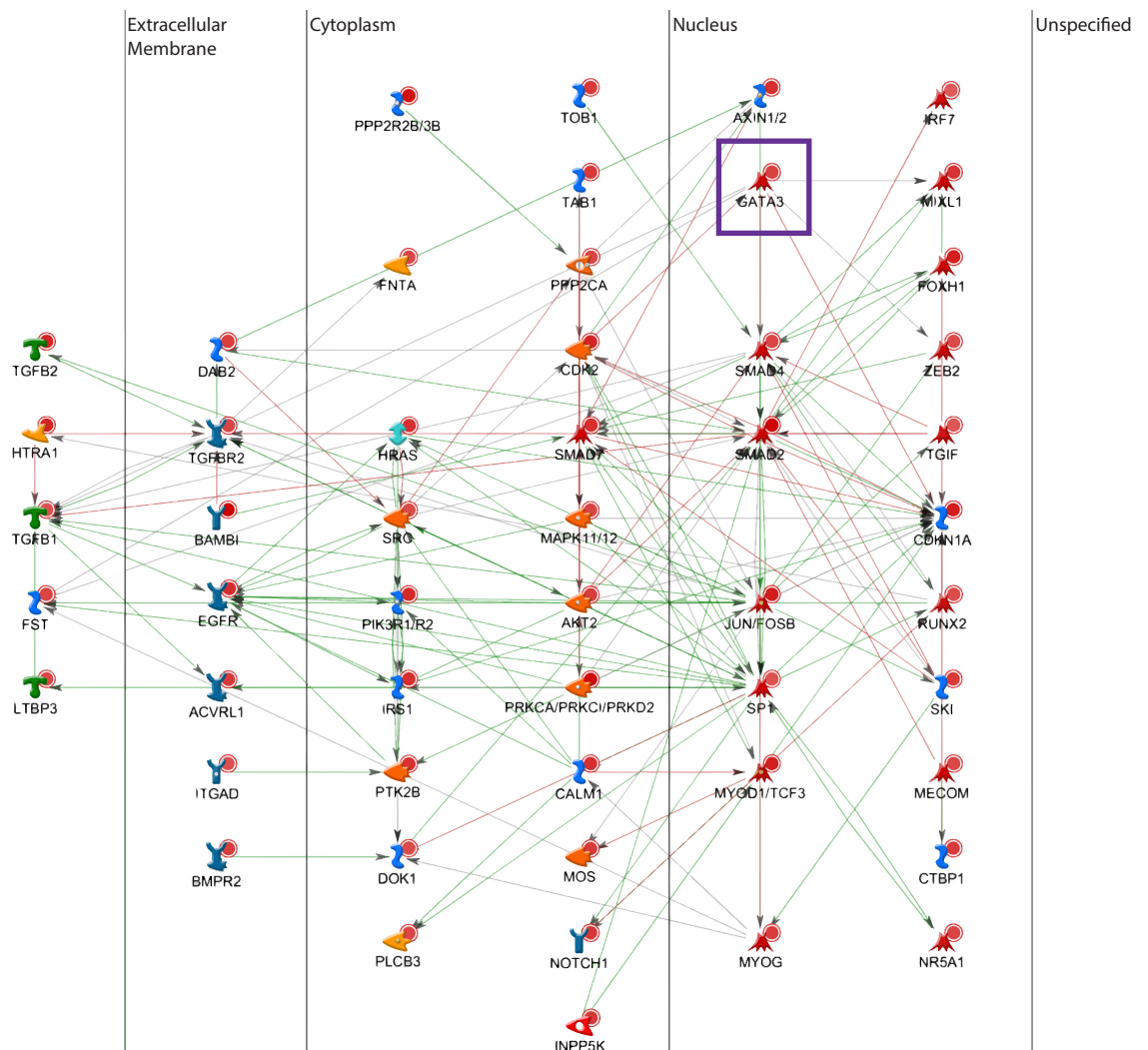
response to interleukin-7	Up	GO Processes	2.45E-04	1.70E-03
Immune response_Platelet activating factor/PTAFR pathway signaling	Up	Pathway Maps	1.17E-04	1.85E-03
Role of Tissue factor-induced Thrombin signaling in cancerogenesis	Up	Pathway Maps	1.56E-04	1.96E-03
Development_TGF-beta receptor signaling	Up	Pathway Maps	1.70E-04	2.08E-03
Immune response_C3a signaling	Up	Pathway Maps	1.87E-04	2.26E-03
interleukin-7-mediated signaling pathway	Up	GO Processes	4.41E-04	2.85E-03
Immune response_IL-4 signaling pathway	Up	Pathway Maps	4.58E-04	4.08E-03
Immune response_IL-5 signaling via JAK/STAT	Up	Pathway Maps	6.15E-05	4.92E-03
Immune response_IFN-alpha/beta signaling via MAPKs	Up	Pathway Maps	7.60E-04	5.77E-03
Cell adhesion_Platelet aggregation	Up	Process Networks	1.84E-03	1.12E-02
Immune response_IL-4-induced regulators of cell growth, survival, differentiation and metabolism	Up	Pathway Maps	2.22E-03	1.27E-02
Immune response_CRTH2 signaling in Th2 cells	Up	Pathway Maps	2.23E-03	1.27E-02
Immune response_IFN-alpha/beta signaling via PI3K and NF-kB pathways	Up	Pathway Maps	2.48E-03	1.38E-02
calcineurin-NFAT signaling cascade	Up	GO Processes	3.76E-03	1.77E-02
regulation of phagocytosis	Up	GO Processes	3.83E-03	1.80E-02
Proliferation_Positive regulation cell proliferation	Up	Process Networks	3.44E-03	1.86E-02
regulation of CD8-positive, alpha-beta T cell extravasation	Up	GO Processes	4.47E-03	2.05E-02
Immune response_CCL2 signaling	Up	Pathway Maps	6.68E-03	2.55E-02
regulation of T cell migration	Up	GO Processes	6.15E-03	2.64E-02
regulation of alpha-beta T cell differentiation	Up	GO Processes	9.57E-03	3.88E-02
Normal and pathological TGF-beta-mediated regulation of cell proliferation	Up	Pathway Maps	1.33E-02	4.13E-02
Immune response_Inhibitory PD-1 signaling in T cells	Up	Pathway Maps	1.37E-02	4.17E-02

Table 7. Enrichment analysis of fatal group DEGs at terminal disease reveals a Th2 and tolerogenic gene signature.

Selected enrichment terms listed were acquired using MetaCoreTM software (Thomson Reuters). Only protein-coding human homologs were included in these analyses. Blue-shaded regions are downregulated, whereas red-shaded regions are upregulated. Abbreviations: FDR (false discovery rate-adjusted p-value); GO (gene ontology).

Gene enrichment for upregulated pathways was characterized by TGF-beta, Wnt, nuclear factor of activated T-cells (NFAT), and programmed cell death signaling. A Th2 signature was also notable based on upregulation of IL-4, IL-5, and chemoattractant receptor-homologous molecule expressed on T-helper type 2 cells (CRTH2) pathways.

CRTH2 is considered a dependable marker for the detection of circulating Th2 cells and stimulates chemotaxis of these cells [210]. TGF-beta is a multifunctional cytokine that can inhibit T- and B-cell proliferation and responsiveness, induce apoptosis, and drive Treg differentiation [211]. Therefore, TGF-beta primarily serves an immunosuppressive or anti-inflammatory role in response to inflammatory processes. A process network map of the “Signal Transduction_TGF-beta, GDF and Activin signaling” pathway is illustrated in Figure 14. As depicted, numerous TGF-beta-related genes, such as TGFB1, TGFB2, and TGFBR2, were upregulated, along with the master regulator transcription factor for Th2 cells, GATA3 [212].



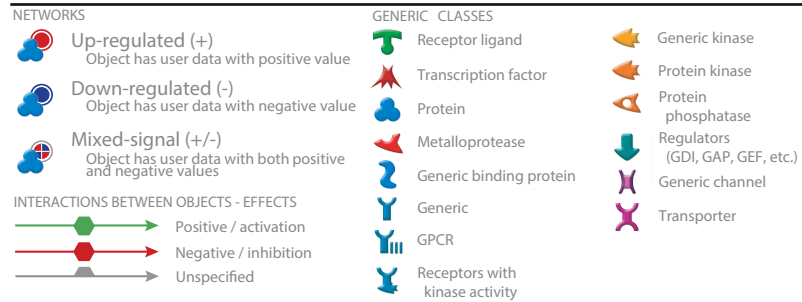


Figure 14. Process network map illustrating direct interactions of DEGs upregulated in the fatal group late in disease that map to “Signal Transduction_TGF-beta, GDF and Activin signaling”.

TGF-beta and related molecules were upregulated in non-survivors. Differentially expressed genes (DEGs) were calculated using EdgeR against a pre-challenge baseline. The network image was created using MetaCore (Thomson Reuters). Note the nuclear expression of GATA3 (the master regulator transcription factor for Th2 cells) boxed in purple. FDR-adjusted p-value for pathway: 1.281E-3.

The Wnt gene family includes a diverse group of lipid-modifying signaling glycoproteins that mediate embryonic development, cell-fate specification, tissue homeostasis, and hematopoiesis [213]. There is also increasing evidence to suggest a regulatory function of Wnt in inflammation, cancers, and infectious diseases. Two highly expressed DEGs in the fatal dataset encoded for the Wnt proteins, Wnt5A (WNT5A; 5.99 logFC; FDR: 3.07E-04) and Wnt6 (WNT6; 7.78 logFC; FDR: 7.77E-05). The “Signal transduction_WNT signaling” and “Development_WNT5A signaling” pathways were also significantly upregulated, with an FDR of 8.89E-09 and 3.16E-06, respectively (Table 7).

Wnt5a was shown to promote the differentiation of DCs to a tolerogenic state. Zhao and colleagues described that increased paracrine Wnt5a-β-catenin-associated metabolic signaling in melanoma cells led to fatty acid oxidation in DCs, thereby increasing indoleamine 2,3-dioxygenase-1 (IDO) activity and decreasing IL-12 expression [214]. Enhanced IDO activity also suppressed effector T-cell activation and

directed successive recruitment of Tregs. Another study suggested that instead Tregs reprogram DC to regulate their function and maturation via increased expression of Wnt5a and attenuation of the NFkB signaling pathway [215]. Treg-conditioned DC secreted less IL-12 and IL-10, and only expressed intermediate levels of costimulatory molecules such as CD80, CD83, and CD86 compared to fully mature DC.

Wnt6 acts on neighboring macrophages to induce proliferation and polarization toward an anti-inflammatory M2 phenotype [216]. IL-4 or IL-13 can also promote macrophages to this alternatively activated state. Schaale et al. discovered the principal source of Wnt6 in granulomatous lesions of *Mycobacterium tuberculosis*-infected mice was foamy macrophages, and expression of this protein reduced TNF-alpha production and increased arginase-1 expression [217].

Provided we observed IL-4 signaling and downmodulation of IL-12 and NFkB pathways in fatal cases, it is possible MARV-Angola proteins interacted with Wnt proteins to foster an immunoregulatory transcriptional program which advanced disease. Other viruses such as influenza, Hepatitis B virus, and certain bunyaviruses, are known to manipulate the host Wnt network to enhance immune evasion and replication [218, 219, 220].

Also upregulated in fatal cases were transcripts mapping to NFAT-calcineurin signaling. The NFAT family of transcription factors consists of 5 members: NFAT1 (NFATp or NFATc2), NFAT2 (NFATc or NFATc1), NFAT3 (NFATc4), NFAT4 (NFATx or NFATc3), and NFAT5 [221]. With the exception of NFAT5 (which is activated by osmotic stress), these proteins are regulated by calcium signaling and play an important role in T-cell development and function, among other cellular processes [221, 222, 223, 224]. Calcineurin directly interacts with NFAT proteins in the presence of

calcium through a conserved motif to dephosphorylate NFAT, resulting in its translocation into the nucleus and transcription of genes [222, 223].

NFAT transcription factors cooperate with STAT proteins to induce cytokine expression and lineage-specific genes within T-cells. For Th1 development, NFAT proteins interact with STAT4 in response to IL-12 receptor engagement to induce IFN-gamma signaling [221]. In turn, IFN-gamma receptor signaling augments STAT1 expression, driving T-bet expression. In contrast, Th2 development is stimulated by the coordination between MAF, NFAT and STAT3/STAT6 proteins to induce the expression of IL-4 and GATA3 expression. Positive-feedback loops maintain expression of the master regulators, T-bet and GATA3. The specific NFAT proteins that dictate Th1 or Th2 cell fate remain controversial, possibly due to whether certain costimulatory molecules are present or absent during T-cell activation.

As mentioned in a previous section, MARV *in vitro* infection of monocyte-derived dendritic cells results in lack of a fully mature activation profile [80]. Suboptimal or prolonged antigen exposure in the absence of adequate T-cell costimulation (e.g. CD28:CD80/CD86 interactions) can cause a gradual loss of T-cell effector functions, with a concurrent rise in expression of inhibitory receptors on these cells [223]. This is known as T-cell exhaustion. One of the hallmarks of this condition is a loss of IL-2 expression and the inability to proliferate in response to antigenic stimuli that ordinarily activate naïve T-cells [222]. Some inhibitory receptors of exhaustion include programmed death receptor 1 (PD-1), lymphocyte activation gene 3 (LAG-3), and cytotoxic T lymphocyte antigen 4 (CTLA-4). Ligands for these molecules include programmed death ligand 1 and 2 (PDL-1/PDL-2), MHC-II, and CD80/CD86, respectively [222, 223]. In fatal monkeys, the “Immune response_Inhibitory PD-1 signaling in T cells” pathway was upregulated (FDR: 4.17E-02) (Table 7), along with

PD-1 (3.09 logFC; FDR: 1.69E-02) and LAG-3 (4.17 log FC; FDR: 1.84E-03) genes. CTLA-4 expression slightly increased (1.21 log FC), but did not meet the ≤ 0.05 FDR threshold for statistical significance. T-cell exhaustion may play a role in filovirus pathogenesis since Ruibal and others showed that CD4⁺ and CD8⁺ T-cells from human survivors during the 2014 EBOV outbreak in West Africa had lower expression of the inhibitory receptors PD-1 and CTLA-4, and immunosuppressive IL-10, compared to non-survivors [225]. Type I IFN is considered a master regulator of IL-10 and the PD-1:PD-L1 axis, and also initiates exhaustion [226, 227, 228, 229, 230]. Blockade of IFN with a monoclonal antibody directed at the IFNAR ameliorated the amounts of IL-10 and PD-1/PD-L1 in treated mice, restored effector T-cell function, and reduced viral titers in a model of chronic Lymphocytic choriomeningitis virus (LCMV) infection [229, 230]. Attenuation of the IFN response also rescued splenic architecture to enable DC: T-cell interactions. Granted the “Immune response_IFN-alpha/beta signaling via PI3K and NF-kB” pathway was significantly upregulated late in disease (FDR: 1.38E-02), dampening the IFN response might represent a potential avenue for ameliorating MVD.

The molecular mechanisms that steer T-cell exhaustion are not fully understood; however, NFAT interactions can facilitate this transcriptional program in the absence of cooperation with its main binding partner, activator protein 1 (AP-1), or without appropriate costimulatory molecules [221]. Noncanonical NFAT complexes with proteins other than AP-1 are thought to direct the tolerogenic signaling cascade. Key regulators of NFAT-associated T-cell anergy/exhaustion were differentially expressed in non-survivors, including the ubiquitin ligases Cbl, Itch, NEDD4, and Grail (Table 8). Cbl, Nedd4, and ITCH interfere with T-cell receptor (TCR) signaling, whereas GRAIL disrupts CD40 ligand signaling and costimulatory pathways [224, 231]. The contribution of specific NFAT proteins to T-cell tolerance has not been fully elucidated, but some

evidence suggests that NFAT1 and NFAT4 are responsible, while NFAT2 may have the opposite function [221].

Other genes implicated in T-cell anergy and exhaustion include IRF4, EOMES, STAT3, GATA3, Blimp-1, FOXP1, IL-6, and T-bet [221, 222, 224]. Some genes in this list are seemingly contradictory as they can also enhance Th1 effector function and memory. For example, EOMES and T-bet help promote Th1 polarization and enhance the cytotoxic activity of CTLs. On the contrary, these transcription factors contribute to and sustain the pool of exhausted CD8⁺ T-cell progenitors. Two progenitor subsets exist: a smaller T-bet^{hi}+PD-1^{mid} subpopulation with some proliferative ability and a larger subpopulation of EOMES^{hi}PD-1^{hi} cells with limited proliferative ability, weak cytokine secretion, and high expression of inhibitory receptors [222]. However, cytolytic activity of CTLs for the latter subset remains intact. Persistent antigen shifts the progenitor pool toward the EOMES^{hi}PD-1^{hi} phenotype. A ratio in favor of EOMES (logFC 3.48; FDR: 2.00E-03) over T-bet (logFC 1.89; FDR: 6.52E-03) in fatal cases may have thus contributed to the loss of transcripts that encode for the Th1 cytokines, IL-2 and IFN-gamma. This phenotype may have also promoted PD-1 expression.

Genes Implicated in Anergy/Exhaustion	logFC	P-value	FDR
Cbl	5.86	2.25E-07	1.11E-04
GRAIL (RNF128)	4.60	2.03E-04	2.63E-03
NFAT1 (NFATp or NFATc2)	4.58	6.25E-06	4.08E-04
IRF4	4.17	1.06E-04	1.81E-03
LAG-3	4.17	1.10E-04	1.84E-03
EOMES	3.48	1.28E-04	2.00E-03
NFAT 3 (NFATc4)	3.10	1.22E-03	8.25E-03
PD-1 (PDCD1 locus)	3.09	3.53E-03	1.69E-02
STAT3	3.08	3.62E-04	3.76E-03
GATA3	3.02	4.36E-03	1.95E-02
NFAT4 (NFATx or NFATc3)	2.96	1.04E-03	7.45E-03
Blimp-1 (PRDM1)	2.80	9.82E-03	3.40E-02

FOXO1	2.66	1.34E-03	8.75E-03
IL-6	2.52	1.29E-02	4.11E-02
ITCH	2.31	2.17E-02	5.88E-02
NEDD4	2.30	6.70E-03	2.61E-02
TGF-beta (TGFB1)	2.23	3.29E-03	1.60E-02
NFAT2 (NFATc or NFATc1)	2.06	3.30E-03	1.60E-02
T-bet (Tbx21)	1.89	2.51E-02	6.52E-02
Th1 Cytokine Genes	logFC	P-value	FDR
IL-2	No reads		
IFNG	No reads		

Table 8. Upregulated DEGs associated with T-cell anergy and exhaustion in the fatal dataset at late disease.

Selected enrichment terms listed were acquired using EdgeR. Only protein-coding human homologs were included in these analyses. FDR values highlighted in yellow indicate statistically significant upregulation of each specific DEG. Abbreviations: DEG (differentially-expressed gene); logFC (log fold-change); FDR (false discovery rate-adjusted p-value).

A PREDOMINANCE OF TH2 AND CD8+ T-CELL TRANSCRIPTS, AND DOWN-REGULATION OF B-CELL MEMORY AND STIMULATED MONOCYTES CORRELATE WITH MARV LETHALITY

To view the distribution of DEGs induced in the fatal dataset across immune cell populations, we performed digital cell quantification (DCQ) analysis using ImmQuant [188, 189]. This software predicts human cell subset quantities based on transcriptional signatures. RNAseq reads at late-disease were compared to a pre-challenge baseline. Most notably, increased cell-type quantities in non-survivors were associated with late-differentiated Th2 and CD8+ T-cell phenotypes (Figure 15). A Th2 signature was anticipated given the extensive IL-4, IL-5, and CRTH2 signaling observed with MetaCore pathway analysis; however, the increase in CD8+ T-cells was unexpected. For downregulated cell subsets, a decrease in expression was noted in B-cell memory IgG and IgA and early-stimulated monocyte populations. This was also predicted since certain B-cell receptor signaling and antigen presentation pathways were down-modulated in this group. When the fatal dataset was restructured to include only untreated controls at the

same disease stage, we detected significantly decreased Th1 and stimulated monocyte/DC quantities (Supplementary Figure 5).

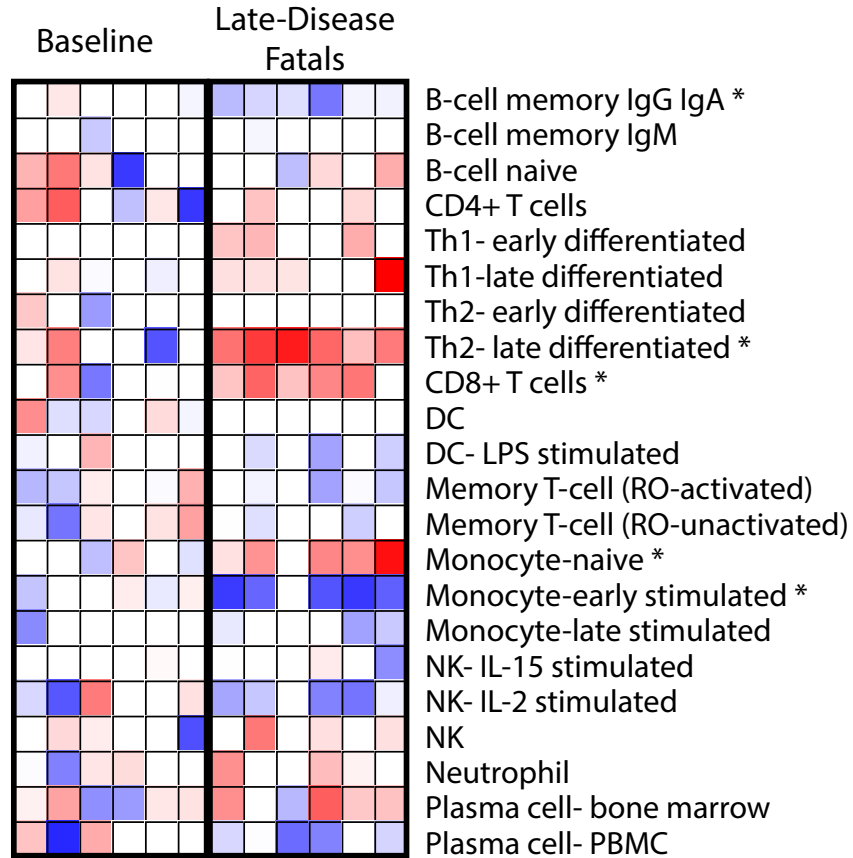


Figure 15. ImmQuant heatmap analysis of the relative contribution of immune cell subsets to differential gene expression within the fatal group.

*We observed an increase in activated Th2 and CD8+ T-cells, and a decrease in B-cell memory IgG/IgA and activated monocyte populations. ImmQuant uses a database based on genome-wide microarray expression profiling of human immune cells from reported studies. Results were calculated using the IRIS algorithm that uses human-based FACS marker genes. The algorithm infers an increase (red) or decrease (blue) in cell-type quantities relative to a pre-challenge baseline. The FDR and p-value were set at ≤ 0.05 and values were based on RPKM expression values for each gene for each sample. Survivors were excluded from the analysis due to the scarcity of DEGs for this dataset. *: Statistically significant putative changes in the cell subset frequency.*

SURVIVOR RESPONSES ARE TH1-SKEWED, WHEREAS FATALS EXHIBIT AN UNPROTECTIVE CYTOTOXIC CD8+T-CELL AND IMMUNOSUPPRESSIVE PHENOTYPE

To confirm whether our sequencing results and related cell subset projections were reflected in the blood compartment, we performed flow cytometry on PBMC from infected macaques. In survivors, the CD8+/CD4+ T-cell ratio remained relatively consistent over the course of the study (except for one outlier corresponding to the sole treated animal that became ill: ΔG Survivor 5) (Figure 16A). In contrast, our results confirmed fatal monkeys had a greater proportion of circulating CD8+ T-cells at late-disease. While we detected degranulating CD8+ T-cells in survivor PBMC, a more substantial quantity was found in fatal cases (Figure 16B).

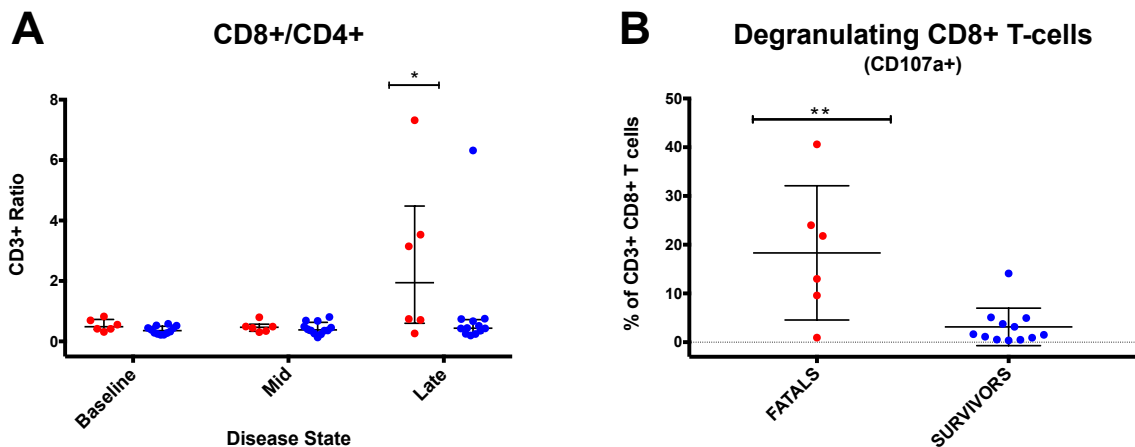


Figure 16. CD8+/CD4+ T-cell ratio and percentage of degranulating CD8+ T-cells in PBMC.

*Non-survivors have a higher CD8+/CD4+ ratio and more degranulating CD8+ T-cells. Stained cell samples were analyzed using a FACS Canto II cytometer and FlowJo software. Approximately 200,000 events were acquired. Only live CD3+ (T-cells) were included in the analysis. CD107a is a marker of degranulation. * $p \leq 0.05$, ** $p \leq 0.01$.*

As gene enrichment pointed to pathways involved in the differentiation and expansion of Tregs, and TGF-beta signaling is known to induce the polarization of naïve T-cells to this subset, we determined if these cells were recruited in non-survivors. Normally, Tregs account for 5-10% of circulating T-cells and are responsible for immune

tolerance and prevention of autoimmunity [232]. Our data revealed this cell population increased to up to ~40% of all CD4+ T-cells at the terminal stage in the fatal group for some animals (Figure 17A). As mentioned, Tregs prevent the induction and proliferation of effector T cells; they also secrete copious amounts of IL-10 and TGF-beta. Th1 cells are thought to correlate with immunity to MARV. Thus, we performed ICS on CD4+ T-cells to see whether a Th1 response was induced in survivors and to determine if Treg recruitment reduced cytokine secretion of this Th subset in fatal cases. We confirmed double positive IL-2- and IFN-gamma-secreting Th1 cells at late disease in surviving animals, but only minute levels in the fatal group (Figure 17B). Since IL-10 is known to down-regulate MHC-II (HLA-DR) expression and is elevated in sepsis [233, 234], we then determined whether antigen presentation was affected by recruitment of Tregs or its effector cytokines. As illustrated in Figure 17C, the mean fluorescent intensity (MFI) of MHC-II was much higher in the survivor versus the fatal group (after values were normalized to a pre-challenge baseline). These data indicate Treg recruitment may enhance disease in MARV-infected monkeys, as these cells can secrete immunosuppressive cytokines, induce apoptosis via TGF-beta signaling, and decrease cytokine release and proliferation of effector T-cells (Figure 17D).

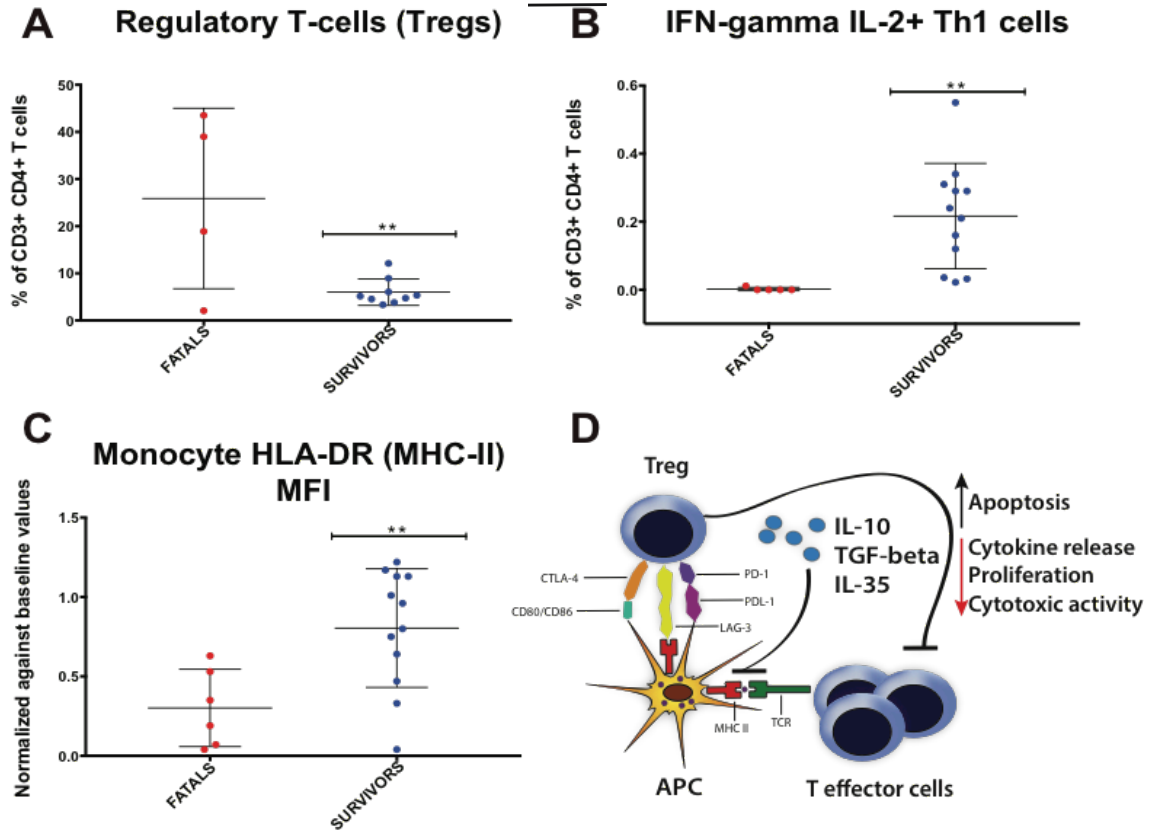


Figure 17. Survivors had a lower percentage of Tregs and more IFN-gamma+ IL-2+ Th1 cells late in disease.

We identified the Treg subset (CD3+CD4+CD25+FOXP3+) in PBMC following an overnight stimulation with phorbol 12-myristate 13-acetate (PMA) and Ionomycin (ION), or a media-only control. Survivors had a lower frequency of Tregs (A) and a higher frequency of IL-2- and IFN-gamma- Th1 cells (B). Th1 cells were surface stained with CD3 and CD4 antibodies before intracellular cytokine staining. PBMC were stimulated with DMSO or an overlapping MARV GP peptide pool (2µg/ml) for 6 hours in the presence of CD28 and CD49d; Brefeldin A protein transport inhibitor was added 2 hours before staining. C) The normalized median fluorescence intensity (MFI) for monocyte HLA-DR (MHC II) expression remained stable in survivor macaques. Monocytes were negatively selected from CD3 (T-cell marker) and CD20 (B-cell marker) populations and positively selected with a CD14 antibody. D) Tregs can suppress the functions of effector T cells via release of inhibitory cytokines such as IL-10, IL-35, and TGF-beta; upregulation of immunosuppressive molecules CTLA-4, LAG-3, and PD-1; and downregulation of antigen presentation. ** $p \leq 0.01$.

Tregs secrete immunosuppressive IL-10 and TGF-beta, and an abundance of TGF-beta isoforms, receptors, and related signaling molecules were upregulated in fatal

macaque blood. Consequently, we measured protein concentration of these cytokines in monkey plasma using multiplex cytokine bead array detection technology. IL-10 levels were elevated at mid- (Figure 18A) and late-disease (Figure 18B) in the fatal group. In line with our sequencing analysis, an increase in TGF-beta was not noted until the terminal stage for non-survivors (Figure 18C-D).

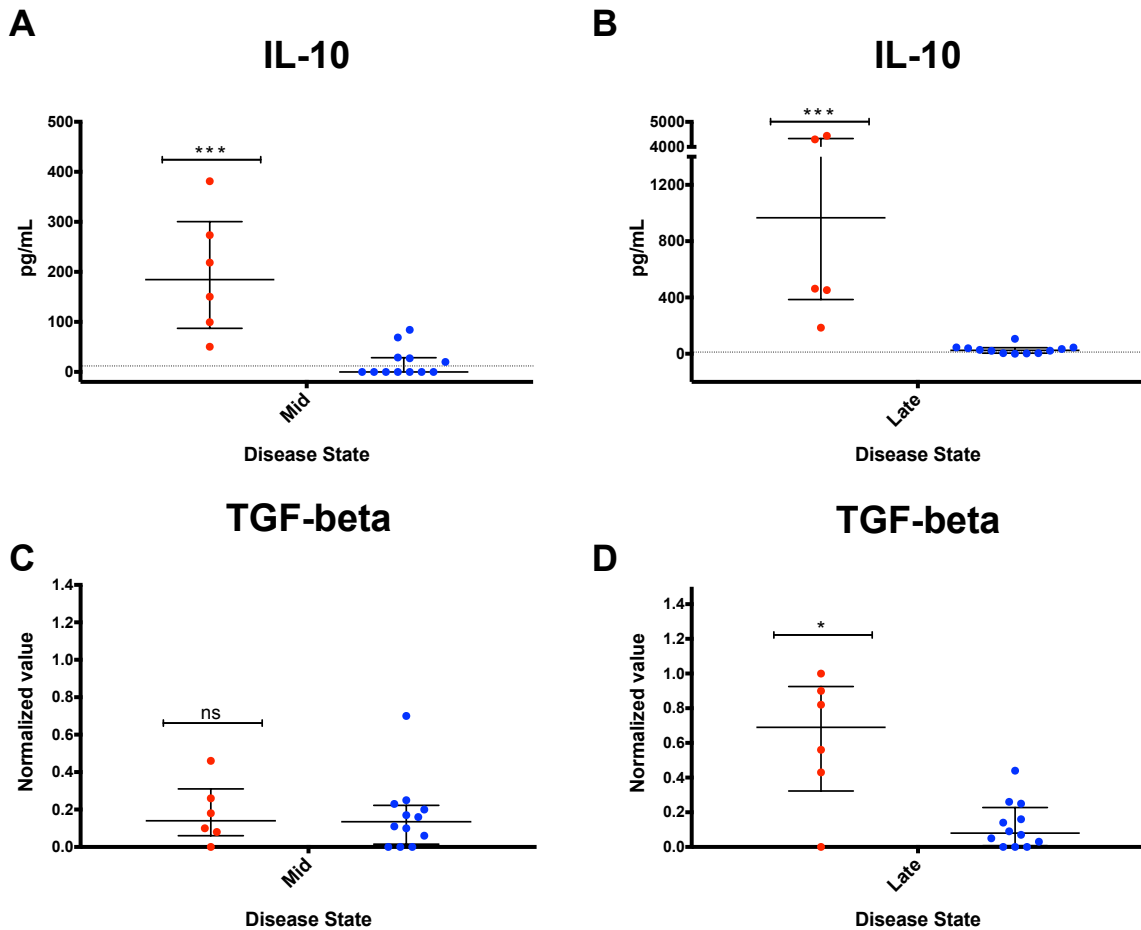


Figure 18. Comparison of concentrations of TGF-beta and IL-10 analytes in the serum of MARV-infected macaques.

*Survivors had lower plasma levels of these cytokines. Increases in IL-10 were observed at A) mid- and B) late-disease, whereas a rise in C) TGF-beta did not occur until late in disease for the fatal group. * $p \leq 0.05$; *** $p \leq 0.001$; ns not significant.*

FATAL CASES ARE ASSOCIATED WITH A LOSS OF TH AND CTL IL-2 EXPRESSION, CONCOMITANT WITH AN INCREASE IN FREQUENCY OF IL-10-SECRETING TREG (CD25+ FOXP3+) AND CD25+ FOXP3- CELLS

Considering numerous genes associated with T-cell anergy and exhaustion were expressed in non-survivors, we next examined shifts of Treg, Th, and CTL populations over the course of infection in these animals. If T-cells are truly “exhausted” in response to MVD, one would expect a weakening of effector function coupled with the expansion of cells with a regulatory capacity. For this evaluation, we tracked the proportion of Tregs at each disease state using flow cytometry. CD3⁺ CD4⁺ T-cell populations were delineated into five groups based on their relative expression of CD25 and FOXP3 (Figure 19A). CD25^{hi} FOXP3⁺ populations are generally recognized as Tregs, while those lacking FOXP3 or CD25 expression are considered conventional or effector T-cells [235]. We observed three FOXP3⁻ populations with no/low (CD25⁻), intermediate (CD25^{int}), and high (CD25^{hi}) expression of CD25. A minor CD25⁻ FOXP3⁺ cell population was designated as “Other”.

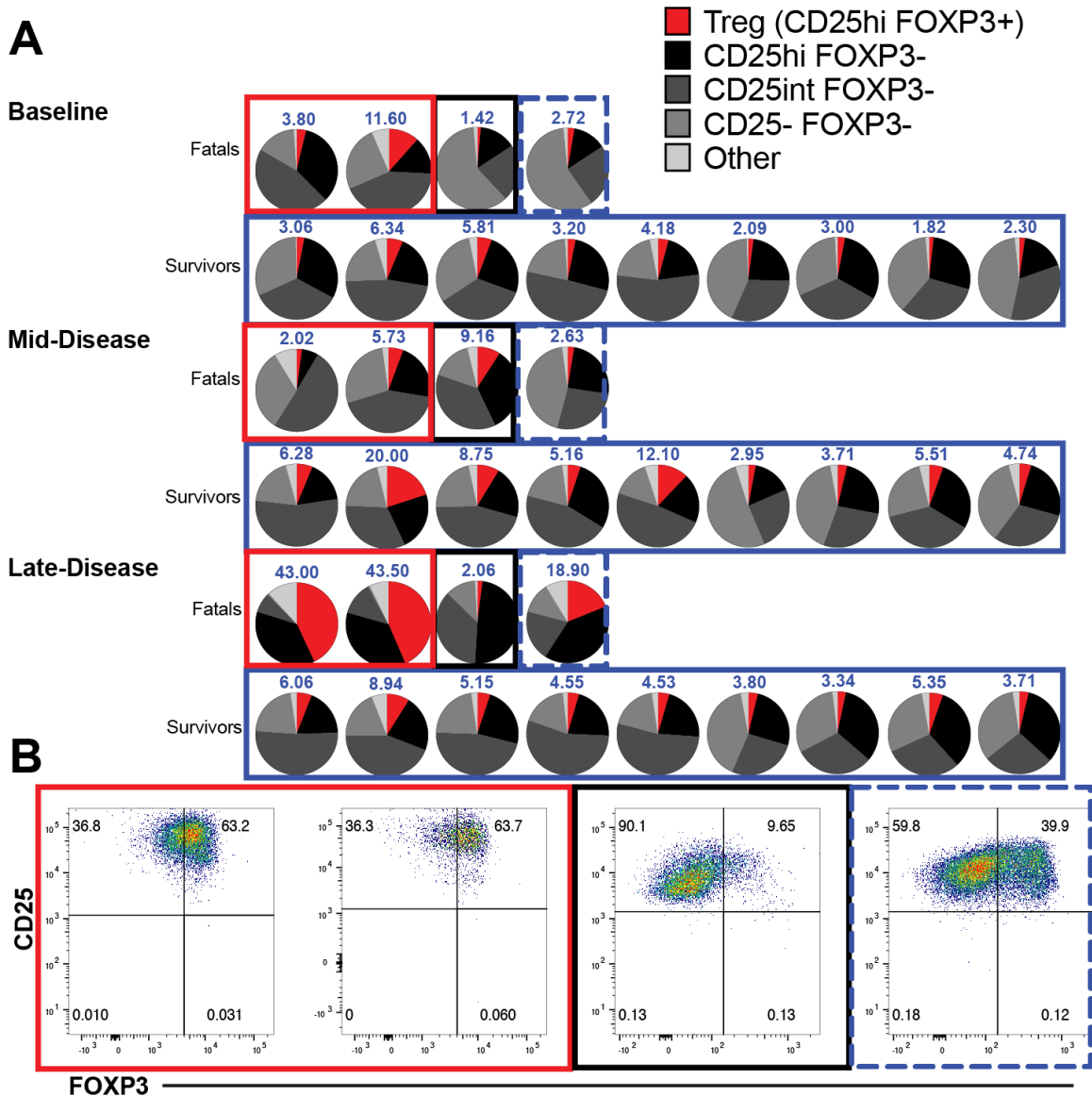


Figure 19. Analysis of shifts in the regulatory T-cells (Treg) population over the course of infection in representative fatal and survivor macaques, and their contribution of IL-10 at late disease.

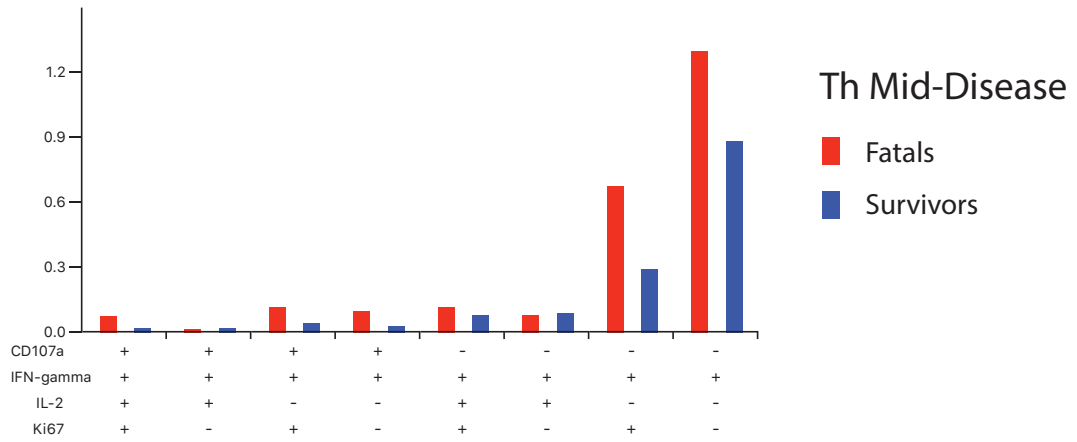
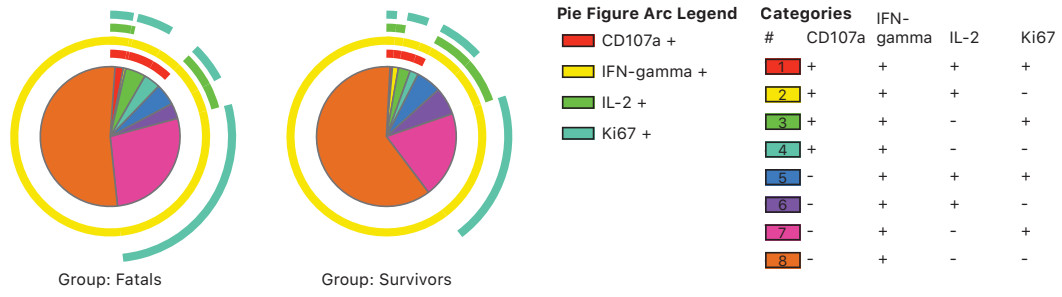
A) Survivors had a relatively stable percentage of Tregs (red slice) over the course of infection, whereas fatals had large fluctuations at mid- and late-disease. The percentage of Tregs is featured above the pie graph for each individual. CD4⁺ T-cells were separated into five groups based on their expression of CD25 and FOXP3. At late disease, the predominant subsets were either Tregs or CD25^{hi} FOXP3⁻ (black slice) populations for fatals. B) The predominant IL-10 producer for the untreated controls was Tregs, whereas the CD25^{hi} FOXP3⁻ population was the main source for the vector control and treated fatal. Boxes: treated survivors (solid blue); untreated controls (red); vector control (black); and treated fatal (perforated blue).

At the baseline, fatal and survivor groups expressed normal amounts of Tregs (Figure 19A). By mid-disease, three of the four featured fatals exhibited a reduction in the percentage of Tregs, whereas survivors had a slight increase in this population. Interestingly, the single treated survivor that showed the most considerable signs of illness had the highest increase (20%) of this cell population at mid-disease. At late-disease, the fatals had a substantial percentage of Tregs (~16-40%), except for the vector control. Instead, the vector control CD4+ T-cell population was mostly characterized by the CD25hi FOXP3- subset and this animal had a ~7% decline of Tregs. The other fatal animals also had a high frequency of the CD25hi FOXP3- subset at the terminal stage.

After scrutinizing all IL-10-producing CD+ T-cell populations in the fatal group, we determined the primary contributors of IL-10 were Tregs and CD25hi FOXP3- cells (Figure 19B). For untreated controls, Tregs were the main producers of IL-10 (~63%). For the vector control and treated fatal, the CD25hi FOXP3- population was the primary source of IL-10 (~60-90%). The function of CD25hi FOXP3- cells has not reached a scientific consensus; however, a few studies have attempted to define some of their characteristics. In a model of acute severe murine spotted fever rickettsiosis, splenic CD25+ FOXP3- T-cells secreted both IFN-gamma and IL-10, and suppressed the proliferation of and IL-2 production by splenic effector T-cells [236]. These cells expressed T-bet and high levels of the inhibitory receptor, CTLA-4. Hence, CD25+ FOXP3-cells might be a mixed pool of effector and regulatory cells or a distinct subset able to secrete both inflammatory and immunosuppressive cytokines. Another possibility is that CD25+ FOXP3- cells represent a particular Treg subset, such as Tr1 cells [237]. These cells exert their suppressive activity via an IL-10 rather than a FOXP3-dependent mechanism [238]. A bona fide marker for Tr1 cells has not yet been identified; nevertheless, these cells are known to secrete TGF-beta, IL-10, and IL-5, and low levels

of effector cytokines [239]. In addition, they express a number of inhibitory receptors, for example, LAG-3.

A



B

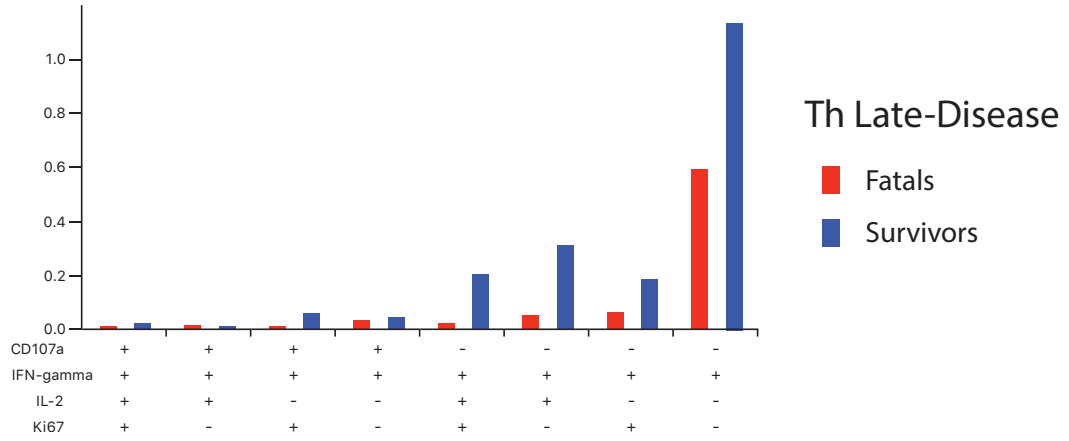
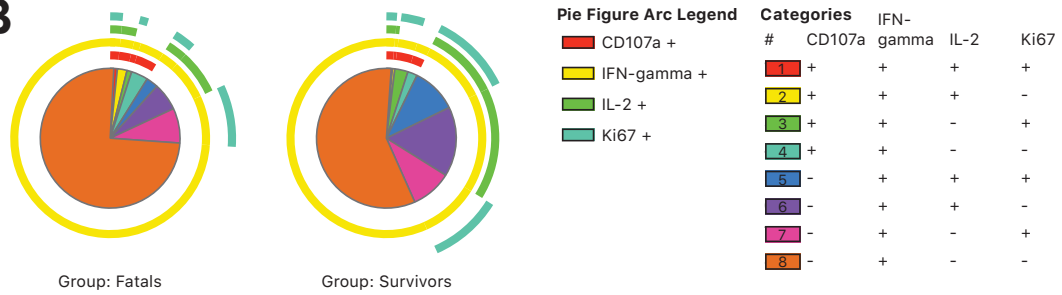


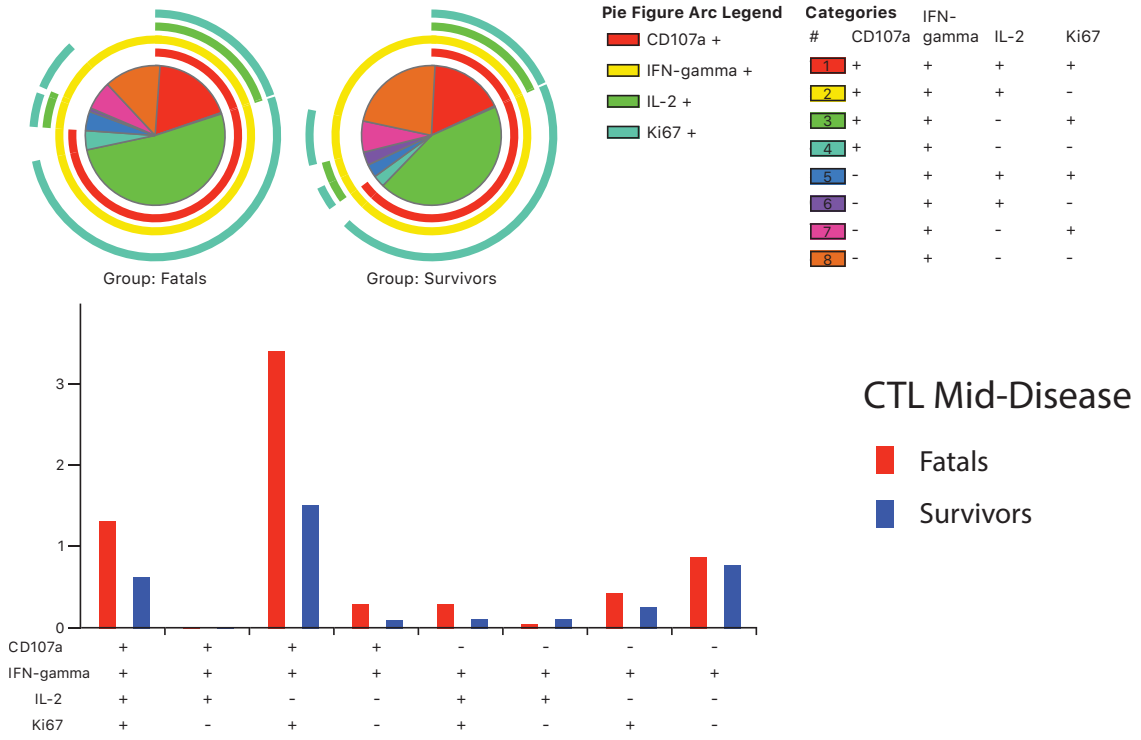
Figure 20. T helper (Th) cell phenotypes in survivors and fatals at mid- and late-disease.

A) Similar phenotypes were observed in fatals and survivors at mid-disease, and both groups had CD3+CD4+ T-cells that secreted IL-2 and IFN-gamma. B) Late-disease in fatals was characterized by a loss of IL-2 expression and limited proliferative ability. Only IFN-gamma+ populations are featured. The various subset phenotypes are denoted by bar and pie graphs. Each slice in the pie graph illustrates the percentage of each subset. CD107a and Ki67 are markers of degranulation and proliferation, respectively. PBMC were stimulated with DMSO or an overlapping MARV GP peptide pool (2µg/ml) for 6 hours in the presence of CD28 and CD49d. Brefeldin A protein transport inhibitor was added 2 hours before staining.

Next, we measured changes in proliferation, degranulation, and polyfunctionality of CD4+ Th1 and CD8+ CTL populations over the course of the study. Phenotypic analysis using SPICE software [240] revealed fatal and survivor T-cells secreted both IL-2 and IFN-gamma at mid-disease for both cell populations, and a similar level of double-positive (IFN-gamma+ and IL-2+) subsets were detected in each group (Figure 20A and Figure 21A). This was unanticipated given MVD is thought to prevent the formation of an adaptive response. For Th1 (IFN-gamma+) cells, the predominant subset was non-proliferative (Ki67-), non-degranulating (CD107-), and IL-2- for both fatal and survivor groups, and a higher percentage was seen in fatal animals (Figure 20A). CTLs appeared more polyfunctional at this disease state compared to the Th population, and more degranulating (CD107+) cells were found (Figure 21A). By the late-disease timepoint, we observed a reduction of Th IL-2-producing cells for the fatal group, and an increase in double-positive cell subsets for the survivors (Figure 20B). A similar trend was observed in CTLs (Figure 21B), although limited polyfunctionality was retained in this population.

A progressive decline in Th1 and CTL effector function for the fatal animals (and an opposite response in survivors) points to an exhaustive phenotype in these animals, possibly precipitated by an increased viral load, transcription of tolerogenic genes, and recruitment of regulatory cells.

A



B

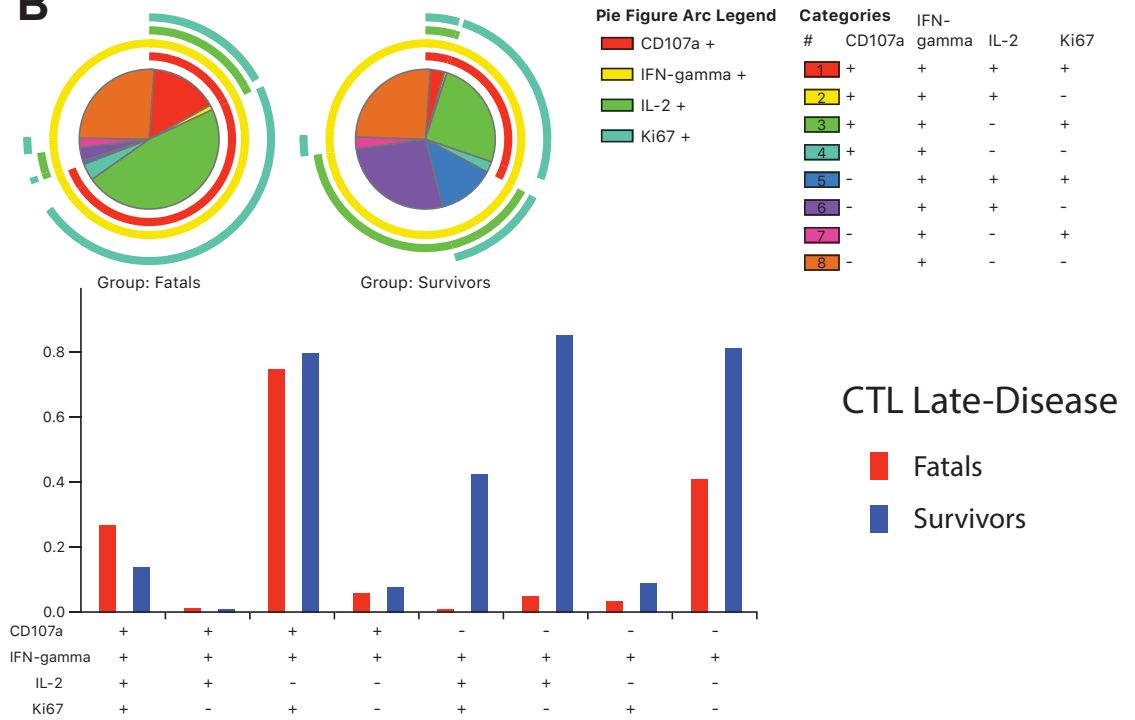


Figure 21. CD8⁺ cytotoxic T-cell (CTL) phenotypes in survivors and fatals at mid- and late-disease.

A) A similar frequency of double-positive (IFN-gamma⁺ IL-2⁺) subsets was observed in fatals and survivors at mid-disease. The frequency of the CD107a⁺ IFN-gamma⁺ IL-2⁺ Ki67⁺ subset appeared slightly higher for the fatal group. B) At late-disease, fatal CTLs had a decline in IL-2 expression and limited proliferative ability, although some polyfunctionality was retained. The various subset phenotypes are denoted by bar and pie graphs. Each slice in the pie graph illustrates the percentage of each subset. CD107a and Ki67 are markers of degranulation and proliferation, respectively. PBMC were stimulated with DMSO or an overlapping MARV GP peptide pool (2µg/ml) for 6 hours in the presence of CD28 and CD49d. Brefeldin A protein transport inhibitor was added 2 hours before staining. CTLs were selected based on their expression of CD3 and CD8. Only IFN-gamma⁺ populations are featured.

MARV-INFECTED PRIMARY HUMAN MONOCYTES EXPRESS LOW LEVELS OF CD80 AND CD86 AND UPREGULATE PDL-1 TO FACILITATE INHIBITORY PD-1 SIGNALING

The suppressive effect of Tregs can be mediated indirectly through the secretion of soluble mediators (i.e. TGF-beta or IL-10), or it can occur via contact-dependent mechanisms [241]. Because we discovered reads mapping to the inhibitory PD-1 cell pathway in the fatal dataset (Table 7) and Tregs maintain PD-1 expression, we next determined whether MARV infection leads to upregulation of inhibitory ligand expression that can facilitate antagonistic receptor interactions. PD-1 is expressed on an assortment of cells, including T-cells, monocytes, dendritic cells, and B-cells [242]. The PD-1 inhibitory ligands, PDL-1 and PDL-2, are typically expressed in APCs but are also expressed in other cell types. Engagement of PDL-1/PDL-2 with a PD-1 receptor transmits a negative signal that inhibits TCR and B-cell receptor (BCR) signaling. This interaction also decreases cytokine production, promotes T-cell exhaustion and dysfunction, and results in the synthesis of IL-10 [243, 244, 245].

For this experiment, we isolated monocytes from three healthy human donors. Monocytes were infected with MARV, rVSVΔG/MARV-Angola-GP, or co-infected at an MOI of 3. Uninfected and LPS-stimulated cells served as negative and positive controls,

respectively. Flow cytometry was performed at 24 and 48 hours post-infection to measure PD-1 and PDL-1 expression, and monocyte activation was determined using the costimulatory markers, CD80 and CD86. Along with TCR: MHC antigen complex signaling, T-cell stimulation occurs by binding of CD80 or CD86 costimulatory ligands on APC to the CD28 receptor. CTLA-4 can also bind CD80 and CD86 with a higher affinity and avidity than CD28, negatively regulating TCR signaling [246]. T-cell activation or inhibition thus depends on the availability of CTLA-4, which can outcompete CD28 for CD80/ CD86 interactions.

Compared to monocytes only infected with rVSV Δ G/MARV-Angola-GP, cells co-infected or only infected with MARV had higher levels of PD-1 and PDL-1 co-expression at 24 hours (Figure 22E). At 48 hours post-infection, approximately 54-71% of MARV- and co-infected monocytes exclusively expressed PDL-1, compared to ~1-7% for cells only infected with rVSV (Figure 22C). No differences were noted between the groups for sole PD-1 expression at either timepoint (Figure 22A). LPS stimulation also resulted in significant increases of these inhibitory molecules (Figures 22A, C, E).

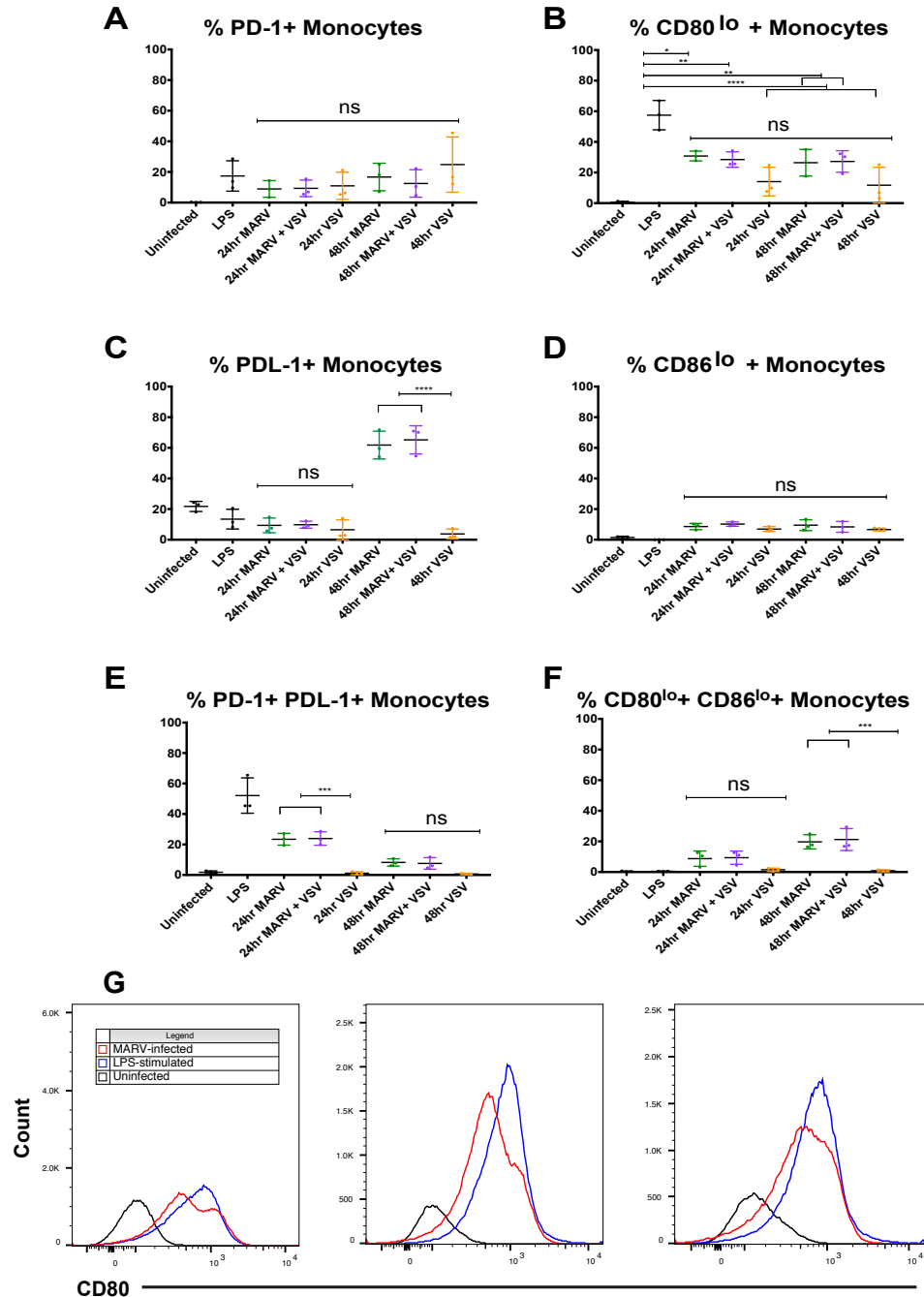


Figure 22. Expression of inhibitory PD-1 and PDL-1, and co-stimulatory CD80 and CD86, molecules in infected human primary monocytes.

Monocytes that were co-infected (MARV+VSV) or only infected with MARV had higher expression of (C) PDL-1, (E) PD-1 and PDL-1 and (F) CD80 and CD86 compared to cells only infected with rVSVΔG/MARV-Angola-GP (written as VSV for the sake of brevity). There were no significant differences in exclusive expression of A) PD-1, B) CD80 and D) CD86 among the infected groups. LPS stimulation resulted in a higher frequency of CD80+ monocytes (B). Histograms of total CD80 expression in uninfected,

*LPS-stimulated, and MARV-infected monocytes for individual donor monocytes is featured in panel G. * $p \leq 0.05$; ** $p \leq 0.01$ *** $p \leq 0.001$; **** $p \leq 0.0001$.*

In terms of activation, all infected monocytes had slight to moderate (lo) upregulation (~3-35%) of CD80 and CD86. There were no significant distinctions between the infected monocyte groups for exclusive expression of CD80 (Figure 22B) or CD86 (Figure 22D) at 24 or 48 hours. However, higher frequencies of CD80+ CD86+ monocytes were observed in the MARV only and co-infected groups at 48 hours post-infection (Figure 22F). Similar to previous reports, monocytes stimulated with LPS only resulted in CD80, not CD86, upregulation [247, 248], and an increased percentage of the CD80+ population was observed in this group compared to MARV, rVSV, or co-infected cells (Figure 22B). CD80 expression in LPS-stimulated versus MARV-infected monocytes was only modestly higher in individual donors (Figure 22G).

These results indicate monocytes express high levels of PD-1 and PDL-1 in response to *in vitro* MARV infection, and are capable of initiating the PD-1: PDL-1 axis. Co-infection of monocytes with rVSV Δ G/MARV-Angola-GP did not appear to attenuate this phenotype.

Recent studies suggest expression of PD-1 on antigen-presenting cells, for example, DCs, impairs their survival and inflammatory cytokine production [243, 244, 245]. Moreover, PD-1-expressing DCs were reported to suppress IL-2 and IFN-gamma production of antigen-specific CTLs [242]. This phenomenon was independent of their expression of other surface signaling molecules, such as CD80, CD86, and CD40. For this reason, it is possible that despite the ability of MARV-infected monocytes to upregulate CD80 and CD86 activation markers, expression of PDL-1 still allows these cells to modulate T-cell function. Infection of monocytes with rVSV Δ G/MARV-Angola-

GP led to low levels of CD80 and CD86 upregulation, but only resulted in negligible PDL-1 expression, which may be critical for stimulation of innate and adaptive immunity.

RVSV POST-EXPOSURE TREATMENT SURVIVAL IS DEPENDENT ON ANTIBODY PRODUCTION

In view of our observed downmodulation of B-cell memory and a pathway involved in B-cell activation and proliferation (as well as the capacity of TGF-beta signaling and Tregs to impair antibody production [249, 250]), we assessed humoral responses via antigen-specific IgM and IgG via ELISAs. For this assay, the serum of monkeys from the high (Figure 23) and low MARV-Angola dose experiments (Figure 24) was monitored. Only treated survivors formed MARV-GP specific antibodies, with the formation of both classes appearing within 6-10 days after treatment (Figures 23 and 24). Low anti-MARV IgM titers (1:100 to 1:1600) generally declined during the convalescent stage (days 21 and 28), conjointly with increasing moderate to high titers of anti-MARV IgG (1:1600 to 1:12800).

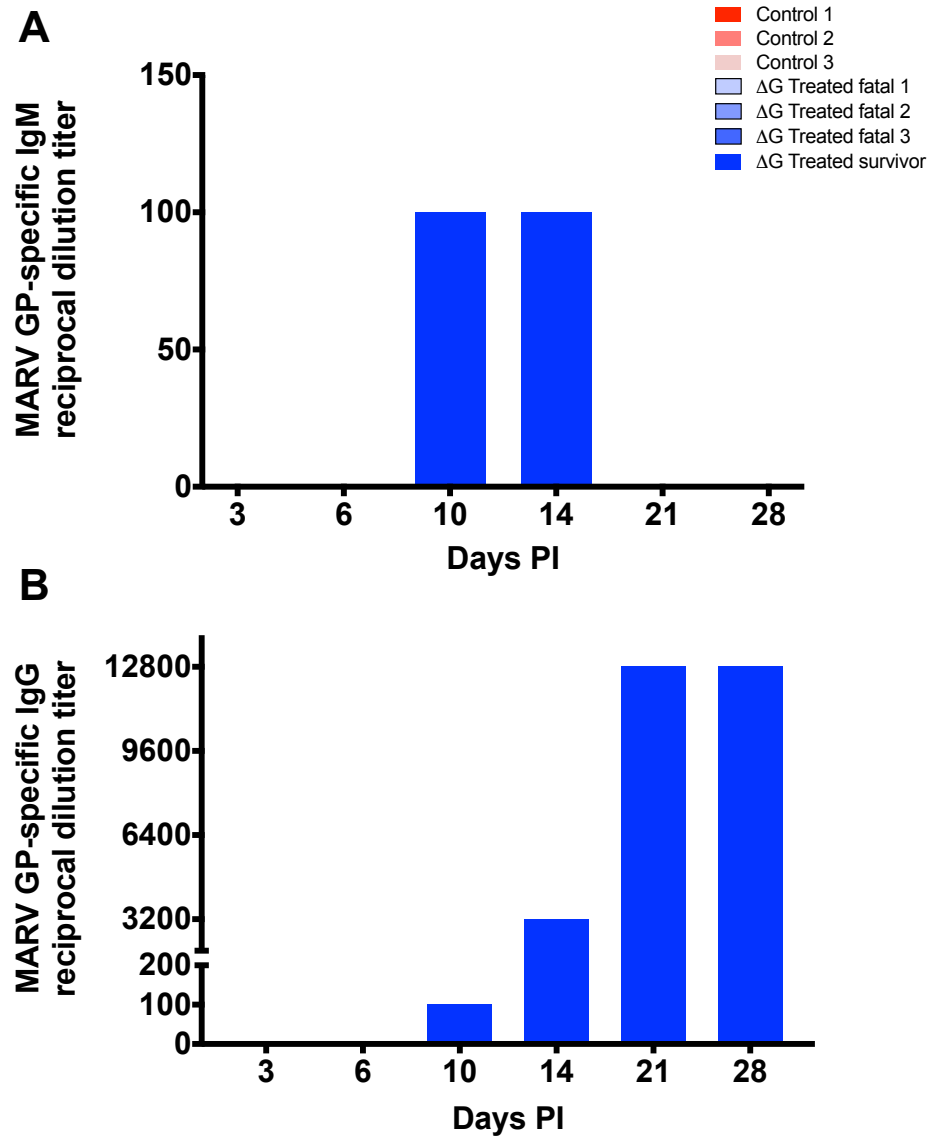


Figure 23. Reciprocal endpoint dilution titers of anti-MARV GP IgM and IgG in the serum of subjects challenged with a high dose MARV-Angola challenge.

Non-survivors were serologically negative. Only MARV GP-specific IgM (A) and IgG (B) titers for the sole survivor are shown and are depicted by blue bars. Abbreviations: MARV (Marburg virus); GP (glycoprotein); ΔG (an animal treated with a rVSV vector expressing a MARV Angola GP in place of the native VSV G); IgM (immunoglobulin M); IgG (immunoglobulin G); PI (post-infection).

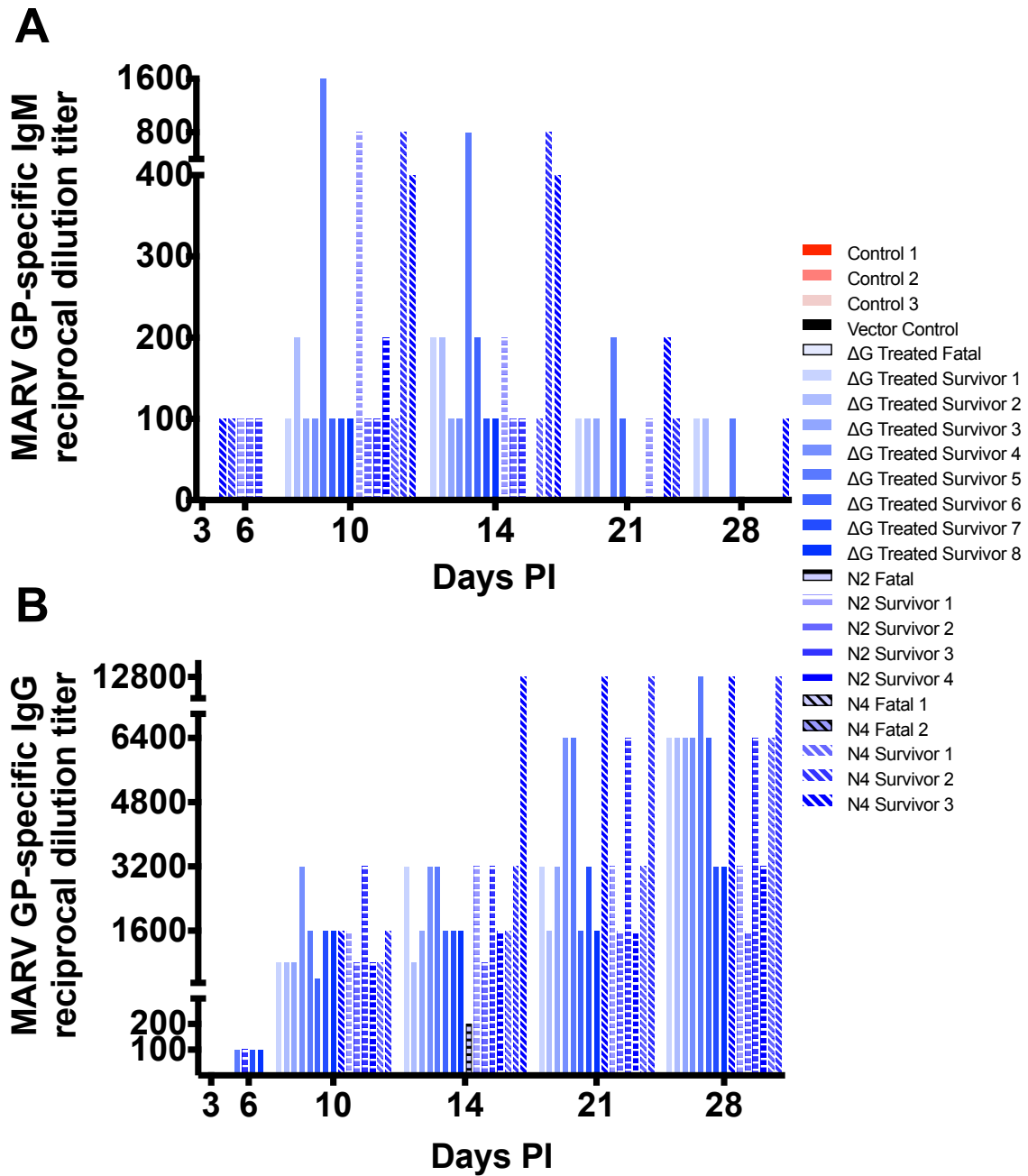


Figure 24. Reciprocal endpoint dilution titers of anti-MARV GP IgM and IgG in the serum of subjects subjected to a low dose MARV-Angola challenge.

Serological titers were evaluated 3, 6, 10, 14, 21, and 28 days after challenge. The untreated controls, vector control, and treated fatals were serologically negative for MARV GP-specific A) IgM and B) IgG; therefore, only treated survivors are depicted (blue bars). To further differentiate between survivors, we used horizontal stripes for N2-treated animals and diagonal stripes for N4-treated animals. Abbreviations: MARV (Marburg virus); GP (glycoprotein); N4 (animal treated with n rVSV vector expressing the nucleoprotein (N) at position 4 in the genome); N2 (animal treated with a rVSV

vector expressing the nucleoprotein (N) at position 2 in the genome); ΔG (an animal treated with a rVSV vector expressing a MARV Angola GP in place of the native VSV G); IgM (immunoglobulin M); IgG (immunoglobulin G); PI (post-infection).

MINIMAL TITERS OF NEUTRALIZING ANTIBODIES WERE FOUND IN TREATED SURVIVOR MACAQUES

Treated survivors produced only low levels of neutralizing antibody. The dilution required to neutralize 50% of MARV plaques ranged from 1:20 to 1:80 for these animals. Neutralizing antibodies did not appear until 10 days post-exposure or prior to the end of the study. These data indicate direct virus neutralization may not be a requirement for protection.

Animal*	MARV Dose	Treatment**	Day 0	Day 6	Day 10	Terminal or Day 28
Control 1	High	None	≤ 10	N.D.	N.D.	≤ 10
Control 2	High	None	≤ 10	N.D.	N.D.	≤ 10
Control 3	High	None	≤ 10	N.D.	N.D.	≤ 10
Treated Fatal 1	High	rVSV Δ G/MARV-Angola-GP	≤ 10	≤ 10	≤ 10	≤ 10
Treated Fatal 2	High	rVSV Δ G/MARV-Angola-GP	≤ 10	≤ 10	≤ 10	≤ 10
Treated Fatal 3	High	rVSV Δ G/MARV-Angola-GP	≤ 10	≤ 10	≤ 10	≤ 10
Treated Survivor	High	rVSV Δ G/MARV-Angola-GP	≤ 10	≤ 10	20	20
Control 1	Low	None	≤ 10	N.D.	N.D.	≤ 10
Control 2	Low	None	≤ 10	N.D.	N.D.	≤ 10
Control 3	Low	None	≤ 10	N.D.	≤ 10	≤ 10
Vector Control	Low	rVSVN4CT1-HIV gag	≤ 10	N.D.	N.D.	≤ 10
Δ G Treated Fatal	Low	rVSV Δ G/MARV-Angola-GP	≤ 10	≤ 10	≤ 10	≤ 10
Δ G Survivor 1	Low	rVSV Δ G/MARV-Angola-GP	≤ 10	≤ 10	≤ 10	40
Δ G Survivor 2	Low	rVSV Δ G/MARV-Angola-GP	≤ 10	≤ 10	≤ 10	40
Δ G Survivor 3	Low	rVSV Δ G/MARV-Angola-GP	≤ 10	≤ 10	20	20
Δ G Survivor 4	Low	rVSV Δ G/MARV-Angola-GP	≤ 10	≤ 10	≤ 10	40
Δ G Survivor 5	Low	rVSV Δ G/MARV-Angola-GP	≤ 10	≤ 10	≤ 10	40
Δ G Survivor 6	Low	rVSV Δ G/MARV-Angola-GP	≤ 10	≤ 10	≤ 10	40
Δ G Survivor 7	Low	rVSV Δ G/MARV-Angola-GP	≤ 10	≤ 10	20	20
Δ G Survivor 8	Low	rVSV Δ G/MARV-Angola-GP	≤ 10	≤ 10	≤ 10	40
N4 Fatal 1	Low	rVSVN4CT1-MARV-Angola GP	≤ 10	≤ 10	≤ 10	≤ 10
N4 Fatal 2	Low	rVSVN4CT1-MARV-Angola GP	≤ 10	≤ 10	≤ 10	≤ 10
N4 Survivor 1	Low	rVSVN4CT1-MARV-Angola GP	≤ 10	≤ 10	≤ 10	40
N4 Survivor 2	Low	rVSVN4CT1-MARV-Angola GP	≤ 10	≤ 10	20	80
N4 Survivor 3	Low	rVSVN4CT1-MARV-Angola GP	≤ 10	≤ 10	20	40
N2 Fatal	Low	rVSVN2CT1-MARV-Angola GP	≤ 10	≤ 10	≤ 10	≤ 10
N2 Survivor 1	Low	rVSVN2CT1-MARV-Angola GP	≤ 10	≤ 10	20	40
N2 Survivor 2	Low	rVSVN2CT1-MARV-Angola GP	≤ 10	≤ 10	≤ 10	20
N2 Survivor 3	Low	rVSVN2CT1-MARV-Angola GP	≤ 10	≤ 10	20	40
N2 Survivor 4	Low	rVSVN2CT1-MARV-Angola GP	≤ 10	≤ 10	≤ 10	40

Table 9. Neutralizing antibody titers.

*Serum was evaluated for neutralizing antibody titers prior to challenge and terminally for untreated controls. Treated macaque sera were additionally evaluated on days 10 and 14 post-challenge. The reciprocal dilution titer of sera that neutralized $\geq 50\%$ of viral plaques is reported. * ΔG (referring to individual monkey treated with rVSV ΔG /MARV-Angola-GP); N4 (referring to individual monkey treated with rVSVN4CT1-MARV-Angola GP); N2 (referring to individual monkey treated with rVSVN2CT1-MARV-Angola GP). **MARV (Marburg virus); rVSV (recombinant vesicular stomatitis virus); MARV-Angola-GP (Marburg virus Angola glycoprotein); N4 (the rVSV nucleoprotein (N) is at position 4 in the genome); N2 (the rVSV nucleoprotein (N) is at position 2 in the genome); CT1 (the native rVSV glycoprotein (G) has a truncated cytoplasmic tail); ΔG (the native VSV G is absent); HIV (human immunodeficiency virus); gag (group-specific antigen). N.D (not determined).*

Conclusions

These analyses add to the limited information pertaining to the systemic host response following MARV infection. Because rVSV post-exposure treatment is only partially protective against a low dose of the Angola variant, we were able to determine immune correlates associated with survival or fatal disease.

In this model, rVSV-treated survivor monkeys induced gene expression changes that were only transiently detected, indicating a tightly controlled host immune response in these animals. Specifically, we observed upregulation of ISGs associated with antiviral activity against VSV and other viruses, such as CMPK2, LY6E, HERC6, and GBP1. The majority of ISGs were type II IFN-related (IFN-gamma). Most importantly, we observed increased transcripts of the ISG STAT4 in this group at mid-disease. STAT4 is an essential transcription factor for Th1 development and is also expressed during Tfh development [200, 201]. Th1 cells secrete IFN-gamma and IL-2 and promote antiviral immunity by fostering antigen presentation, activating macrophages and NK cells, and assisting in the production of antibodies [200]. Moreover, skewing towards this T effector subset was seen in survivors from a MARV outbreak in Uganda [130]. Tfh cells promote

B-cell memory, plasma cell differentiation, antibody affinity maturation, and immunoglobulin class switching [201]. Th1 and Tfh responses likely contribute to protection as we only detected double positive IL-2 and IFN-gamma Th1 cells and GP-specific antibodies in survivors at late-disease. Further, we did not detect upregulation of tolerogenic genes in these animals at mid- or late-disease. Consistent with previous findings for preventative vaccination and post-exposure treatment with rVSV vectors, only low levels of neutralizing antibodies were produced in these animals. Non-neutralizing mechanisms, such as ADCC or complement-mediated cytotoxicity, probably elicit protection.

In the fatal group, transcription of type I IFN genes did not occur until late in disease, though signaling was robust at this stage. The timing and magnitude of the IFN response may be crucial factors for protective immunity against MVD. Sustained IFN signaling for certain virus infections can actually elicit immunosuppression. Blockade of the IFNAR rescues this phenotype and can decrease cell exhaustion markers, improve antiviral responses, and promote Th1 differentiation in late-primed virus-specific CD4+ T-cells [251].

Down-regulated pathways in the fatal dataset included TLR, NFkB, and IL-12 signaling, while upregulated genes and pathways were associated with Th2 and TGF-beta signaling, Treg differentiation, and T-cell exhaustion. Th2 and Treg cells and their effector cytokines (IL-4, IL-10, IL-13, TGF-beta) are known to inhibit Th1 differentiation and cytokine production [252]. Impaired IL-12 signaling may also have contributed to the loss of IL-2 expression in Th1 cells and CTLs in this study since this cytokine drives Th1 differentiation. Further, we noted genes mapping to inhibitory PD-1 signaling in T-cells. *In vitro*, we demonstrated that MARV infection of human primary monocytes led to higher expression of PDL-1 that engages this inhibitory receptor, which may cause

effector T cell dysfunction and exhaustion. Finally, secretion of immunosuppressive IL-10 by Tregs and/or CD25⁺ FOXP3⁻ CD4⁺ T-cells likely prompted downregulation of MHC-II expression in monocytes, interfering with humoral immunity [233, 234].

One limitation of this study is that although we detected IL-4 and other Th2 gene signatures in the fatal group, we did not test whether circulating Th2 cells were actually recruited in the blood or secondary lymphoid organs. We will need to perform this analysis in future studies. It would also be worthwhile to determine whether Tregs remain in the blood compartment or migrate into tissues to elicit their immunosuppressive effects.

Another caveat is that in addition to Th2 (IL-4, IL-6, and IL-13) and Treg (IL-10 and TGF-beta) cytokines, we also noted induction of Th1 (IFN-gamma, IL-12, and IL-18) and Th17 (IL-17) cytokines in the plasma of fatal animals (Supplementary Figure 6). IFN-gamma secreted by cells other than antigen-specific Th1 cells, e.g. CD8⁺ T cells, might be more harmful than beneficial. Effects must be proximal to the initial activation site, or else, this cytokine can promote apoptosis and T-cell contraction [253]. Indeed, recruitment and degranulation of CD8⁺ T-cells did not appear to ameliorate disease in fatal cases. Also, with the exception of IL-18, Th1 and Th17 cytokines were not secreted until the terminal stage of disease, concurrent with the recruitment of Th2 and Treg populations. The latter cells may mitigate any effects of Th1 and Th17 functions. IL-18 does not activate STAT4 expression in Th1 cells. Instead, it operates through MyD88 and IRAK pathways leading to activation of transcription factors such as NFkB and AP-1 [254]. NFkB was significantly downregulated in fatal animals; therefore, this pathway might be ineffective for activation of Th1 immunity.

In summary, survivors had early upregulation of innate antiviral genes and Th1-skewed immunity, whereas in nonsurvivors the immune response was associated with TGF-beta and IL-4 signaling, and an exhaustive phenotype. This study emphasizes the importance of Th1 immunity in protection against MARV infection. MARV may have evolved mechanisms to suppress Th1 signaling in hosts by provoking a Th2 and immunosuppressive response in order to promote viral replication. Although immune tolerance prevents autoimmunity and mitigates tissue damage from pro-inflammatory mediators, consequences of this phenotype include loss of effector function, sustained upregulation of inhibitory receptors, and secretion of immunosuppressive cytokines, all of which promote viral replication [255]. A balance of pro- and anti-inflammatory cellular processes is presumably pivotal for immunity against MVD.

CHAPTER 5: PROPOSED MECHANISM OF RVSV-MEDIATED POST-EXPOSURE PROTECTION AGAINST MARBURG ANGOLA VIRUS

Following stimulation of the CD4 T-cell receptor with an APC-presented antigen peptide-MHC-II complex, naïve CD4⁺T cells differentiate into several Th lineages depending on the cytokine milieu of the microenvironment (Figure 25). CTLs are instead primed by MHC-I presentation to stimulate their cytotoxic activity. Several Th subsets have been identified, including Th1, Th2, Th17, Tfh, and Treg effector cells, all of which serve discrete functions. To differentiate into these lineages, a complex network of cytokine signaling pathways, along with subsequent activation of specific transcription factors, is required [256].

PAMPs and DAMPs engage RLRs, TLRs, CLRs, and NLRs to activate APC and induce IFN and antiviral signaling [257]. These cells subsequently secrete cytokines that determine the cytokine environment for T-cell differentiation. Secretion of IL-12 initiates development of antiviral Th1 cells, which in turn, increases antigen presentation, activation of macrophages and NK cells, and production of IgG opsonizing antibodies. STAT4 is a key early transcription factor for this subset, and T-bet is a master regulator [200]. STAT4 and T-bet have unique signaling pathways that coordinate with one another to further enhance the Th1 response. IL-2, IL-4, and IL-6 signaling causes differentiation of the Th2 lineage, consequently resulting in upregulation of STAT6 and GATA3 in these cells [256]. The Th2 subset secretes IL-4, IL-5, IL-10, and IL-13, and is important in defense against extracellular pathogens. It is also responsible for B-cell IgE switching and secretion. For Th17 cells, IL6 and TGF-beta are the two chief signaling cytokines involved in their differentiation. The Th17 subset is characterized by secretion of IL-17 and IL-22, tissue inflammation, autoimmunity, and release of antimicrobial

peptides. Th1-associated IFN-gamma suppresses Th2 and Th17 development and Th2-associated GATA3 can suppress Th1 STAT4 expression. This provides a positive feedback loop to maintain their effector phenotypes.

Commitment to the Tfh lineage is mediated by IL-6 and IL-21 [258]. These cells are important in humoral immunity and can be split into various subtypes (Tfh1, Tfh2, Tfh10, etc.) [259]. They interact with antigen-primed B cells to facilitate long-lived memory B cells and Ig-producing plasma cells. In mice, Tfh1 IFN-gamma favors IgG2a production (IgG1 and IgG3 equivalent in humans [92]), Tfh2 IL-4 results in the production of IgE and IgG1, and Tfh10 IL-10 promotes IgA secretion.

The polarization of the Treg subset is primarily mediated by TGF-beta expression [258]. These cells develop in the thymus (natural Tregs) or in peripheral lymphoid tissues after antigen priming (induced Treg). Natural Tregs do not require antigen priming for forkhead transcription factor (FOXP3) expression. These cells secrete IL-10, TGF-beta, and IL-35, and function in the maintenance of tolerance to self and foreign antigens [260]. After pathogen clearance, these cells negatively regulate immune and Th effector responses to protect the host against inflammation-mediated immunopathology and tissue destruction. To prevent this damage, they secrete immunosuppressive cytokines and upregulate receptors, such as PD-1 and CTLA-4, to dampen the immune response.

In this study, rVSV-mediated innate immune activation, antibody production, and T-cell responses likely acted together to elicit protection in survivors. Polarization towards the Th1 effector subset in survivors probably reflects secretion of IL-12 by DCs and other APCs early in infection [91]. In these animals, we found early upregulation of genes associated with antiviral responses, type I and II IFN signaling, and STAT4. In contrast, fatal animals did not upregulate type I IFN responses until end-stage disease.

This finding goes against the current dogma that the IFN response is dampened in response to MARV infection. However, MARV proteins possibly antagonized ISG induction early in infection, which deferred initiation of innate and adaptive immunity. VP40 is known to interfere with the JAK/STAT signaling pathway by blocking the phosphorylation of JAKs to prevent type I and II signaling [122]; VP35 antagonizes RIG-I/MDA-5 RLR signaling by interfering with IRF proteins [125]. These viral proteins may have prevented key antiviral innate pathways from being activated, resulting in an inappropriate adaptive response (commitment to Th2 and Treg lineages or an exhaustive phenotype). Another possibility is that rVSV is a more potent inducer of ISGs or activates alternative signaling pathways. Although MARV may weaken or overcome the effects of ISG activation, it may be more vulnerable to rVSV innate responses early in disease. Once a high level of MARV replication is achieved, the virus may be able to overcome these antiviral responses. This is supported by the fact that the terminal viral load titers were lower in treated fatals, while viremia was low or absent in treated survivors. In addition, co-infection with rVSV *in vitro* did not reduce inhibitory PDL-1 expression. In conclusion, rVSV innate immune responses in protected animals keep MARV replication in check until an adaptive response is formed. Treatment with rVSV also contributes to protection by facilitating polarization to more effective T-cell responses, such as antiviral Th1 and antibody-promoting Tfh cells.

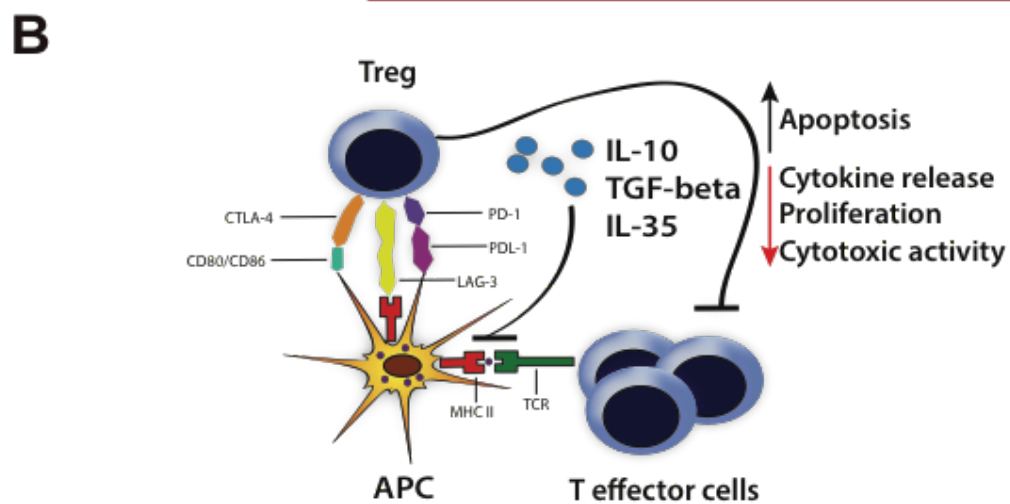
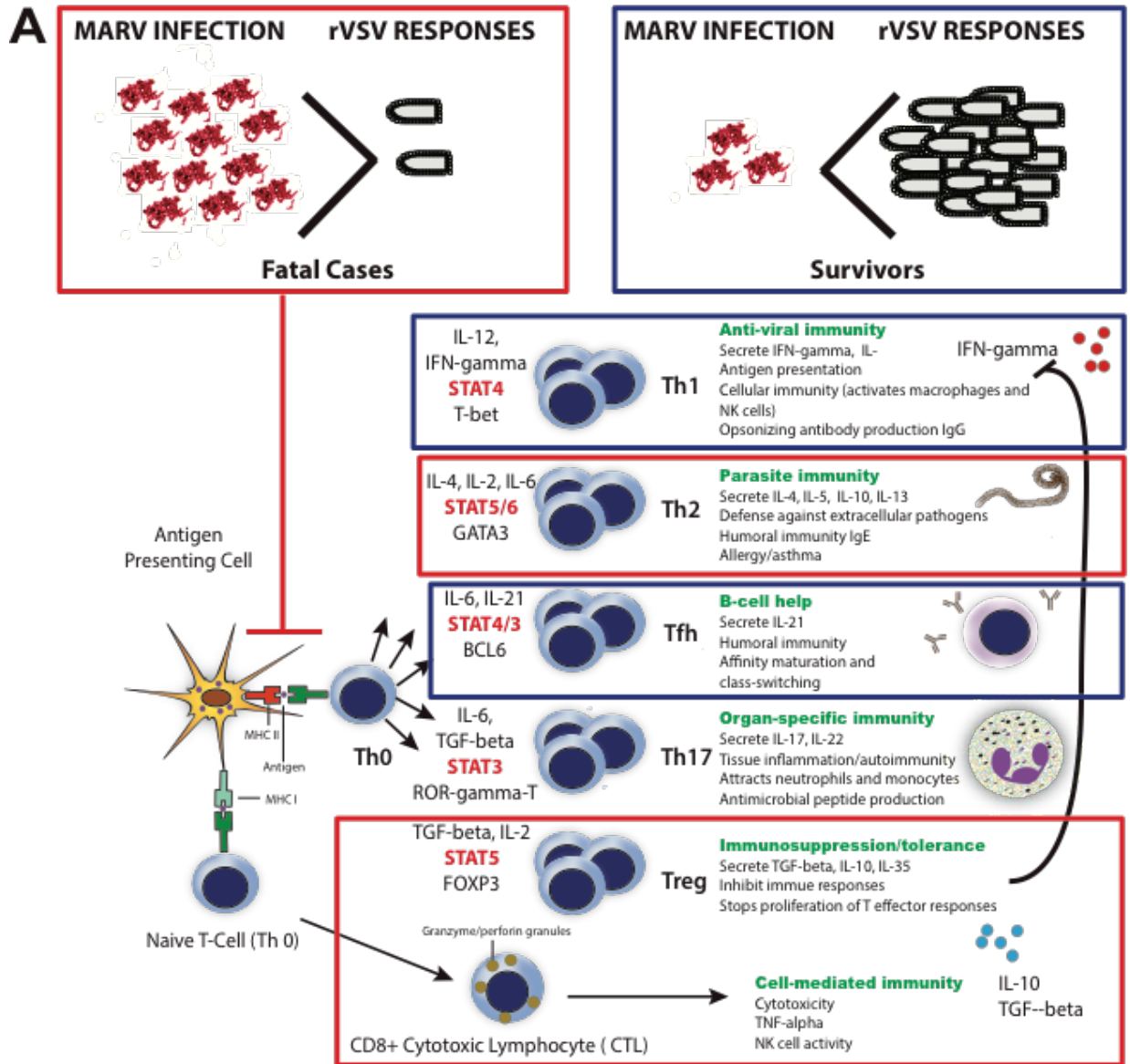


Figure 25. Proposed mechanism for rVSV-mediated post-exposure protection.

A) Treatment with rVSV keeps MARV replication in check by stimulating expression of interferon-related antiviral genes and Th1- and Tfh-associated STAT4. If viral load becomes too great, MARV may overcome these immune responses leading to disease and/or death. In response to antigen stimulation and a specific cytokine milieu, naïve T-cells differentiate into various effector subsets. CTL priming is mediated by interaction with the MHC-I antigen complex, while MHC-II antigen complexes prime T effector cells. In survivors, rVSV treatment polarizes naïve T-cells towards the Th1 effector subtype. In fatal cases, MARV polarizes naïve T-cells towards CTL, Th2 and Treg subsets. Th2 and Treg IL-10 production may also impair T helper immunity and antibody production by down-modulating MHC-II expression. Red boxes: predicted detrimental host responses; blue boxes: predicted beneficial host responses; bold red text: early transcription factors for each Th subset. B) The engagement of Treg PD-1, LAG-3 and CTLA-4 receptors contributes to T-cell dysfunction and exhaustion. The secretion of immunosuppressive cytokines induces apoptosis and inhibits proliferation and cytokine production of T effector cells.

CHAPTER 6: FUTURE STUDIES

Projects in the future will focus on three main themes: testing the potential mechanisms of rVSV-mediated post-exposure treatment survival and failure proposed in this dissertation, identifying alternative mechanisms elicited by rVSV treatment, and improving our vector to extend the treatment window.

First, ISGSs identified by RNAseq following rVSV treatment (e.g. CMPK2, LY6E, HERC6, and GBP1) could be used in a siRNA screen to see whether these genes directly interfere with MARV replication or budding. To test whether Th1 and Tfh cells contribute to protection, we could challenge STAT4 knock-out mice to determine if they have enhanced susceptibility to MARV disease since both effector subsets express this transcription factor. One disadvantage of this method is that it would require the use of an adapted virus for this animal model. Moreover, mice do not recapitulate many aspects of disease seen in humans [15]. A better option might be to employ clustered regularly interspaced short palindromic repeats (CRISPR) genome-editing technology [261]. This would allow us to excise the STAT4 gene in a more suitable animal model, i.e. NHPs. If we are successful, we could further delineate between Th1- versus Tfh-mediated protection by knocking down their respective master regulators, T-bet and BCL6. If ISGs from our RNAi screen demonstrate antiviral activity against MARV, these could also be explored using this approach. If we face difficulties with these methods, we could simplify our strategy by depleting CD4⁺ T-cells in the NHP rVSV post-exposure model. We would expect to see higher mortality in the CD4⁺-depleted group.

One concern we had for our RNAseq analysis was that gene expression changes in T- and B-cell populations would be diluted given they only represent a minority of

cells in peripheral blood. This may have precluded us from identifying additional immune signatures associated with protection. Total lymphocytes only account for ~30% of cells in whole blood, and effector cells are scarce in comparison [262]. Purification of CD20+ (B-cell), CD4+, and CD8+ populations might yield more relevant results, especially since we were unable to detect many B-cell signatures in the survivor group. We could also isolate Tregs from infected monkeys, and co-culture these populations with effector cells to see whether they inhibit proliferation or suppress cytokine secretion in response to stimulation.

One mechanism that has not yet been discussed is the potential ability of rVSV to outcompete MARV for target cells or elicit superinfection resistance (the phenomenon of virus-infected cells having decreased susceptibility to re-infection). An early antagonistic interaction between these viruses may reduce MARV viral replication, allowing sufficient time for the host to form protective adaptive responses. Early target cells for MARV include monocytes and dendritic cells, with successive spread to hepatocytes, kidney cells, adrenal cells, and fibroblasts [68]. Given the MARV GP mediates entry and fusion into susceptible cells [36, 37], rVSV is thought to infect similar cell types (since it also expresses this protein). We performed an experiment in healthy donor PBMC to see if this hypothesis had credibility. PBMC were infected with rVSV Δ G/MARV-Angola-GP for 14 hours, stained with various markers to identify infected cell populations, and positive cells were enumerated using an Amnis imaging cytometer. Similar to MARV, lymphocytes were incapable of becoming infected with our rVSV vector, only monocytes and dendritic cells were susceptible (Figure 26).

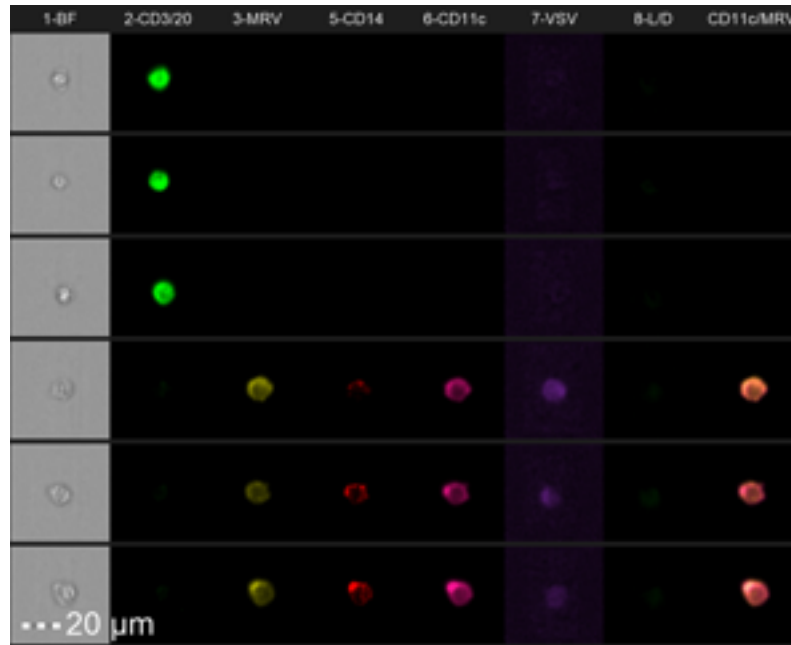


Figure 26. Representative Amnis cytometer image demonstrating rVSV Δ G/MARV-Angola-GP preferentially infects monocytes.

PBMC from human donors were infected with a high MOI of rVSV Δ G/MARV-Angola-GP for 14 hours. Cells were subsequently stained for immunophenotyping surface markers to delineate the various cells. Fluorochrome-conjugated antibodies directed at CD3 (T-cells), CD20 (B-cells), CD14 (monocytes), and CD11c (dendritic cells and monocytes) were used to identify T-cells, B-cells, and dendritic cell (CD14-) populations, respectively. To confirm infection, we used VSV N and MARV GP antibodies. Abbreviations: MRV (Marburg virus-infected); VSV (rVSV Δ G/MARV-Angola-GP-infected); L/D (live/dead stain, no staining means the cell is viable); CD11cMRV (merged MRV and CD11c channels).

After confirming rVSV Δ G/MARV-Angola-GP infects similar cell types, we next tested whether infection with rVSV prevented MARV replication. Vero E6 (NHP kidney), Huh7 (human liver) and HepG2 (human liver) cell lines, representing secondary target cells for MARV, were infected with MARV-Angola, rVSV Δ G/MARV-Angola-GP, or were co-infected at a saturating MOI of 3 of each virus. Cell lysates and supernatants were collected in Trizol and Trizol LS, respectively. RT-qPCR was performed to detect the level of viral replication.

rVSV Δ G/MARV-Angola-GP-infected cells had 3-5 logs more copies per ml in cell lysates and supernatants (Figure 27). However, no major difference in replication was noted in individually-infected versus co-infected wells at 1, 24, or 48 hours.

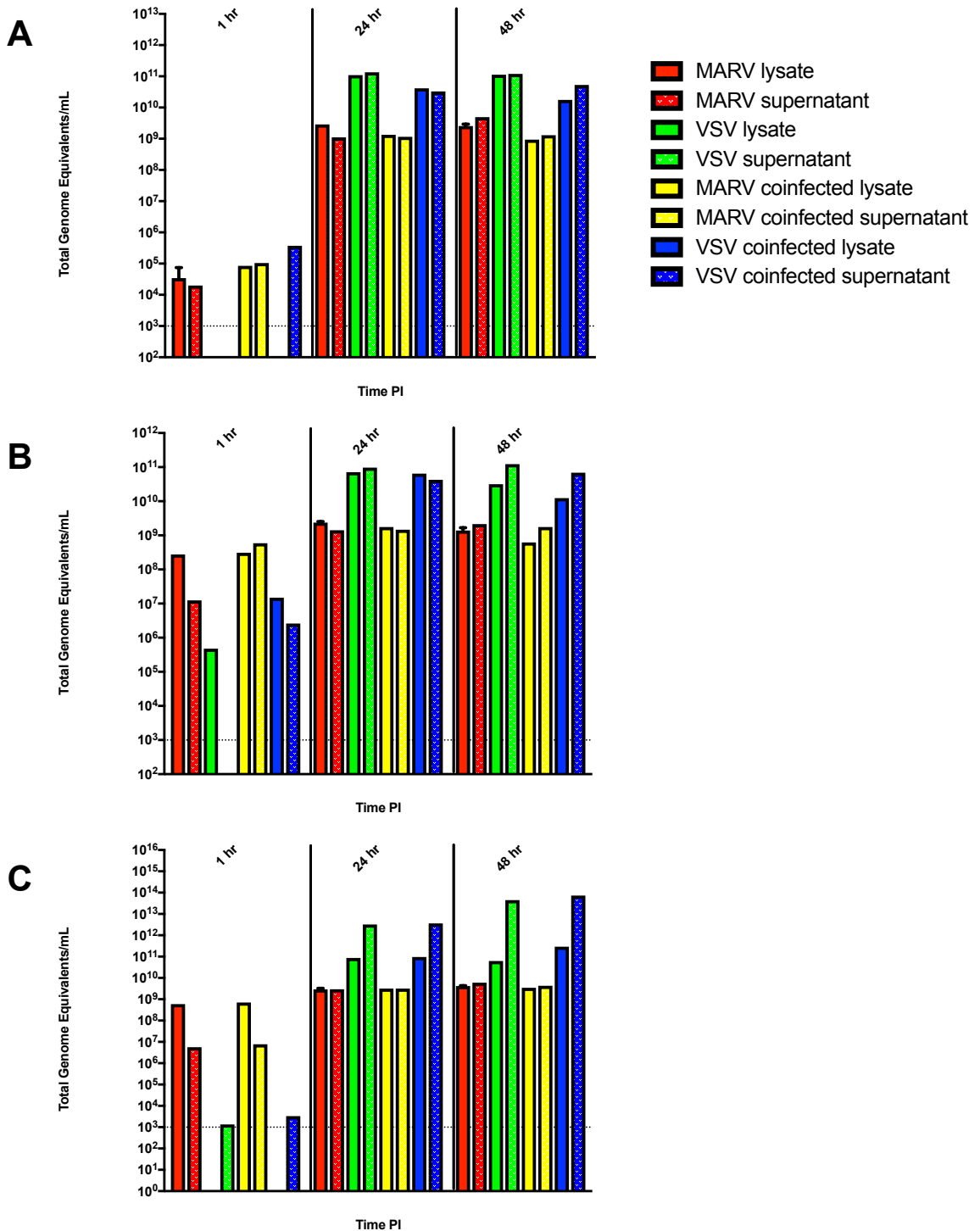


Figure 27. RT-qPCR of VeroE6, Huh7, and HepG2 wells infected with rVSVΔG/MARV-Angola-GP and/or MARV.

rVSVΔG/MARV-Angola-GP GP grows to higher titers than MARV in VeroE6 (A), Huh7 (B), and HepG2 (C) cells. Two-step PCR was performed to select only genome equivalents. RNA isolation was performed using Direct-zol RNA MiniPrep kits (Zymo Research) according to the manufacturer directions. Primers and FAM-labeled probes for MARV Angola-L, VSV-M, and beta-actin (to normalize expression) were used to record fluorescent signal. Uninfected Vero E6, Huh7, and HepG2 cells, and wells without template RNA added were used as negative controls. BioRad CFX manager software was used for analysis and compared to standard curves to generate total genome equivalents. No statistical significance was noted between the groups.

Successful co-infection of both viruses in VeroE6 (Figure 28A-I) and HepG2 cells (Figure 28J-R) was confirmed using an immunofluorescence assay. Briefly, cells were infected as previously described for the RT-qPCR analysis and stained at 1 (Figure 28A-C, J-L), 24 (Figure 28D-F, M-O), and 48 (Figure 28G-I, P-R) hours post-infection. rVSVΔG/MARV-Angola-GP led to rapid cytopathic effects, with extensive cell rounding and detachment by 24 hours (Figure 28E, N). At 48 hours post-infection, very few live cells were present (Figure 28H, Q). MARV infection also caused cell death and detachment (Figure 28D, G, M, P), but to a much lesser extent at these timepoints. Most cells positive for rVSVΔG/MARV-Angola-GP antigen also expressed MARV VP40 (Figure 28F, I, O, R), indicating rVSVΔG/MARV-Angola-GP was unable to prevent MARV entry or induce superinfection resistance in co-infected cells at these conditions.

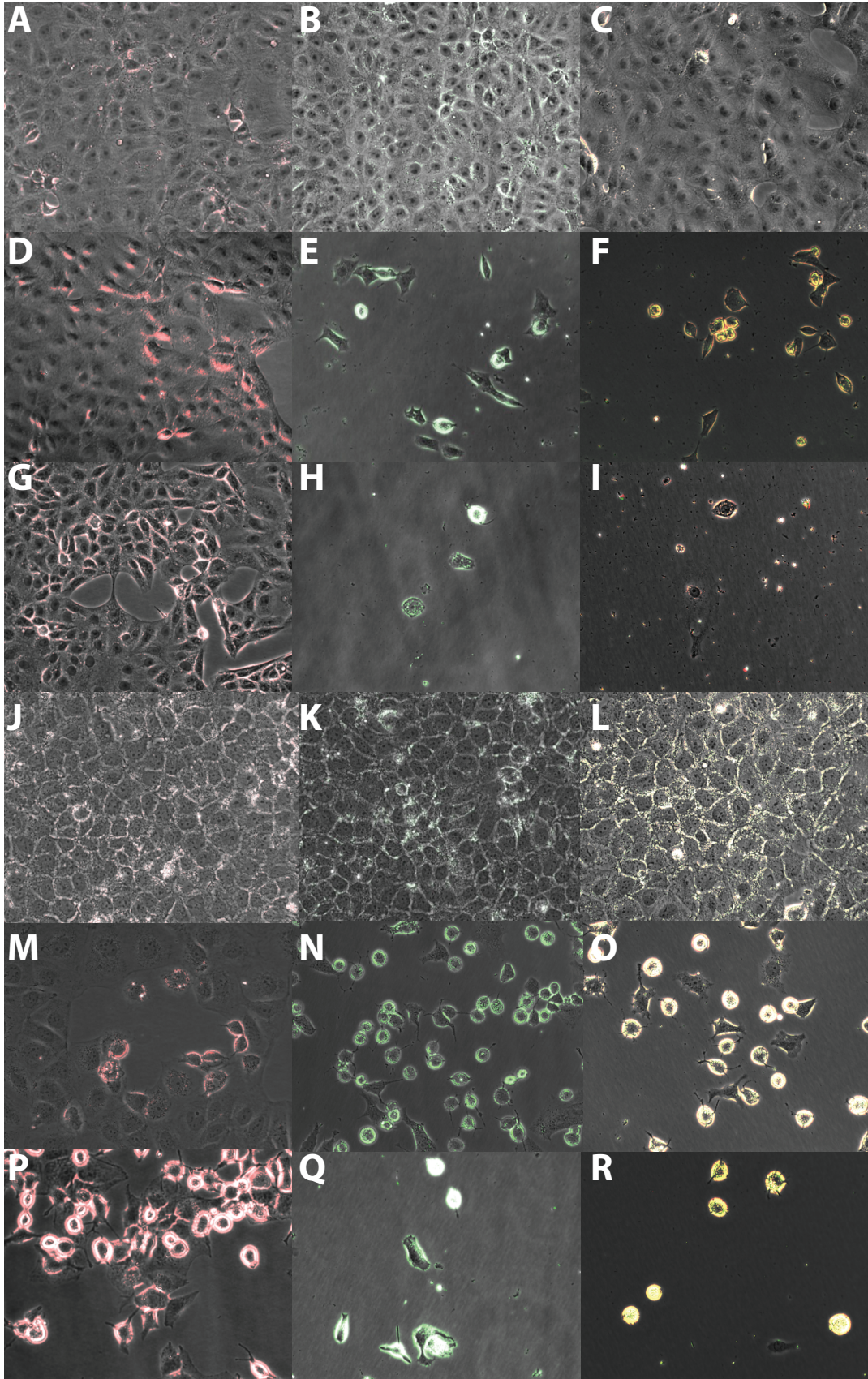


Figure 28. Immunofluorescence assay of VeroE6 and HepG2 wells infected with rVSVΔG/MARV-Angola-GP and/or MARV.

rVSVΔG/MARV-Angola-GP infection leads to rapid cell death and does not prevent MARV entry in co-infected kidney (A-I) and liver (J-R) cell lines. Cells were infected (MOI of 3) with MARV (A, D, G, J, M, P), rVSVΔG/MARV-Angola-GP (B, D, H, N, Q), or simultaneously co-infected with both viruses (C, E, I, O, R), and stained for their respective antigens at 1 (A-C, J-M), 24 (D-F, N-O), and 48 (G-I, P-R) hours post-infection. The co-infected images are an overlay of MARV and rVSV-stained images. Plates were immersed in 10% neutral buffered formalin for 24 hours and fresh fixative was added the next day prior to immunostaining. Wells were washed in PBS-100mM glycine and subsequently permeabilized in 1% Triton-X in PBS-100mM glycine for 15 minutes at RT. Cells again were washed with PBS-100mM glycine, blocked with 10% heat-inactivated goat serum, and a 1:500 dilution of polyclonal rabbit-anti-MARV-VP40 (Integrated Biotherapeutics, Inc.) and/or monoclonal mouse-anti-VSV-nucleoprotein (Clone 10G4 Kerafast) primary antibody was added. After a one-hour incubation, cells were washed three times and incubated for one hour with a 1:1000 dilution of Alexa 488 goat-anti-rabbit and Alexa568 goat-anti-mouse (ThermoFisher) secondary antibodies to generate a fluorescent signal. Plates were visualized immediately with a fluorescence microscope.

To validate these results, further evaluation is needed at various MOIs to test for viral interference. More time may be needed to establish an antiviral response in response to rVSV infection to interfere with MARV entry. Also, assays need to be performed in human PBMC, which elicit more robust innate immune signaling.

To augment protection in the post-exposure model, we suggest the use of Th1-skewing adjuvants. A poly:IC derivative, poly: ICLC, performed well in clinical studies and greatly improved CD4+, CD8+, and Tfh responses, as well as antibody titers [263]. Poly: ICLC is a stabler form of poly: IC that, *in vivo*, induces a clear Th1 phenotype evident by the induction of type I IFN, IL-12, TNF-alpha, IFN-gamma, IL-6, and a number of chemokines [264]. The mechanism of Th1 skewing for this adjuvant is dependent on TLR3 and MDA-5 signaling.

To promote T-cell effector responses we could additionally perform an antibody-mediated PDL-1 blockade. Poly: ICLC and PDL-1 inhibitors are thought to work

synergistically to elicit protective immunity [265]. Immunomodulating agents directed at PD-1 or LAG-3 might also provide some benefit against MARV [266, 267, 268]. Targeting LAG-3 might be a better option given its ability to impede Treg suppressive activity and downregulate inhibitory LAG-3 signals in activated T-cells [268]. Hopefully, these treatment enhancements would help elicit protection in non-responders.

Another way to boost our treatment is to design rVSVs that express short hairpin RNAs (shRNAs) to deliver temporal RNAi activity. Other RNAi treatments, such as SNALPs, have been highly effective against MARV disease (especially against the most highly transcribed NP protein) [158, 159]. This method would boost protection by reducing viral replication, as a high viral load is associated with poor prognosis. shRNAs will be designed to complement MARV mRNAs. shRNAs will be theoretically transcribed by the viral polymerase and recognized by and loaded into RNAi machinery. Ultimately, this would result in degradation of MARV mRNAs, thereby reducing viral replication in the host.

To generate a database of shRNA duplex candidates targeting MARV NP mRNA, we used siRNA wizard v3.1, s-Biopredsi, i-Score, Reynold, and DSIR algorithms to predict the most functional shRNAs. Sequence targets that shared 16 or more contiguous base homology with human mRNAs, as well as those that did not share 100% nucleotide sequence identity among three additional MARV variants, were excluded. Each shRNA duplex consisted of a 21nt sense sequence, linker hairpin loop (TCAAGAG), and an antisense sequence. These sequences were cloned into a standard pcDNA3.1 vector to pre-screen shRNA knockdown activity. As illustrated in Figure 29, the NP-1165 candidate was able to inhibit NP expression at 100ng and 200ng concentrations. A scrambled shRNA targeting MARV NP and a shRNA targeting Renilla luciferase (rLuc) were synthesized to serve as negative and positive controls, respectively. We will next

clone this shRNA sequence into a rVSV expressing MARV-Angola-GP and recover the virus using reverse genetics. If successful, this optimization strategy would be particularly beneficial because an exclusive selection of conserved sequences would likely protect against multiple MARV variants.

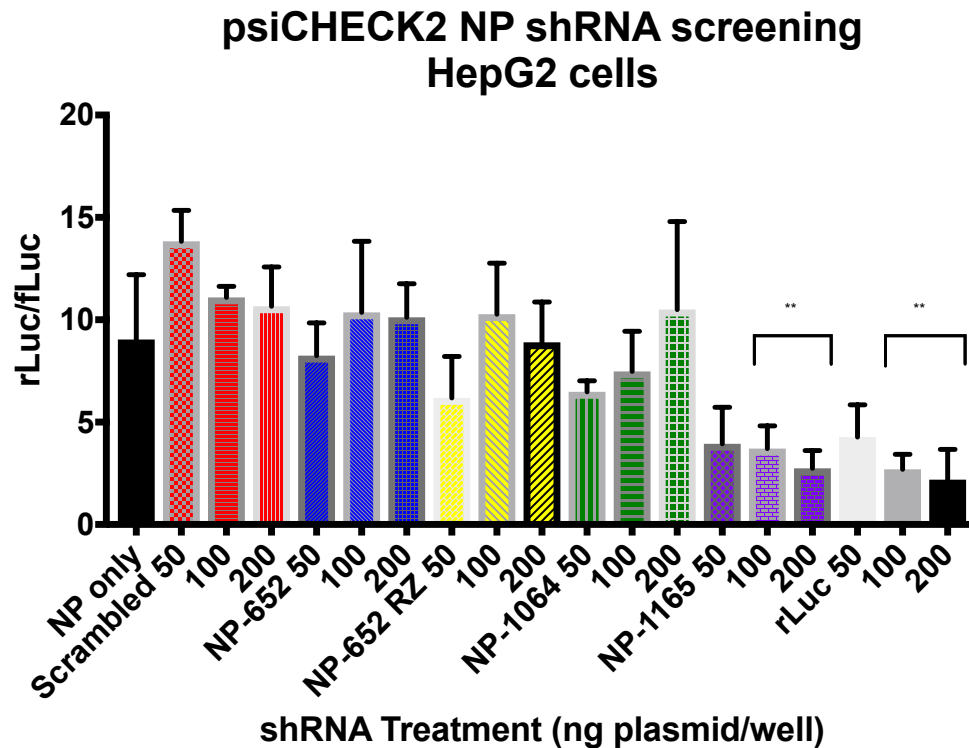


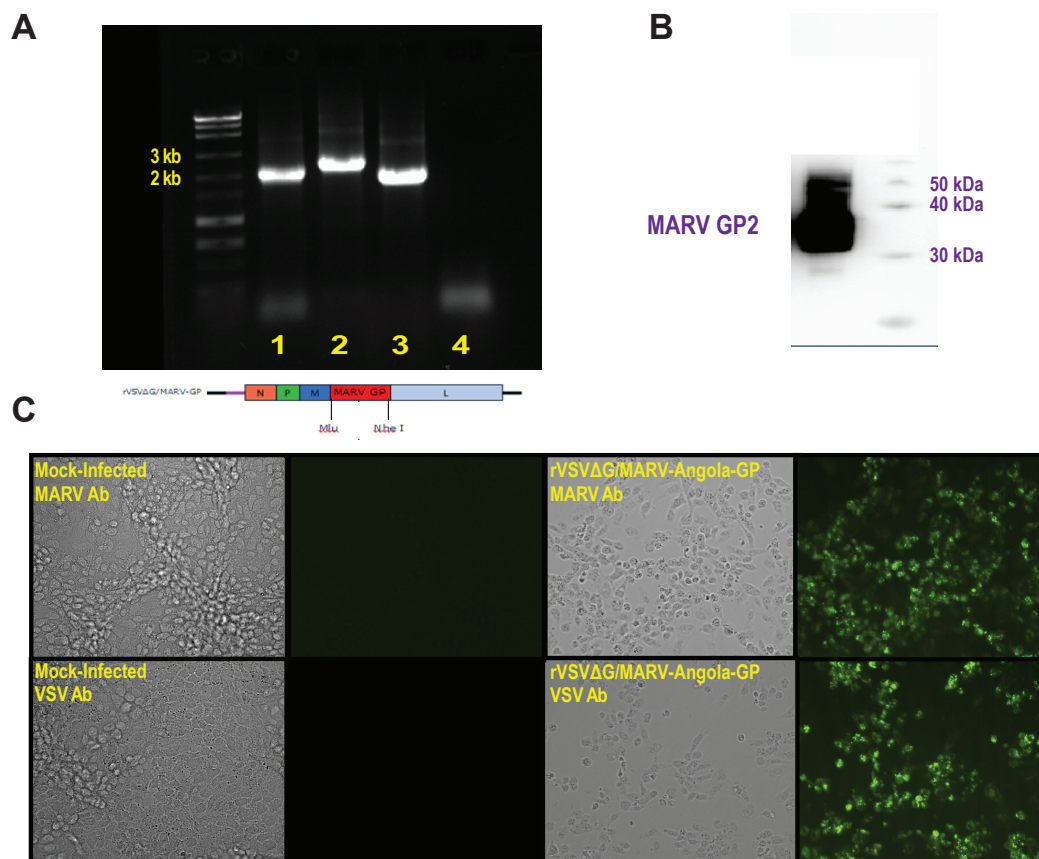
Figure 29. In vitro screening of plasmids expressing selected shRNAs.

shRNA genes were assembled into a T7 expression vector (pcDNA3.1) via restriction site-mediated integration. Plasmids were sequenced to confirm successful insertion. Tekmira Pharmaceuticals Corporation kindly provided us with their optimized dual luciferase reporter system to test mRNA knockdown efficacy. The MARV NP gene was cloned into the multiple cloning site (MCS) of a psiCHECK2 vector (Promega) containing firefly luciferase (Luc) and Renilla luciferase (rLuc) genes. The MARV NP gene is fused to a RLuc reporter gene, so that if shRNA is unable to bind the target mRNA, translation of the shRNA: RLuc fusion mRNA occurs, emitting light detectable by a luminometer when luciferin substrate is added. If shRNA binds the target mRNA, degradation of the fusion mRNA should occur via induction of RNAi. HepG2 cells were reverse-transfected into a Lipofectamine 2000 (Invitrogen) mixture containing 0.75 µg of psiCHECK2 plasmid, various concentrations of shRNA plasmids (50 ng, 100ng, 200ng), and 1 µg T7 pCAGGs into 24-well plates. The rLuc signal (reflecting MARV target gene expression) was normalized to the firefly Luc signal and expressed as a percentage of

*gene expression relative to the nonspecific scrambled shRNA control. A shRNA targeting rLuc served as a positive control. ** $p \leq 0.01$*

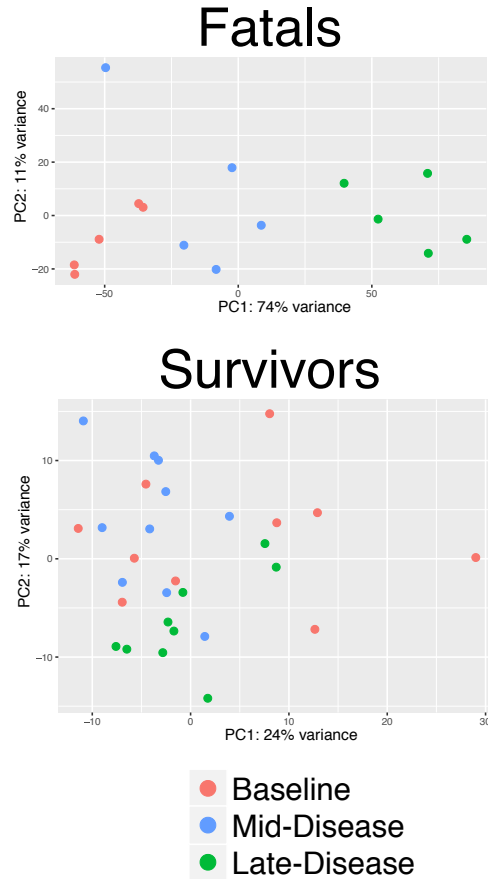
Much remains to be clarified with respect to the relative importance of these newly identified mechanisms. Post-exposure protection mediated by rVSV is likely multifactorial. Based on our analyses, innate and adaptive immunity appear pivotal for protection. Performing more in-depth analyses as proposed in this chapter, will shed further light on mechanisms. Immunotherapy with PDL-1/PD-1/LAG-3 inhibitors, Th1-skewing adjuvants, or a re-designed shRNA-expressing vector, will hopefully push us further towards our goal of extending the treatment window.

SUPPLEMENTARY FIGURES



Supplementary Figure 1. Confirmation of recovery of rVSVΔG/MARV-Angola-GP.

A) *cDNA amplification of recovered virus from Trizol-extracted RNA (Vero cell supernatants). Lane 1: MARV GP primers; Lane 2: VSV primers flanking GP region; Lane 3: MARV GP-forward primer within GP region and VSV L- reverse primer; and Lane 4: (-) control, only primers added.* B) *Western blot confirming protein expression of the MARV GP2 subunit. A primary rabbit anti-MARV GP polyclonal antibody (IBT Bioservices) and secondary goat anti-rabbit HRP antibody were used for detection.* C) *Immunofluorescence assay demonstrating infectivity of rVSVΔG/MARV-Angola-GP in Vero cells. Vero cells were infected at a low MOI and collected at 48 hours post-infection. A rabbit anti-MARV GP polyclonal antibody or VSV M (Kerafast) was used as a primary antibody. AlexaFluor 488 secondary antibody was used to generate a fluorescent signal.*



Supplementary Figure 2. PCA of survivor and fatal group individuals at baseline, mid-disease, and late-disease.

Similar clustering of untreated, vector control-treated, and treated fatal samples were observed following viremia-based normalization. We observed dimensional separation for the fatals. The survivors had less clear separation at the baseline, but tended to cluster at mid- and late-disease. EdgeR was used to plot overall expression values. Red dots represent baseline values, blue dots represent mid-disease values and green dots represent late-disease values.

Monkey	Group	Mid-Disease	Late-Disease	Final Disposition
Control 1	Fatal	3	6	Succumbed on day 8
Control 2	Fatal	6	9	Succumbed on day 9
Control 3	Fatal	6	10	Succumbed on day 10
Vector Control	Fatal	6	10	Succumbed on day 12
Δ G Treated Fatal	Fatal	6	10	Succumbed on day 11
Δ G Survivor 1	Survivor	6	10	Survived to day 28

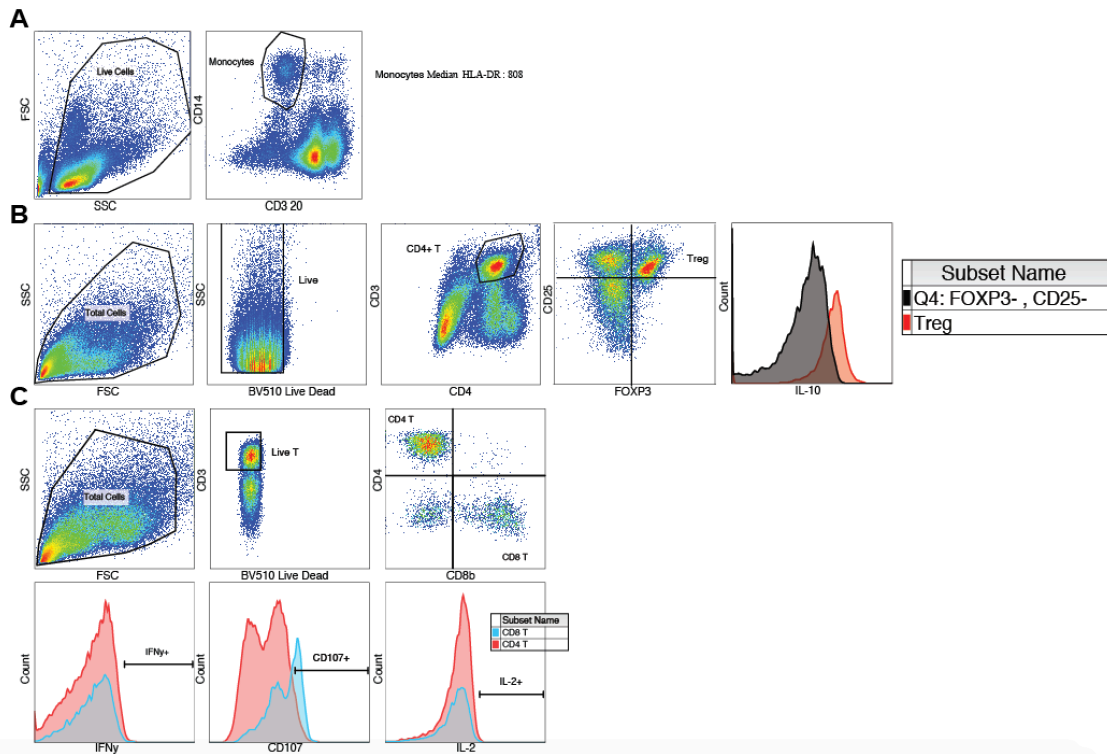
ΔG Survivor 2	Survivor	6	10	Survived to day 28
ΔG Survivor 3	Survivor	6	10	Survived to day 28
ΔG Survivor 4	Survivor	6	10	Survived to day 28
ΔG Survivor 5	Survivor	6	10	Survived to day 28
ΔG Survivor 6	Survivor	6	10	Survived to day 28
ΔG Survivor 7	Survivor	6	10	Survived to day 28
ΔG Survivor 8	Survivor	6	10	Survived to day 28
N2 Fatal	Fatal	10	14	Succumbed on day 14
N2 Survivor 1	Survivor	6	10	Survived to day 28
N2 Survivor 2	Survivor	6	10	Survived to day 28
N2 Survivor 3	Survivor	6	10	Survived to day 28
N2 Survivor 4	Survivor	6	10	Survived to day 28

Supplementary Table 1. Normalization of samples for RNAseq, flow cytometry, and cytokine analyses.

Samples from MARV-Angola-infected were normalized based upon the first detectable viremia in these animals (mid-disease). Late-disease corresponded to 0-2 days before the animal succumbed to MVD. The median timepoints for these disease stages were used to define mid- (6 days post-exposure) and late-disease (10 days post-exposure) stages in the survivor dataset.

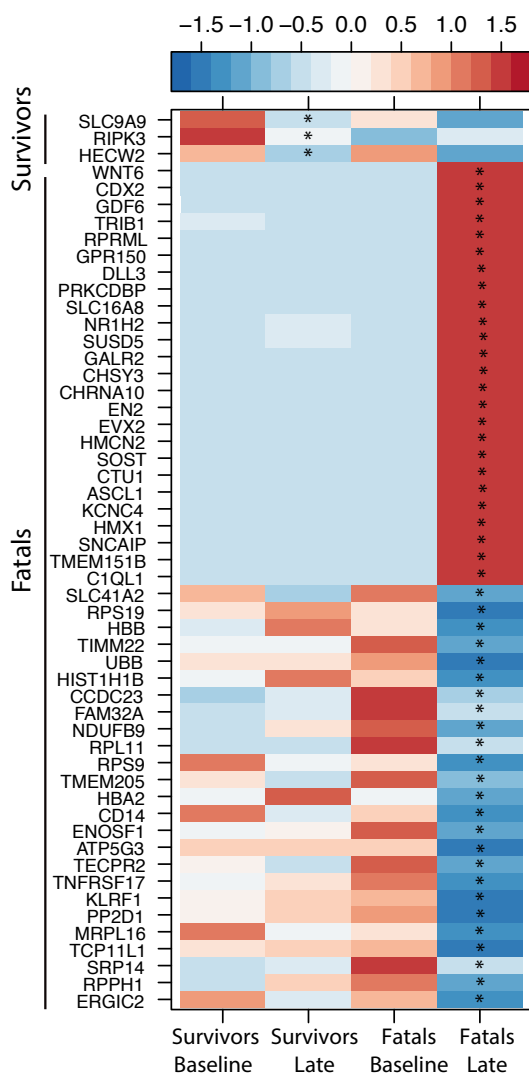
Fluorochrome	Monocyte HLA-DR MFI	T helper 1 (Th1)/CTL	Regulatory T-cell (Treg)
FITC	CD3 (BD, SP34-2) CD20 (BD, 2H7)	Ki67 (BD, B56)	CD3 (BD, SP34-2)
PE	CD16 (Biolegend, 3G8)	CD8b (BD, 2ST8.5H7)	FOXP3 (Biolegend, 259D)
PerCP/Cy5.5	CD123 (Biolegend, 6H6)	CD4 (Tonbo, OKT4)	CD4 (Tonbo, OKT4)
PE/Cy7	CD11c (Biolegend, 3.9)	IFN-gamma (Biolegend, B27)	IL-10 (Biolegend, JES3-9D7)
APC	CD14 (Biolegend, M5E2)	CD107a (Biolegend, H4A3)	
APC/Cy7	HLA-DR (Biolegend, L243)	IL-2 (Biolegend, MQ1-17H12)	CD25 (Biolegend, M-A251)
Pacific Blue		CD3 (BD, SP34-2)	
BV510		BD Horizon Fixable Viability Stain 510	BD Horizon Fixable Viability Stain 510
Purified (no fluorochrome)		CD28 (Biolegend, CD28.2) CD49d (Biolegend, 9F10)	

Supplementary Table 2. Antibodies used for flow cytometric analysis of immune cell subsets in rhesus monkeys (manufacturer and clone are indicated in parentheses).



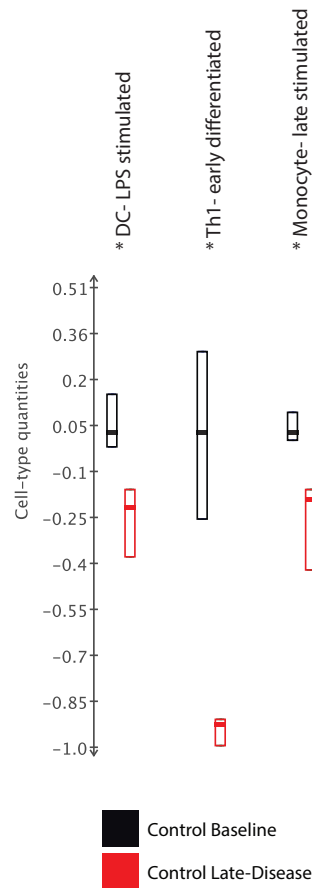
Supplementary Figure 3. PBMC flow cytometry gating strategy.

*A) Monocytes were identified based on lack of CD3 (T-cell) and CD20 (B-cell) expression, and positive CD14 expression. The mean fluorescence intensity of HLA-DR was then calculated within this population. B) After live/dead staining, regulatory T-cells (Tregs) were positively selected for the following markers: CD3, CD4, CD25, and FOXP3. PBMC were stimulated for 6 hours or overnight with a media-only control, or 50ng/ml phorbol 12-myristate 13 acetate (PMA) and 1 μ g/ml ionomycin calcium salt from *Streptomyces conglobatus* (ION). C) To identify Th1 and CTL populations, cells were stained with CD3, CD4, CD8b, IL-2, IFN-gamma, and CD107a fluorochrome-conjugated antibodies. T helper 1 (Th1) cells were identified by their expression of CD3, CD4, IL-2, and IFN-gamma. CTLs were identified by their expression of CD3, CD8, and the degranulation marker, CD107. PBMC were stimulated with a DMSO negative control, or 2 μ g/ml of an overlapping MARV GP peptide pool, for 6 hours in the presence of CD28, CD49d, and CD107. Brefeldin A was added two hours before performing intracellular staining. A B C) Approximately 200,000 events were collected on a BD FACS Canto II cytometer and analyzed using FACS Diva and FlowJo software.*



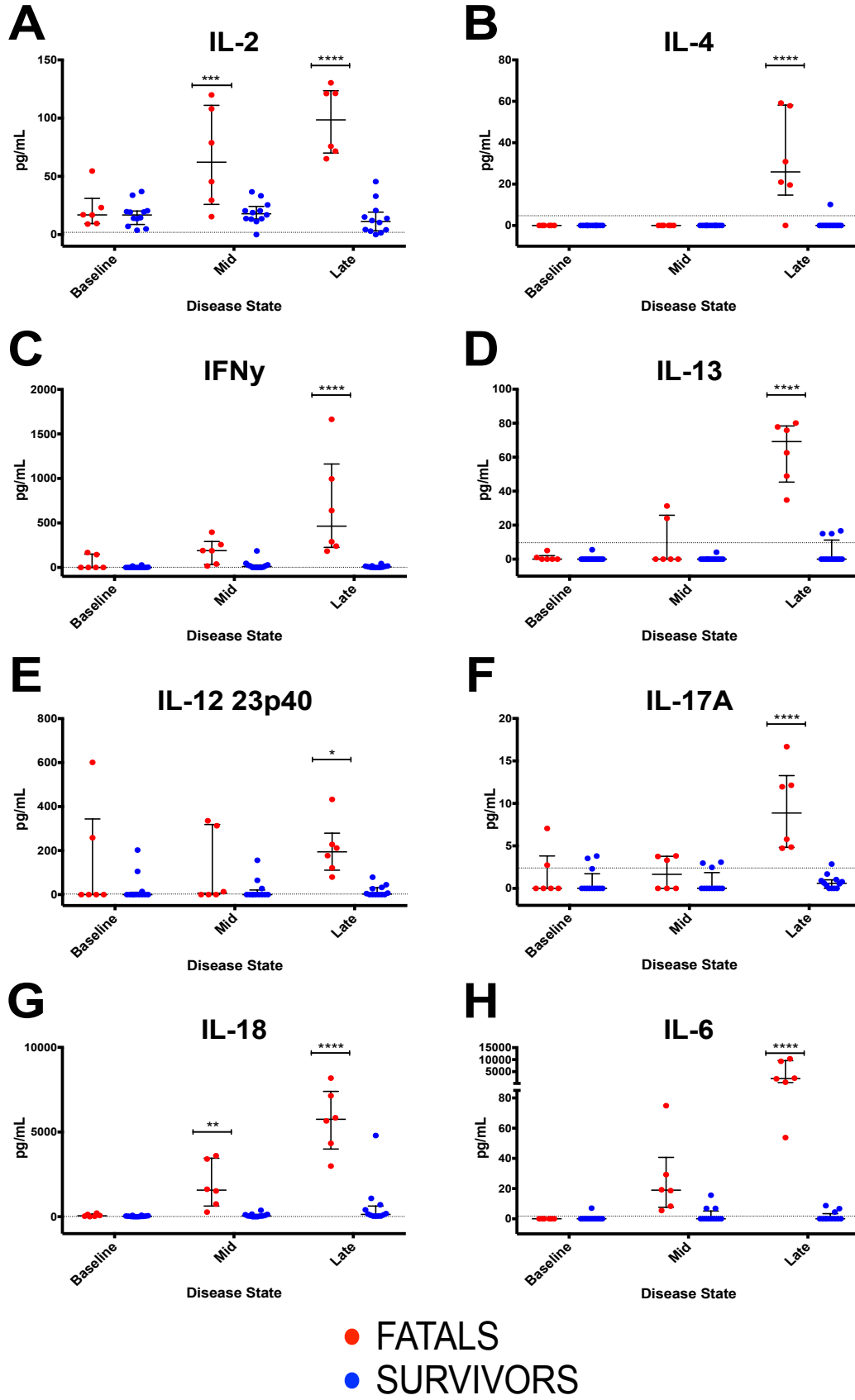
Supplementary Figure 4. Heatmap comparison of the most highly upregulated and downregulated DEGS at late-disease for each group.

*Only three genes were upregulated in survivors at this disease stage. DEGs were calculated using EdgeR against a pre-challenge baseline to establish the most highly expressed genes based on log fold-change. This heatmap was based on scaled RPKM values within that set of genes (red represents increased expression while blue represents decreased expression); each column represents the median RPKM values for each time point. Only human homologs and protein-coding genes were analyzed. *: statistically significant, FDR-corrected p-value of ≤ 0.05 .*



Supplementary Figure 5. ImmQuant comparative view analysis of the relative contribution of immune cell subsets to differential gene expression within the control group.

Fewer cell-type quantities of stimulated DCs and monocytes were observed, as well as significant downregulation of Th1 cells, in untreated controls. ImmQuant uses a database based on genome-wide microarray expression profiling of human immune cells from reported studies. Results were calculated using the Digital Cell Quantifier (DCQ) algorithm with human-based FACS marker genes. The algorithm infers an increase or decrease in cell-type quantities relative to a Dy 0 baseline.”” indicates statistically significant putative changes in cell subset frequency.*



Supplementary Figure 6. Plasma levels of cytokines measured by Milliplex NHP 23-plex cytokine bead arrays.

Red dots represent animals in the fatal dataset; blue dots represent animals in the treated survivor dataset. *p-value ≤ 0.05 ; **p-value ≤ 0.01 ; ***p-value ≤ 0.001 ; ****p-value ≤ 0.0001 .

REFERENCES

1. Amarasinghe, G. K., Bào, Y., Basler, C. F., Bavari, S., Beer, M., Bejerman, N., ... Kuhn, J. H. (2017). Taxonomy of the order Mononegavirales: update 2017. *Archives of Virology*, 162(8): 2493–2504.
2. Kuhn, J. H. (2008). *Filoviruses, A Compendium of 40 years of Epidemiological, Clinical, and Laboratory Studies*. Vienna, Austria: Springer Verlag.
3. Galindo, P., Srihongse, S., de Rodaniche, E. and Grayson, M. A. (1966). An ecological survey for arboviruses in Almirante, Panama, 1959–1962. *Am. J. Trop. Med. Hyg.* 15: 385–400.
4. Peralta, P. H., and Shelokov, A. (1966). Isolation and characterization of arboviruses from Almirante, Republic of Panama. *Am. J. Trop. Med. Hyg.* 15: 369–378.
5. Sudia, W. D., Fields, B. N. and Calisher, C. H.. (1967). The isolation of vesicular stomatitis virus (Indiana strain) and other viruses from mosquitoes in New Mexico, 1965. *Am. J. Epidemiol.* 86: 598–602.
6. Walton, T. E., Webb, P. A., Kramer, W. L., Smith, G. C., Davis, T., Holbrook, F. R., Moore, C. G., Schiefer, T. J., Jones, R. H., Janney, G. C. (1987). Epizootic vesicular stomatitis in Colorado, 1982: epidemiologic and entomologic studies. *Am. J. Trop. Med. Hyg.* 36:166–176.
7. Fields, B. N., Knipe, D. M., and Howley, P. M. (2013). *Fields Virology: Sixth Edition*. Philadelphia, PA: Lippincott, Williams, and Wilkins.
8. Pattnaik, A. K. and Whitt, M. A. (2014). *Biology and pathogenesis of rhabdo- and filoviruses*. Hackensack, NJ: World Scientific Publishing Co.
9. Geisbert, T. W. and Feldmann, H. (2011). Recombinant Vesicular Stomatitis Virus–Based Vaccines Against Ebola and Marburg Virus Infections. *The Journal of Infectious Diseases*, 204(Suppl 3): S1075–S1081.
10. Geisbert, T. W., Jones, S., Fritz, E. A., Shurtleff, A. C., Geisbert, J. B., Liebscher, R., ... Feldmann, H. (2005). Development of a New Vaccine for the Prevention of Lassa Fever. *PLoS Medicine*, 2(6): e183.
11. Zehender, G., Sorrentino, C., Veo, C., Fiaschi, L., Giofrè, S., Ebranati, E., ... Galli, M. (2016). Distribution of Marburg virus in Africa: An evolutionary approach. *Infection, Genetics and Evolution*, 44: 8–16.
12. Smith, D. H., Johnson, B. K., Isaacson, M., Swanapoel, R., Johnson, K. M., Killey, M., et al. (1982). Marburg-virus disease in Kenya. *Lancet*. 1: 816–20.

13. Towner, J. S., Khristova, M. L., Sealy, T. K., Vincent, M. J., Erickson, B. R., Bawiec, D. A., ... Nichol, S. T. (2006). Marburgvirus Genomics and Association with a Large Hemorrhagic Fever Outbreak in Angola. *Journal of Virology*, 80(13): 6497–6516.
14. Geisbert, T. W., Daddario-DiCaprio, K. M., Geisbert, J. B., et al. (2007). Marburg Virus Angola Infection of Rhesus Macaques: Pathogenesis and Treatment with Recombinant Nematode Anticoagulant Protein c2. *J Infect Dis.* 196(Suppl 2): S372-S381.
15. Geisbert, T. W., Strong, J. E., Feldmann, H. (2015). Considerations in the Use of Nonhuman Primate Models of Ebola Virus and Marburg Virus Infection. *J Infect Dis.* 212(January): S91-S97.
16. Fernando, L. , Qiu, X. , Melito, P. L. et al. (2015). Immune response to Marburg virus Angola infection in nonhuman primates. *J Infect Dis.* 212(suppl 2): S234–41.
17. Peters, D., Müller, G., Slenczka, W. (1971) Morphology, Development, and Classification of the Marburg Virus. In: Martini G.A., Siebert R. (eds) *Marburg Virus Disease*. Berlin, Heidelberg: Springer.
18. Geisbert, T. W., Jahrling, P. B. (1995). Differentiation of filoviruses by electron microscopy. *Virus Res.* 39: 129–150.
19. Feldmann, H., Mühlberger, E., Randolph, A., Will, C., Kiley, M. P., Sanchez, A., Klenk, H. D. (1992). Marburg virus, a filovirus: Messenger RNAs, gene order, and regulatory elements of the replication cycle. *Virus Res.* 24: 1–19.
20. Mühlberger, E. (2007). Filovirus replication and transcription. *Future Virology.* 2: 205–215.
21. Brauburger, K., Hume, A. J., Mühlberger, E., & Olejnik, J. (2012). Forty-five years of marburg virus research. *Viruses*, 4(10): 1878–1927.
22. Dolnik, O., Kolesnikova, L., Welsch, S., Strecker, T., Schudt, G., & Becker, S. (2014). Interaction with Tsg101 Is Necessary for the Efficient Transport and Release of Nucleocapsids in Marburg Virus-Infected Cells. *PLoS Pathogens*, 10(10): e1004463.
23. Mühlberger, E., Lötfering, B., Klenk, H. D., Becker, S. (1998). Three of the four nucleocapsid proteins of Marburg virus, NP, VP35, and L, are sufficient to mediate replication and transcription of Marburg virus-specific monocistronic minigenomes. *J. Virol.* 72: 8756–8764.
24. Becker, S., Rinne, C., Hofsäss, U., Klenk, H. D., Mühlberger, E. (1998). Interactions of Marburg virus nucleocapsid proteins. *Virology* 249: 406–417.
25. Wenigenrath, J., Kolesnikova, L., Hoenen, T., Mittler, E., Becker, S. (2010). Establishment and application of an infectious virus-like particle system for Marburg virus. *J. Gen. Virol.* 91: 1325–1334.
26. Kolesnikova, L., Mittler, E., Schudt, G., Shams-Eldin, H., Becker, S. (2012). Phosphorylation of Marburg virus matrix protein VP40 triggers assembly of

- nucleocapsids with the viral envelope at the plasma membrane. *Cell Microbiol.* 14: 182–197.
27. Kolesnikova, L., Strecker, T., Morita, E., Zielecki, F., Mittler, E., Crump, C., Becker, S. (2009). Vacuolar protein sorting pathway contributes to the release of Marburg virus. *J. Virol.* 83: 2327–2337.
 28. Urata, S., Noda, T., Kawaoka, Y., Morikawa, S., Yokosawa, H., Yasuda, J. (2007). Interaction of Tsg101 with Marburg virus VP40 depends on the PPPY motif, but not the PT/SAP motif as in the case of Ebola virus, and Tsg101 plays a critical role in the budding of Marburg virus-like particles induced by VP40, NP, and GP. *J. Virol.* 81: 4895–4899.
 29. Urata, S. and Yasuda, J. (2010). Regulation of Marburg virus (MARV) budding by Nedd4.1: a different WW domain of Nedd4.1 is critical for binding to MARV and Ebola virus VP40. *J. Gen. Virol.* 91: 228–234.
 30. Feldmann, H., Will, C., Schikore, M., Slenczka, W., Klenk, H.D. (1991). Glycosylation and oligomerization of the spike protein of Marburg virus. *Virology.* 182: 353–356.
 31. Geyer, H., Will, C., Feldmann, H., Klenk, H. D., Geyer R. Carbohydrate structure of Marburg virus glycoprotein. *Glycobiology,* 2: 299–312.
 32. Becker, S., Klenk, H. D., Mühlberger, E. (1996). Intracellular transport and processing of the Marburg virus surface protein in vertebrate and insect cells. *Virology.* 225: 145–155.
 33. Sanger, C., Mühlberger, E., Lotfering, B., Klenk, H. D., Becker, S. (2002). The Marburg virus surface protein GP is phosphorylated at its ectodomain. *Virology.* 295: 20–29.
 34. Funke, C., Becker, S., Dartsch, H., Klenk, H. D., Mühlberger, E. (1995). Acylation of the Marburg virus glycoprotein. *Virology.* 208: 289–297.
 35. Volchkov, V. E., Volchkova, V. A., Stroher, U., Becker, S., Dolnik, O., Cieplik, M., Garten, W., Klenk, H. D., Feldmann, H. (2000). Proteolytic processing of Marburg virus glycoprotein. *Virology,* 268: 1–6.
 36. Kondratowicz, A. S., Lennemann, N. J., Sinn, P. L., Davey, R. A., Hunt, C. L., Moller-Tank, S., Meyerholz, D. K., Rennert, P., Mullins, R. F., Brindley, M., Sandersfeld, L. M., Quinn, K., et al. (2011). T-cell immunoglobulin and mucin domain 1 (TIM-1) is a receptor for Zaire Ebolavirus and Lake Victoria Marburgvirus. *Proc. Natl. Acad. Sci. U.S.A.* 108: 8426–8431.
 37. Koellhoffer, J. F., Malashkevich, V. N., Harrison, J. S., Toro, R., Bhosle, R. C., Chandran, K., Almo, S. C., Lai, J. R. (2012). Crystal Structure of the Marburg Virus GP2 core domain in its post-fusion conformation. *Biochemistry.* 51(39): 7665-7675.
 38. Modrof, J., Mühlberger, E., Klenk, H. D., Becker, S. (2002). Phosphorylation of VP30 Impairs Ebola Virus transcription. *J. Biol. Chem.* 277: 33099-33104.

39. Fowler, T., Bamberg, S., Möller, P., Klenk, H. D., Meyer, T. F., Becker, S., and Rudel, T. (2005). Inhibition of Marburg virus protein expression and viral release by RNA interference. *J. Gen. Virol.* 86: 1181-1188.
40. Bamberg, S., Kolesnikova, L., Möller, P., Klenk, H. D., Becker, S. (2005). VP24 of Marburg virus influences formation of infectious particles. *J. Virol.* 79: 13421–13433.
41. Poch, O., Blumberg, B. M., Bougueleret, L., Tordo, N. (1990). Sequence comparison of five polymerases (L proteins) of unsegmented negative-strand RNA viruses: theoretical assignment of functional domains. *J. Gen. Virol.* 71: 1153–1162.
42. Matsuno, K., Kishida, N., Usami, K., Igarashi, M., Yoshida, R., Nakayama, E., Shimojima, M., Feldmann, H., Irimura, T., Kawaoka, Y., Takada, A. (2010). Different potential of C-type lectin mediated entry between Marburg virus strains. *J. Virol.* 84: 5140–5147.
43. Gramberg, T., Hofmann, H., Möller, P., Lalor, P. F., Marzi, A., Geier, M., Krumbiegel, M., Winkler, T., Kirchhoff, F., Adams, D. H., Becker, S., Munch, J., Pohlmann, S. (2005). LSECTin interacts with filovirus glycoproteins and the spike protein of SARS coronavirus. *Virology.* 340: 224–236.
44. Becker, S., Spiess, M., and Klenk, H. D. (1995). The asialoglycoprotein receptor is a potential liver-specific receptor for Marburg virus. *J Gen Virol.* 76: 393–9.
45. Hunt, C. L., Kolokoltsov, A. A, Davey, R. A., Maury, W. (2011). The Tyro3 receptor kinase Axl enhances macropinocytosis of Zaire ebolavirus. *J Virol.* 85: 334–347.
46. Shimojima, M., Takada, A., Ebihara, H., Neumann, G., Fujioka, K., Irimura, T., Jones, S., Feldmann, H., and Kawaoka, Y. (2006). Tyro3 family-mediated cell entry of Ebola and Marburg viruses. *J. Virol.* 80: 10109–10116.
47. Kondratowicz, A. S., Lennemann, N. J., Sinn, P. L., Davey, R. A., Hunt, C. L., Moller-Tank, S., ... Maury, W. (2011). Tcellimmunoglobulin and mucin domain 1 (TIM-1) is a receptor for Zaire Ebola virus and Lake Victoria Marburg virus. *PNAS.* 108(20): 8426-8431.
48. Nanbo, A., Imai, M., Watanabe, S., Noda, T., Takahashi, K., Neumann, G., Halfmann, P., Kawaoka, Y. (2010). Ebolavirus is internalized into host cells via macropinocytosis in a viral glycoprotein-dependent manner. *PLoS Pathog* 6:e1001121. [10.1371/journal.ppat.1001121](https://doi.org/10.1371/journal.ppat.1001121).
49. Kolokoltsov, A. A., Albrecht, T., and Davey, R. A. (2010). Cellular entry of Ebola virus involves uptake by a macropinocytosis-like mechanism and subsequent trafficking through early and late endosomes. *PLoS Pathog* 6:e1001110. [10.1371/journal.ppat.1001110](https://doi.org/10.1371/journal.ppat.1001110). Accessed February 05, 2018.

50. Carette, J. E., Raaben, M., Wong, A. C., Herbert, A. S., Obernosterer, G., Mulherkar, N., Kuehne, A. I., Kranzusch, P. J., Griffin, A. M., Ruthel, G., et al. (2011). Ebola virus entry requires the cholesterol transporter Niemann-Pick C1. *Nature*. 477: 340–343.
51. Weissenhorn, W., Carfi, A., Lee, K. H., Skehel, J.J., and Wiley, D. C. (1998). Crystal structure of the Ebola virus membrane fusion subunit, GP2, from the envelope glycoprotein ectodomain. *Mol. Cell*. 2: 605–616.
52. Mittler, E., Kolesnikova, L., Strecker, T., Garten, W., Becker, S. (2007). Role of the transmembrane domain of marburg virus surface protein GP in assembly of the viral envelope. *J. Virol.* (81): 3942–3948.
53. Garoff, H., Hewson, R., and Opstelten, D.-J. E. (1998). Virus Maturation by Budding. *Microbiology and Molecular Biology Reviews*, 62(4): 1171–1190.
54. Gaudier, M., Gaudin, Y., and Knossow, M. (2002). Crystal structure of vesicular stomatitis virus matrix protein. *The EMBO Journal*, 21(12): 2886–2892.
55. Finkelshtein, D., Werman, A., Novick, D., Barak, S., and Rubinstein, M. (2013). LDL receptor and its family members serve as the cellular receptors for vesicular stomatitis virus. *Proc Natl Acad Sci U S A*. 110(18): 7306–11.
56. 1. Li, J. and Zhang, Y. (2012). Messenger RNA Cap Methylation in Vesicular Stomatitis Virus, a Prototype of Nonsegmented Negative-Sense RNA Virus, Methylation - From DNA, RNA and Histones to Diseases and Treatment, Prof. Anica Dricu (Ed.), InTech. Available from: <https://www.intechopen.com/books/methylation-from-dna-rna-and-histones-to-diseases-and-treatment/messenger-rna-cap-methylation-in-vesicular-stomatitis-virus-a-prototype-of-non-segmented-negative-se>. Accessed February 04, 2018.
57. Carneiro, F. A., Bianconi, M. L., Weissmüller, G., Stauffer, F., and Da Poian, A. T. (2002). Membrane Recognition by Vesicular Stomatitis Virus Involves Enthalpy-Driven Protein-Lipid Interactions. *Journal of Virology*. 76(8): 3756–3764.
58. Mire, C. E., White, J. M., and Whitt, M. A. (2010). A Spatio-Temporal Analysis of Matrix Protein and Nucleocapsid Trafficking during Vesicular Stomatitis Virus Uncoating. *PLoS Pathog*, 6(7): e1000994.
59. Ogino, T. (2014). Capping of vesicular stomatitis virus pre-mRNA is required for accurate selection of transcription stop–start sites and virus propagation. *Nucleic Acids Research*, 42(19): 12112–12125.
60. Amman, B. R., Carroll, S. A., Reed, Z. D., Sealy, T. K., Balinandi, S., Swanepoel, R., Kemp, A., Erickson, B. R., Comer, J. A., et al. (2012). Seasonal pulses of Marburg virus circulation in juvenile *Rousettus aegyptiacus* bats coincide with periods of increased risk of human infection. *PLoS Pathog* 8: e1002877. Accessed February 03, 2018.

61. Towner, J. S., Amman, B. R., Sealy, T. K., Carroll, S. A., Comer, J. A., Kemp, A., Swanepoel, R., Paddock, C. D., Balinandi, S., et al. (2009). Isolation of Genetically Diverse Marburg Viruses from Egyptian Fruit Bats. *PLoS Pathog* 5: e1000536. Accessed January 26, 2018.
62. Martini, G. A. (1969). Marburg agent disease: In man. *Trans. R. Soc. Trop. Med. Hyg.* 63: 295–302.
63. Slenczka, W. G. (1999). The Marburg virus outbreak of 1967 and subsequent episodes. *Curr. Top. Microbiol. Immunol.* 235: 49–75.
64. Stille, W., Böhle, E. (1971). Clinical course and prognosis of Marburg virus (green monkey) disease. In *Marburg virus disease*, Martini, G.A., Siebert, R. Eds., pp. 10–18. Berlin: Springer.
65. Hartman, A. L., Towner, J. S., and Nichol, S. T. (2010). Ebola and marburg hemorrhagic fever. *Clin. Lab. Med.* 30: 161–177.
66. Mehedi, M., Groseth, A., Feldmann, H., and Ebihara, H. (2011). Clinical aspects of Marburg hemorrhagic fever. *Future Virol.* 6: 1091–1106.
67. Kortepeter, M. G., Bausch, D. G., Bray, M. (2011). Basic clinical and laboratory features of filoviral hemorrhagic fever. *J. Infect. Dis.* 204: S810–6.
68. Ströher, U., West, E., Bugany, H., Klenk, H. D., Schnittler, H. J., Feldmann, H. (2001). Infection and activation of monocytes by Marburg and Ebola viruses. *J. Virol.* 75: 11025–11033.
69. Schnittler, H. J. and Feldmann, H. (1998). Marburg and Ebola hemorrhagic fevers: does the primary course of infection depend on the accessibility of organ-specific macrophages? *Clin. Infect. Dis.* 27: 404–406.
70. Hensley, L. E., Alves, D. A., Geisbert, J. B., Fritz, E. A., Reed, C., Larsen, T., Geisbert, T. W. (2011). Pathogenesis of Marburg hemorrhagic fever in cynomolgus macaques. *J. Infect. Dis.* 204: S1021–S1031.
71. Fritz, E. A., Geisbert, J. B., Geisbert, T. W., Hensley, L. E., Reed, D. S. (2008). Cellular immune response to Marburg virus infection in cynomolgus macaques. *Viral Immunol.* (21): 355–363.
72. Lin, K. L., Twenhafel, N. A., Connor, J. H., Cashman, K. A., Shamblin, J. D., Donnelly, G. C., ... Goff, A. J. (2015). Temporal Characterization of Marburg Virus Angola Infection following Aerosol Challenge in Rhesus Macaques. *Journal of Virology*, 89(19): 9875–9885.
73. Alves, D. A., Glynn, A. R., Steele, K. E., Lackemeyer, M. G., Garza, N. L., Buck, J. G., Mech, C., Reed, D. S. (2010). Aerosol exposure to the angola strain of marburg virus causes lethal viral hemorrhagic Fever in cynomolgus macaques. *Vet. Pathol.* 47: 831–851.
74. Stroher, U., West, E., Bugany, H., Klenk, H. D., Schnittler, H. J., and Feldmann, H. (2001). Infection and Activation of Monocytes by Marburg and Ebola Viruses. *Journal of Virology*, 75(22): 11025–11033.

75. Böckeler, M., Ströher, U., Seebach, J., Afanasieva, T., Suttorp, N., Feldmann, H., & Schnittler, H. (2007). Breakdown of Paraendothelial Barrier Function during Marburg Virus Infection Is Associated with Early Tyrosine Phosphorylation of Platelet Endothelial Cell Adhesion Molecule-1. *The Journal of Infectious Diseases*, 196(s2): S337–S346.
76. Feldmann, H., Bugany, H., Mahner, F., Klenk, H. D., Drenckhahn, D., & Schnittler, H. J. (1996). Filovirus-induced endothelial leakage triggered by infected monocytes/macrophages. *Journal of Virology*, 70(4): 2208–14.
77. Stille, W., Boehle, E.. (1971). Clinical course and prognosis of Marburg virus ('green-monkey') disease. In: Martini GA, Siegert R, editors. *Marburg Virus Disease*. Springer-Verlag; NY, USA.
78. Bente, D., Gren, J., Strong, J.E., Feldmann, H. (2009). Disease modeling for Ebola and Marburg viruses. *Dis. Model Mech.* 2(1–2): 12–17.
79. Egbring, R., Slenczka, W., Baltzer, G. (1971). Clinical manifestations and mechanism of the haemorrhagic diathesis in Marburg virus disease. In: Martini GA, Siegert R, editors. *Marburg Virus Disease*. Springer-Verlag; NY, USA.
80. Bosio, C. M., Aman, M. J., Grogan, C., Hogan, R., Ruthel, G., Negley, D., ... Schmaljohn, A. (2003). Ebola and Marburg Viruses Replicate in Monocyte-Derived Dendritic Cells without Inducing the Production of Cytokines and Full Maturation. *The Journal of Infectious Diseases*, 188(11): 1630–1638.
81. Bosio, C. M., Moore, B. D., Warfield, K. L., Ruthel, G., Mohamadzadeh, M., Aman, M. J., and Bavari, S. (2004). Ebola and Marburg virus-like particles activate human myeloid dendritic cells. *Virology*, 326(2): 280–287.
82. Geisbert, T.W., Hensley, L.E., Gibb, T.R., Steele, K.E., Jaax, N.K., Jahrling, P.B. (2000). Apoptosis induced in vitro and in vivo during infection by Ebola and Marburg viruses. *Lab. Invest.* 80: 171–186.
83. Murphy, F. A., Simpson, D. I. H., Whitfield, S. G., et al. (1971). Marburg virus infection in monkeys. *Lab Invest*, 1971(24): 279-291.
84. Kumar, H., Kawai, T., and Akira, S. (2011). "Pathogen Recognition by the Innate Immune System". *International Reviews of Immunology*. 30 (1): 16–34.
85. Seong S. Y., Matzinger P. (2004). "Hydrophobicity: an ancient damage-associated molecular pattern that initiates innate immune responses". *Nature Reviews. Immunology*. 4(6): 469–78.
86. Thompson, M. R., Kaminski, J. J., Kurt-Jones, E. A., and Fitzgerald, K. A. (2011). Pattern Recognition Receptors and the Innate Immune Response to Viral Infection. *Viruses*, 3(6): 920–940.
87. Liu, Y. J. (2005). "IPC: professional type 1 interferon-producing cells and plasmacytoid dendritic cell precursors". *Annu Rev Immunol*. 23: 275–306.

88. Kiu, H., and Nicholson, S. E. (2012). Biology and significance of the JAK/STAT signalling pathways. *Growth Factors* (Chur, Switzerland), 30(2): 88–106.
89. Keskinen, P., Ronni, T., Matikainen, S., Lehtonen, A., and Julkunen, I. (1997). Regulation of HLA class I and II expression by interferons and influenza A virus in human peripheral blood mononuclear cells. *Immunology*. 91(3): 421–429.
90. Vilček, J., and Le, J. (1998). Interferon γ A2 - Delves, Peter J. *BT - Encyclopedia of Immunology* (Second Edition) (pp. 1421–1426). Oxford: Elsevier.
91. Hsieh, C. S., Macatonia, S. E., Tripp, C. S., Wolf, S. F., O'Garra, A., Murphy, K. M. (1993). Development of TH1 CD4+ T cells through IL-12 produced by Listeria-induced macrophages. *Science*, 260 (5107): 547–9.
92. Murphy, K, Travers, P, and Walport, M. (2008). *Janeway's Immunobiology*. Seventh edition. New York: Garland Science.
93. Kato, H., Takeuchi, O., Sato, S., Yoneyama, M., Yamamoto, M., Matsui, K., ... Akira, S. (2006). Differential roles of MDA5 and RIG-I helicases in the recognition of RNA viruses. *Nature*. 441: 101.
94. Hornung, V., Ellegast, J., Kim, S., Brzózka, K., Jung, A., Kato, H., ... Hartmann, G. (2006). 5'-Triphosphate RNA Is the Ligand for RIG-I. *Science*, 314(5801): 994 LP-997.
95. Loo, Y. M., Fornek, J., Crochet, N., Bajwa, G., Perwitasari, O., Martinez-Sobrido, L., ... Gale, M. (2008). Distinct RIG-I and MDA5 Signaling by RNA Viruses in Innate Immunity . *Journal of Virology*. 82(1): 335–345.
96. Liu, S. Y., Sanchez, D. J., Aliyari, R., Lu, S., and Cheng, G. (2012). Systematic identification of type I and type II interferon-induced antiviral factors. *Proceedings of the National Academy of Sciences*. 109(11): 4239–4244.
97. Reikine, S., Nguyen, J. B., and Modis, Y. (2014). Pattern Recognition and Signaling Mechanisms of RIG-I and MDA5. *Frontiers in Immunology*. 5: 342.
98. Satoh, T., Kato, H., Kumagai, Y., Yoneyama, M., Sato, S., Matsushita, K., ... Takeuchi, O. (2010). LGP2 is a positive regulator of RIG-I- and MDA5-mediated antiviral responses. *Proceedings of the National Academy of Sciences of the United States of America*. 107(4): 1512–1517.
99. Delneste, Y., Beauvillain, C., Jeannin, P. (2007). "Innate immunity: structure and function of TLRs". *Med Sci (Paris)*. 23 (1): 67–73.
100. Takeda, K., Kaisho, T., and Akira, S. (2003). Toll Like Receptors. *Annual Review of Immunology*. 21(1): 335–376.
101. Honda, K., and Taniguchi, T. (2006). IRFs: master regulators of signalling by Toll-like receptors and cytosolic pattern-recognition receptors. *Nature Reviews Immunology*. 6: 644.

102. Edelmann, K. H., Richardson-Burns, S., Alexopoulou, L., Tyler, K. L., Flavell, R. A., and Oldstone, M. B. A. (2004). Does Toll-like receptor 3 play a biological role in virus infections? *Virology*. 322(2): 231–238.
103. Georgel, P., Jiang, Z., Kunz, S., Janssen, E., Mols, J., Hoebe, K., ... Beutler, B. (2007). Vesicular stomatitis virus glycoprotein G activates a specific antiviral Toll-like receptor 4-dependent pathway. *Virology*. 362(2): 304–313.
104. Verhelst, J., Hulpiau, P., and Saelens, X. (2013). Mx Proteins: Antiviral Gatekeepers That Restrain the Uninvited. *Microbiology and Molecular Biology Reviews*, 77(4): 551–566.
105. Sarojini, S., Theofanis, T., and Reiss, C. S. (2011). Interferon-Induced Tetherin Restricts Vesicular Stomatitis Virus Release in Neurons. *DNA and Cell Biology*. 30(12): 965–974.
106. Baltzis, D., Qu, L. K., Papadopoulou, S., Blais, J. D., Bell, J. C., Sonenberg, N., Koromilas, A. E. (2004). Resistance to vesicular stomatitis virus infection requires a functional cross talk between the eukaryotic translation initiation factor 2a kinases PERK and PKR. *J. Virol.* 78: 12747–12761.
107. Wagner, R. R., and Huang, A. S. (1966). Inhibition of RNA and interferon synthesis in Krebs-2 cells infected with vesicular stomatitis virus. *Virology*. 28(1): 1–10.
108. Black, B. L., Rhodes, R. B., McKenzie, M., and Lyles, D. S. (1993). The role of vesicular stomatitis virus matrix protein in inhibition of host-directed gene expression is genetically separable from its function in virus assembly. *Journal of Virology*. 67(8): 4814–4821.
109. D'agostino, P. M., Amenta, J. J., and Reiss, C. S. (2009). IFN- β -Induced Alteration of VSV Protein Phosphorylation in Neuronal Cells. *Viral Immunology*. 22(6): 353–369.
110. Kash, J. C., Mühlberger, E., Carter, V., Grosch, M., Perwitasari, O., Proll, S. C., ... Katze, M. G. (2006). Global Suppression of the Host Antiviral Response by Ebola- and Marburgviruses: Increased Antagonism of the Type I Interferon Response Is Associated with Enhanced Virulence. *Journal of Virology*. 80(6): 3009–3020.
111. Valmas, C., Grosch, M. N., Schümann, M., Olejnik, J., Martinez, O., Best, S. M., ... Mühlberger, E. (2010). Marburg virus evades interferon responses by a mechanism distinct from ebola virus. *PLoS Pathogens*, 6(1): e1000721.
112. Bray, M. (2001). The role of the Type I interferon response in the resistance of mice to filovirus infection. *Journal of General Virology*. 82(6): 1365–1373.
113. Bray, M., Raymond, J. L., Geisbert, T., and Baker, R. O. (2002). 3-Deazaneplanocin A induces massively increased interferon- α production in Ebola virus-infected mice. *Antiviral Research*. 55(1): 151–159.
114. Smith, L. M., Hensley, L. E., Geisbert, T. W., Johnson, J., Stossel, A., Honko, A., ... Karp, C. L. (2013). Interferon- β Therapy Prolongs Survival in Rhesus

- Macaque Models of Ebola and Marburg Hemorrhagic Fever. *The Journal of Infectious Diseases*. 208(2): 310–318.
115. Jahrling, P. B., Geisbert, T. W., Geisbert, J. B., Swearingen, J. R., Bray, M., Jaax, N. K., ... Peters, C. J. (1999). Evaluation of Immune Globulin and Recombinant Interferon- α 2b for Treatment of Experimental Ebola Virus Infections. *The Journal of Infectious Diseases*. 179(Supplement_1): S224–S234.
 116. Messaoudi, I., Amarasinghe, G.K., and Basler, C.F. (2015). Filovirus pathogenesis and immune evasion: insights from Ebola virus and Marburg virus. *Nat. Rev. Microbiol.* 13 (11): 663-676.
 117. Bale, S., Julien, J.-P., Bornholdt, Z. A., Kimberlin, C. R., Halfmann, P., Zandonatti, M. A., ... Saphire, E. O. (2012). Marburg Virus VP35 Can Both Fully Coat the Backbone and Cap the Ends of dsRNA for Interferon Antagonism. *PLoS Pathogens*, 8(9): e1002916.
 118. Ramanan, P., Edwards, M. R., Shabman, R. S., Leung, D. W., Endlich-Frazier, A. C., Borek, D. M., ... Amarasinghe, G. K. (2012). Structural basis for Marburg virus VP35-mediated immune evasion mechanisms. *Proceedings of the National Academy of Sciences of the United States of America*, 109(50): 20661–20666.
 119. Lofts, L. L., Ibrahim, M. S., Negley, D. L., Hevey, M. C., Schmaljohn, A. L. (2007). Genomic differences between guinea pig lethal and nonlethal Marburg virus variants. *J. Infect. Dis.* 196(Suppl. 2): S305–S312.
 120. Lofts, L. L., Wells, J. B., Bavari, S., & Warfield, K. L. (2011). Key Genomic Changes Necessary for an In Vivo Lethal Mouse Marburgvirus Variant Selection Process. *Journal of Virology*, 85(8): 3905–3917.
 121. Qiu, X., Wong, G., Audet, J., Cutts, T., Niu, Y., Booth, S., & Kobinger, G. P. (2014). Establishment and Characterization of a Lethal Mouse Model for the Angola Strain of Marburg Virus. *Journal of Virology*, 88(21): 12703–12714.
 122. Valmas, C., and Basler, C. F. (2011). Marburg Virus VP40 Antagonizes Interferon Signaling in a Species-Specific Manner. *Journal of Virology*. 85(9): 4309–4317.
 123. Bray, M. (2001). The role of the Type I interferon response in the resistance of mice to filovirus infection. *Journal of General Virology*, 82(6): 1365–1373.
 124. Guito, J. C., Albariño, C. G., Chakrabarti, A. K., and Towner, J. S. (2017). Novel activities by ebolavirus and marburgvirus interferon antagonists revealed using a standardized in vitro reporter system. *Virology*. 501: 147–165.
 125. Edwards, M. R., Liu, G., Mire, C. E., Sureshchandra, S., Luthra, P., Yen, B., ... Basler, C. F. (2016). Differential regulation of interferon responses by Ebola and Marburg virus VP35 proteins. *Cell Reports*. 14(7): 1632–1640.

126. Köhl, A., Banning, C., Marzi, A., Votteler, J., Steffen, I., Bertram, S., ... Pöhlmann, S. (2011). The Ebola Virus Glycoprotein and HIV-1 Vpu Employ Different Strategies to Counteract the Antiviral Factor Tetherin. *The Journal of Infectious Diseases*. 204(Suppl 3): S850–S860.
127. Noyori, O., Matsuno, K., Kajihara, M., Nakayama, E., Igarashi, M., Kuroda, M., ... Takada, A. (2013). Differential potential for envelope glycoprotein-mediated steric shielding of host cell surface proteins among filoviruses. *Virology*. 446(1–2): 152–161.
128. Edwards, M. R., Johnson, B., Mire, C. E., Xu, W., Shabman, R. S., Speller, L. N., ... Basler, C. F. (2014). The Marburg virus VP24 protein interacts with Keap1 to activate the cytoprotective antioxidant response pathway. *Cell Reports*. 6(6): 1017–1025.
129. Connor, J. H., Yen, J., Caballero, I. S., Garamszegi, S., Malhotra, S., Lin, K., ... Goff, A. J. (2015). Transcriptional Profiling of the Immune Response to Marburg Virus Infection. *Journal of Virology*. 89(19): 9865–9874.
130. Stonier, S. W., Herbert, A. S., Kuehne, A. I., Sobarzo, A., Habibulin, P., Dahan, C. V. A., ... Dye, J. M. (2017). Marburg virus survivor immune responses are Th1 skewed with limited neutralizing antibody responses. *J Exp Med*. 214(9): 2563-2572.
131. Tanaka, T., Hu-Li, J., Seder, R. A., Fazekas de St Groth, B., and Paul, W. E. (1993). Interleukin 4 suppresses interleukin 2 and interferon gamma production by naive T cells stimulated by accessory cell-dependent receptor engagement. *Proceedings of the National Academy of Sciences of the United States of America*. 90(13): 5914–5918.
132. World Health Organization. Marburg virus disease. Fact sheet, October 2017. Geneva, Switzerland: World Health Organization. Available at: http://www.who.int/mediacentre/factsheets/fs_marburg/en/. Accessed 17 Nov 2017.
133. World Health Organization. Disease outbreak news- Marburg virus disease- Uganda and Kenya, 15 Nov 2017. Geneva, Switzerland: World Health Organization. Available at: <http://www.who.int/csr/don/7-november-2017-marburg/en/>. Accessed 17 Nov 2017.
134. Benda, P., Vallo, P., Hulva, P., and Horáček, I. (2012). The Egyptian fruit bat *Rousettus aegyptiacus* (Chiroptera: Pteropodidae) in the Palaearctic: Geographical variation and taxonomic status. 67(6): 1230–1244. Poland: Biologia.
135. Alibek, Steven. (1999). *Biohazard: The Chilling True Story of the Largest Covert Biological Weapons Program in the World—Told from Inside by the Man Who Ran It*. New York: Random House.
136. Ignatyev, G. M., Agafonov, A. P., Streltsova, M. A., Kashentseva, E. A. (1996). Inactivated Marburg virus elicits a nonprotective immune response in Rhesus monkeys. *J Biotechnol*. 44: 111–118.

137. Hevey, M., Negley, D., Pushko, P., Smith, J., Schmaljohn, A. (1998). Marburg virus vaccines based upon alphavirus replicons protect guinea pigs and nonhuman primates. *Virology*. 251: 28–37.
138. Hevey, M., Negley, D., Staley, A., Schmaljohn A. (2001). Determination of vaccine components required for protecting cynomolgus macaques against genetically divergent isolates of Marburg virus. 20th Annual meeting of the American Society of Virology, Madison, Wisconsin, USA.
139. Swenson, D.L., Warfield, K.L., Larsen, T., Alves, D.A., Coberley, S.S., Bavari, S. (2008). Monovalent virus-like particle vaccine protects guinea pigs and nonhuman primates against infection with multiple Marburg viruses. *Expert Rev. Vaccines*. 7(4): 417–429.
140. Riemenschneider, J., Garrison, A., Geisbert, J., Jahrling, P., Hevey, M., Negley, D., ... Schmaljohn, C. (2003). Comparison of individual and combination DNA vaccines for B. anthracis, Ebola virus, Marburg virus and Venezuelan equine encephalitis virus. *Vaccine*, 21(25–26): 4071–4080.
141. Geisbert, T.W., Bailey, M., Geisbert, J.B., Asiedu, C., Roederer, M., Grazia-Pau, M., Custers, J., Jahrling, P., Goudsmit, J., Koup, R., Sullivan, N.J. (2010). Vector choice determines immunogenicity and potency of genetic vaccines against Angola Marburg virus in nonhuman primates. *J. Virol.* 84: 10386–10394.
142. Swenson, D. L., Wang, D., Luo, M., Warfield, K. L., Woraratanadharm, J., Holman, D. H., ... Pratt, W. D. (2008). Vaccine To Confer to Nonhuman Primates Complete Protection against Multistrain Ebola and Marburg Virus Infections . *Clinical and Vaccine Immunology*, 15(3): 460–467.
143. 1. Jones, S. M., Feldmann, H., Ströher, U., Geisbert, J. B., Fernando, L., Grolla, A., ... Geisbert, T. W. (2005). Live attenuated recombinant vaccine protects nonhuman primates against Ebola and Marburg viruses. *Nature Medicine*, 11(7): 786–790.
144. Daddario-DiCaprio, K. M., Geisbert, T. W., Geisbert, J. B., Ströher, U., Hensley, L. E., Grolla, A., ... Jones, S. M. (2006). Cross-Protection against Marburg Virus Strains by Using a Live, Attenuated Recombinant Vaccine. *Journal of Virology*. 80(19): 9659–9666.
145. Geisbert, T. W., Daddario-DiCaprio, K. M., Geisbert, J. B., Reed, D. S., Feldmann, F., Grolla, A., ... Feldmann, H. (2008). Vesicular stomatitis virus-based vaccines protect nonhuman primates against aerosol challenge with Ebola and Marburg viruses. *Vaccine*, 26(52): 6894–6900.
146. Geisbert, T. W., Geisbert, J. B., Leung, A., Daddario-DiCaprio, K. M., Hensley, L. E., Grolla, A., & Feldmann, H. (2009). Single-Injection Vaccine Protects Nonhuman Primates against Infection with Marburg Virus and Three Species of Ebola Virus. *Journal of Virology*, 83(14): 7296–7304.
147. Daddario-DiCaprio, K. M., Geisbert, T. W., Ströher, U., Geisbert, J. B., Grolla, A., Fritz, E. A., ... Feldmann, H. (2006). Postexposure protection

- against Marburg haemorrhagic fever with recombinant vesicular stomatitis virus vectors in non-human primates: an efficacy assessment. *Lancet* (London, England), 367(9520): 1399–404.
148. Geisbert, T. W., Hensley, L. E., Geisbert, J. B., et al. (2010). Postexposure treatment of Marburg virus infection. *Emerg Infect Dis.* 16: 1119–1122.
 149. Geisbert, T. W., Daddario-Dicaprio, K. M., Lewis, M. G., Geisbert, J. B., Grolla, A., et al. (2008) Vesicular stomatitis virus-based ebola vaccine is well-tolerated and protects immunocompromised nonhuman primates. *PLoS Pathog* 4: e1000225.
 150. Mire, C. E., Miller, A. D., Carville, A., Westmoreland, S. V., Geisbert, J. B., Mansfield, K. G., Feldmann, H., Hensley, L. E., Geisbert, T. W. (2012). Recombinant vesicular stomatitis virus vaccine vectors expressing filovirus glycoproteins lack neurovirulence in nonhuman primates. *PLoS Negl Trop Dis.* 6(3): e1567.
 151. Marzi, A., Feldmann, F., Geisbert, T. W., Feldmann, H., & Safronetz, D. (2015). Vesicular stomatitis virus-based vaccines against lassa and ebola viruses. *Emerging Infectious Diseases*, 21(2): 305–307.
 152. Mire, C. E., Geisbert, J. B., Agans, K. N., Satterfield, B. a, Versteeg, K. M., Fritz, E. a, ... Geisbert, T. W. (2014). Durability of a vesicular stomatitis virus-based marburg virus vaccine in nonhuman primates. *PloS One*, 9(4): e94355.
 153. Bray, M., Paragas, J. (2002). Experimental therapy of filovirus infections. *Antiviral Res.* 54: 1-17.
 154. Warren, T. K., Wells, J., Panchal, R. G., Stuthman, K. S., Garza, N. L., Van Tongeren, S. A., ... Bavari, S. (2014). Protection against filovirus diseases by a novel broad-spectrum nucleoside analogue BCX4430. *Nature*, 508(7496): 402–405.
 155. Warren, T. K., Whitehouse, C. A., Wells, J., Welch, L., Charleston, J. S., Heald, A., ... Bavari, S. (2016). Delayed Time-to-Treatment of an Antisense Morpholino Oligomer Is Effective against Lethal Marburg Virus Infection in *Cynomolgus Macaques*. *PLoS Neglected Tropical Diseases*, 10(2): 1–18.
 156. Warren, T. K., Warfield, K. L., Wells, J., Swenson, D. L., Donner, K.S ., Van Tongeren, S. A., Garza, N. L., Dong, L., Mourich, D. V., Crumley, S., et al. (2010). Advanced antisense therapies for postexposure protection against lethal filovirus infections. *Nat. Med.* 16: 991–994.
 157. Dye, J. M. et al. (2012). Postexposure antibody prophylaxis protects nonhuman primates from filovirus disease. *Proc. Natl Acad. Sci. USA* 109: 5034–5039.
 158. Thi, E. P., Mire, C. E., Ursic-Bedoya, R., Geisbert, J. B., Lee, A. C. H., Agans, K. N., ... Geisbert, T. W. (2014). Marburg virus infection in

- nonhuman primates: Therapeutic treatment by lipid-encapsulated siRNA. *Science Translational Medicine*, 6(250): 250ra116-250ra116.
159. Thi, E. P., Mire, C. E., Lee, A. C. H., Geisbert, J. B., Ursic-Bedoya, R., Agans, K. N., ... Geisbert, T. W. (2017). siRNA rescues nonhuman primates from advanced Marburg and Ravn virus disease. *Journal of Clinical Investigation*. 127(12): 4437–4448.
 160. Mire, C. E., Geisbert, J. B., Borisevich, V., et al. (2017). Therapeutic treatment of Marburg and Ravn virus infection in nonhuman primates with a human monoclonal antibody. *Sci Transl Med*. 5(9): 384.
 161. King, L. B., Fusco, M. L., Flyak, A. I., Ilinykh, P. A., Huang, K., Gunn, B., ... Saphire, E. O. (2018). The Marburgvirus-Neutralizing Human Monoclonal Antibody MR191 Targets a Conserved Site to Block Virus Receptor Binding. *Cell Host & Microbe*, 23(1): 101–109.e4.
 162. Fedorov, Y., Anderson, E. M., Birmingham, A., Reynolds, A., Karpilow, J., Robinson, K., ... Khvorova, A. (2006). Off-target effects by siRNA can induce toxic phenotype. *RNA*. 12(7): 1188–1196.
 163. Tabll, A., Abbas, A. T., El-Kafrawy, S., and Wahid, A. (2015). Monoclonal antibodies: Principles and applications of immunodiagnosis and immunotherapy for hepatitis C virus. *World Journal of Hepatology*, 7(22): 2369–2383.
 164. Khurana, S., Fuentes, S., Coyle, E. M., Ravichandran, S., Davey, R. T., and Beigel, J. H. (2016). Human antibody repertoire after VSV-Ebola vaccination identifies novel targets and virus-neutralizing IgM antibodies. *Nature Medicine*. 22(12): 1439–1447.
 165. Farooq, F., Beck, K., Paolino, K. M., Phillips, R., Waters, N. C., Regules, J. A., & Bergmann-Leitner, E. S. (2016). Circulating follicular T helper cells and cytokine profile in humans following vaccination with the rVSV-ZEBOV Ebola vaccine. *Scientific Reports*. 6: 1–9.
 166. Menicucci, A. R., Sureshchandra, S., Marzi, A., Feldmann, H., and Messaoudi, I. (2017). Transcriptomic analysis reveals a previously unknown role for CD8+ T-cells in rVSV-EBOV mediated protection. *Scientific Reports*. 7(1): 919.
 167. Dahlke, C., Kasonta, R., Lunemann, S., Krähling, V., Zinser, M. E., Biedenkopf, N., ... Lapujade, O. (2017). Dose-dependent T-cell Dynamics and Cytokine Cascade Following rVSV-ZEBOV Immunization. *EBioMedicine*. 19: 107–118.
 168. Maloy, K. J., Burkhart, C., Junt, T. M., Odermatt, B., Oxenius, A., Piali, L., ... Hengartner, H. (2000). Cd4+ T Cell Subsets during Virus Infection: Protective Capacity Depends on Effector Cytokine Secretion and on Migratory Capability. *The Journal of Experimental Medicine*. 191(12): 2159–2170.

169. Marzi, A., Hanley, P. W., Haddock, E., Martellaro, C., Kobinger, G., and Feldmann, H. (2016). Efficacy of Vesicular Stomatitis Virus–Ebola Virus Postexposure Treatment in Rhesus Macaques Infected With Ebola Virus Makona. *The Journal of Infectious Diseases*. 214(Suppl 3): S360–S366.
170. Martins, K., Cooper, C., Warren, T., Wells, J., Bell, T., Raymond, J., ... Bavari, S. (2014). Characterization of Clinical and Immunological Parameters During Ebola Virus Infection of Rhesus Macaques. *Viral Immunology*, 28(1): 32–41.
171. Wong, G., Qiu, X., De La Vega, M. A., Fernando, L., Wei, H., Bello, A., ... Kobinger, G. (2016). Pathogenicity Comparison between the Kikwit and Makona Ebola Virus Variants in Rhesus Macaques. *Journal of Infectious Diseases*, 214(April): S281–S289.
172. Marzi, A., Engelmann, F., Feldmann, F., Haberthur, K., Shupert, W. L., Brining, D., ... Messaoudi, I. (2013). Antibodies are necessary for rVSV/ZEBOV-GP-mediated protection against lethal Ebola virus challenge in nonhuman primates. *Proceedings of the National Academy of Sciences of the United States of America*. 110(5): 1893–1898.
173. Borio, L., Inglesby, T., Peters, C. J., et al. (2002). Hemorrhagic fever viruses as biological weapons: medical and public health management. *JAMA*. 287:2391–2405.
174. Henao-Restrepo, A. M., Camacho, A., Longini, I. M., et al. (2017). Efficacy and effectiveness of an rVSV-vectored vaccine expressing Ebola surface glycoprotein: final results from the Guinea ring vaccination, open-label, cluster-randomised trial (Ebola Ça Suffit!). *Lancet*. 389(10068): 505-518.
175. Kennedy, S. B., Bolay, F., Kieh, M., et al. (2017). Phase 2 Placebo-Controlled Trial of Two Vaccines to Prevent Ebola in Liberia. *N Engl J Med*. 377(15): 1438-1447.
176. Cross, R. W., Fenton, K. A., Geisbert, J. B., Ebihara, H., Mire, C. E., Geisbert, T. W. (2015). Comparison of the Pathogenesis of the Angola and Ravn Strains of Marburg Virus in the Outbred Guinea Pig Model. *J Infect Dis*. 212: S258-S270.
177. Johnston, S. C., Lin, K. L., Twenhafel, N. A., et al. (2015). Dose response of MARV/Angola infection in cynomolgus macaques following im or aerosol exposure. *PLoS One*. 10: 9.
178. Cooper, D., Wright, K. J., Calderon, P. C., et al. (2008). Attenuation of Recombinant Vesicular Stomatitis Virus-Human Immunodeficiency Virus Type 1 Vaccine Vectors by Gene Translocations and G Gene Truncation Reduces Neurovirulence and Enhances Immunogenicity in Mice. *J Virol*. 82(1): 207-219.
179. Whitt, M.A., Geisbert, T.W., Mire, C.E. (2016). Single-Vector, Single-Injection Recombinant Vesicular Stomatitis Virus Vaccines Against High-

- Containment Viruses. In: Thomas S. (eds) Vaccine Design. Methods in Molecular Biology, vol 1403. New York, NY: Humana Press.
180. Roberts, A., L. Buonocore, R. Price, J. Forman, and J. K. Rose. 1999. Attenuated vesicular stomatitis viruses as vaccine vectors. *J. Virol.* 73: 3723-3732.
 181. Flanagan, E. B., J. M. Zamparo, L. A. Ball, L. L. Rodriguez, and G. W. Wertz. 2001. Rearrangement of the genes of vesicular stomatitis virus eliminates clinical disease in the natural host: new strategy for vaccine development. *J. Virol.* 75: 6107-6114.
 182. Schnell, M. J., L. Buonocore, E. Boritz, H. P. Ghosh, R. Chernish, and J. K. Rose. 1998. Requirement for a non-specific glycoprotein cytoplasmic domain sequence to drive efficient budding of vesicular stomatitis virus. *EMBO J.* 17: 1289-1296.
 183. Witko, S. E., Kotash, C. S., Nowak, R. M., Johnson, J. E., Boutilier, L. A. C., Melville, K. J., ... Parks, C. L. (2006). An efficient helper-virus-free method for rescue of recombinant paramyxoviruses and rhabdoviruses from a cell line suitable for vaccine development. *Journal of Virological Methods*, 135(1): 91–101.
 184. Jia, X., Yuan, S., Wang, Y., Fu, Y., Ge, Y., Ge, Y., ... Xu, A. (2017). The role of alternative polyadenylation in the antiviral innate immune response. *Nature Communications*, 8: 1–12.
 185. Kandasamy, R. K., Vladimer, G. I., Snijder, B., Müller, A. C., Rebsamen, M., Bigenzahn, J. W., ... Superti-Furga, G. (2016). A time-resolved molecular map of the macrophage response to VSV infection. *Npj Systems Biology and Applications*, 2(1): 16027.
 186. Turner, J. R. (2009). "Intestinal mucosal barrier function in health and disease". *Nat Rev Immunol.* 9: 799–809.
 187. Rusinova, I., Forster, S., Yu, S., Kannan, A., Masse, M., Cumming, H., Chapman, R., Hertzog, P.J. (2013). INTERFEROME v2. 0: an updated database of annotated interferon-regulated genes. *Nucleic Acids Research*. 41(database issue): D1040-D1046.
 188. Frishberg, A., Brodt, A., Steurman, Y., and Gat-Viks, I. (2016). ImmQuant: a user-friendly tool for inferring immune cell-type composition from gene-expression data. *Bioinformatics.* 32(24): 3842–3843.
 189. Abbas, A. R. et al. (2005) Immune response in silico (IRIS): immune-specific genes identified from a compendium of microarray expression data. *Genes. Immun.*, 6, 319–331. ImmQuant: a user-friendly tool for inferring immune cell type composition from gene-expression data (PDF Download Available). Available from: https://www.researchgate.net/publication/306247856_ImmQuant_a_user_friendly_tool_for_inferring_immune_cell_type_composition_from_gene-expression_data. Accessed Feb 05, 2018.

190. Van Agthoven, T., van Agthoven, T. L., Dekker, A., van der Spek, P. J., Vreede, L., & Dorssers, L. C. (1998). Identification of BCAR3 by a random search for genes involved in antiestrogen resistance of human breast cancer cells. *The EMBO Journal*, 17(10): 2799–2808.
191. Roxrud, I., Raiborg, C., Gilfillan, G.D., Stromme, P., Stenmark, H. (2009). Dual degradation mechanisms ensure disposal of NHE6 mutant protein associated with neurological disease. *Exp Cell Res*, 315(17): 3014–27.
192. Newton, K., Dugger, D. L., Wickliffe, K. E., Kapoor, N., De Almagro, M. C., Vucic, D., ... Dixit, V. M. (2014). Activity of protein kinase RIPK3 determines whether cells die by necroptosis or apoptosis. *Science*, 343(6177): 1357–1360.
193. Shu, Q., Lennemann, N. J., Sarkar, S. N., Sadovsky, Y., & Coyne, C. B. (2015). ADAP2 Is an Interferon Stimulated Gene That Restricts RNA Virus Entry. *PLOS Pathogens*, 11(9): e1005150.
194. Chen, Y. L., Lin, D. W., & Chang, Z. F. (2008). Identification of a putative human mitochondrial thymidine monophosphate kinase associated with monocytic/macrophage terminal differentiation. *Genes to Cells*, 13(7): 679–689.
195. Su, B., Waneck, G. L., Flavell, R. A., and Bothwell, A. L. (1991) The glycosyl phosphatidylinositol anchor is critical for Ly-6A/E-mediated T cell activation. *J Cell Biol*, 112: 377-384.
196. Backes, S., Langlois, R. A., Schmid, S., Varble, A., Shim, J. V., Sachs, D., & tenOever, B. R. (2014). The Mammalian Response to Virus Infection Is Independent of Small RNA Silencing. *Cell Reports*, 8(1): 114–125.
197. Szklarczyk, D., Franceschini, A., Wyder, S., Forslund, K., Heller, D., Huerta-Cepas, J., ... von Mering, C. (2015). STRING v10: protein–protein interaction networks, integrated over the tree of life. *Nucleic Acids Research*, 43(D1): D447–D452.
198. Anderson, S. L., Carton, J. M., Lou, J., Xing, L., & Rubin, B. Y. (1999). Interferon-induced guanylate binding protein-1 (GBP-1) mediates an antiviral effect against vesicular stomatitis virus and encephalomyocarditis virus. *Virology*, 256(1): 8–14.
199. Shydlovskiy, S., Zienert, A. Y., Ince, S., Dovengerds, C., Hohendahl, A., Dargazanli, J. M., ... Herrmann, C. (2017). Nucleotide-dependent farnesyl switch orchestrates polymerization and membrane binding of human guanylate-binding protein 1. *Proceedings of the National Academy of Sciences*, 114(28): E5559–E5568.
200. Thieu, V. T., Yu, Q., Chang, H. C., Yeh, N., Nguyen, E. T., Sehra, S., and Kaplan, M. H. (2008). Stat4 is required for T-bet to promote IL-12-dependent Th1 fate determination. *Immunity*. 29(5): 679–690.

201. Weinstein, J. S., Laidlaw, B. J., Lu, Y., Wang, J. K., Schulz, V. P., Li, N., ... Craft, J. (2018). STAT4 and T-bet control follicular helper T cell development in viral infections. *The Journal of Experimental Medicine*. 215(1): 337-355.
202. Oppmann, B., Lesley, R., Blom, B., Timans, J. C., Xu, Y., Hunte, B., ... Kastelein, R. A. (2000). Novel p19 protein engages IL-12p40 to form a cytokine, IL-23, with biological activities similar as well as distinct from IL-12. *Immunity*. 13(5): 715-725.
203. Chew, L.-J., Shen, W., Ming, X., Senatorov, V. V., Chen, H.-L., Cheng, Y., ... Gallo, V. (2011). Sox17 regulates the Wnt/beta-catenin signaling pathway in oligodendrocyte progenitor cells. *The Journal of Neuroscience: The Official Journal of the Society for Neuroscience*, 31(39): 13921-13935.
204. Rui, L., Yuan, M., Frantz, D., Shoelson, S., & White, M. F. (2002). SOCS-1 and SOCS-3 block insulin signaling by ubiquitin-mediated degradation of IRS1 and IRS2. *Journal of Biological Chemistry*, 277(44): 42394-42398.
205. Chen, L., Neville, R. D., Michael, D. R., Martin, J., Luo, D. D., Thomas, D. W., ... Bowen, T. (2012). Identification and analysis of the human hyaluronan synthase 1 gene promoter reveals Smad3- and Sp3-mediated transcriptional induction. *Matrix Biology*, 31(7-8): 373-379.
206. Meran, S., Thomas, D.W., Stephens, P., Enoch, S., Martin, J., Steadman, R., Phillips, A.O. (2008). Hyaluronan facilitates transforming growth factor-beta1-mediated fibroblast proliferation. *J. Biol. Chem.* 283: 6530-6545.
207. Wu, C., Thalhamer, T., Franca, R. F., Xiao, S., Wang, C., Hotta, C., ... Kuchroo, V. K. (2014). Galectin-9-CD44 interaction enhances stability and function of adaptive regulatory T cells. *Immunity*, 41(2): 270-282.
208. Fernandis, A. Z., Cherla, R. P., & Ganju, R. K. (2003). Differential regulation of CXCR4-mediated T-cell chemotaxis and mitogen-activated protein kinase activation by the membrane tyrosine phosphatase, CD45. *Journal of Biological Chemistry*, 278(11): 9536-9543.
209. Schneider, P. (2005). The role of APRIL and BAFF in lymphocyte activation. *Current Opinion in Immunology*, 17(3): 282-289.
210. Cosmi, L., Annunziato, F., Galli MIG, Maggi RME, Nagata, K., and Romagnani, S. (2000). CRTH2 is the most reliable marker for the detection of circulating human type 2 Th and type 2 T cytotoxic cells in health and disease. *European Journal of Immunology*, 30(10): 2972-9.
211. Schuster, N., and Krieglstein, K. (2002). Mechanisms of TGF-β-mediated apoptosis. *Cell and Tissue Research*. 307(1): 1-14.
212. Zhu, J., Yamane, H., Cote-Sierra, J., Guo, L., & Paul, W. E. (2006). GATA-3 promotes Th2 responses through three different mechanisms: Induction of Th2 cytokine production, selective growth of Th2 cells and inhibition of Th1 cell-specific factors. *Cell Research*, 16(1): 3-10.

213. Brandenburg, J., & Reiling, N. (2016). The Wnt blows: On the functional role of Wnt signaling in mycobacterium tuberculosis infection and beyond. *Frontiers in Immunology*, 7(DEC): 1–11.
214. Zhao, F., Xiao, C., Evans, K. S., Theivanthiran, T., DeVito, N., Holtzhausen, A., ... Hanks, B. A. (2018). Paracrine Wnt5a- β -Catenin Signaling Triggers a Metabolic Program that Drives Dendritic Cell Tolerization. *Immunity*, 48(1): 147–160.e7.
215. Mavin, E., Nicholson, L., Rafez Ahmed, S., Gao, F., Dickinson, A., & Wang, X. (2017). Human Regulatory T Cells Mediate Transcriptional Modulation of Dendritic Cell Function. *The Journal of Immunology*, 198(1): 138–146.
216. Villaseñor, T., Madrid-Paulino, E., Maldonado-Bravo, R., Urbán-Aragón, A., Pérez-Martínez, L., & Pedraza-Alva, G. (2017). Activation of the Wnt pathway by Mycobacterium tuberculosis: A Wnt-Wnt Situation. *Frontiers in Immunology*, 8(FEB): 1–16.
217. Schaale, K., Brandenburg, J., Kispert, A., Leitges, M., Ehlers, S., & Reiling, N. (2013). Wnt6 Is Expressed in Granulomatous Lesions of Mycobacterium tuberculosis-Infected Mice and Is Involved in Macrophage Differentiation and Proliferation. *The Journal of Immunology*, 191(10): 5182–5195.
218. More, S., Yang, X., Zhu, Z., Bamunuarachchi, G., Guo, Y., Huang, C., ... Liu, L. (2018). Regulation of influenza virus replication by Wnt/ β -catenin signaling. *PLoS ONE*, 13(1): 1–21.
219. Daud, M., Rana, M.A., Husnain, T. et al. (2017). Modulation of Wnt signaling pathway by hepatitis B virus. *Arch Virol*.162 (10): 2937-2947.
220. Harmon, B., Bird, S. W., Schudel, B. R., Hatch, A. V., Rasley, A., & Negrete, O. A. (2016). A Genome-Wide RNA Interference Screen Identifies a Role for Wnt/ β -Catenin Signaling during Rift Valley Fever Virus Infection. *Journal of Virology*, 90(16): 7084–7097.
221. Macian, F. (2005). NFAT proteins: Key regulators of T-cell development and function. *Nature Reviews Immunology*, 5(6): 472–484.
222. Wherry, E. J., & Kurachi, M. (2015). Molecular and cellular insights into T cell exhaustion. *Nature Reviews Immunology*, 15(8): 486–499.
223. Kahan, S. M., Wherry, E. J., & Zajac, A. J. (2015). T cell exhaustion during persistent viral infections. *Virology*, 479–480: 180–193.
224. Atfield, A. D., Liu, P., & Penninger, J. M. (2006). The biochemical mechanisms of T-cell anergy. *Current Immunology Reviews*, 2(1): 73–99.
225. Ruibal, P., Oestereich, L., Lüdtkke, A., Becker-Ziaja, B., Wozniak, D. M., Kerber, R., ... Muñoz-Fontela, C. (2016). Unique human immune signature of Ebola virus disease in Guinea. *Nature*, 533(7601): 100–104.
226. Wang, Y., Swiecki, M., Cella, M., Alber, G., Schreiber, R. D., Gilfillan, S., & Colonna, M. (2012). Timing and magnitude of type I interferon responses by

- distinct sensors impact CD8 T cell exhaustion and chronic viral infection. *Cell Host & Microbe*, 11(6): 631–642.
227. Oldstone, M. B. A. (2015). A Jekyll and Hyde Profile: Type 1 Interferon Signaling Plays a Prominent Role in the Initiation and Maintenance of a Persistent Virus Infection. *Journal of Infectious Diseases*, 212(April): S31–6.
 228. Cheng, L., Ma, J., Li, J., Li, D., Li, G., Li, F., ... Zhang, L. (2017). Blocking type I interferon signaling enhances T cell recovery and reduces HIV-1 reservoirs. *The Journal of Clinical Investigation*, 127(1): 269–279.
 229. Teijaro, J.R., Ng, C., Lee, A.M., et al. (2013). Persistent LCMV infection is controlled by blockade of type I interferon signaling. *Science* 340: 207–11.
 230. Wilson, E.B., Yamada, D.H., Elsaesser, H., et al. (2013). Blockade of chronic type I interferon signaling to control persistent LCMV infection. *Science* 340: 202–7.
 231. Kuklina, E. M. (2013). Molecular mechanisms of T-cell anergy. *Biochemistry (Mosc)*, 78(2): 144–156.
 232. Singer, B. D., King, L. S., and D'Alessio, F. R. (2014). Regulatory T Cells as Immunotherapy. *Frontiers in Immunology*, 5: 46.
 233. Lee, J., Tam, H., Adler, L., Ilstad-Minnihan, A., Macaubas, C., and Mellins, E. D. (2017). The MHC class II antigen presentation pathway in human monocytes differs by subset and is regulated by cytokines. *PLoS ONE*, 12(8): e0183594.
 234. Chaudhry, H., Zhou, J., Zhong, Y., Ali, M. M., McGuire, F., Nagarkatti, P. S., and Nagarkatti, M. (2013). Role of Cytokines as a Double-edged Sword in Sepsis. *In Vivo (Athens, Greece)*. 27(6): 669–684.
 235. Huang, H., Dawicki, W., Zhang, X., Town, J., & Gordon, J. R. (2010). Tolerogenic Dendritic Cells Induce CD4⁺CD25^{hi}Foxp3⁺ Regulatory T Cell Differentiation from CD4⁺CD25⁻/loFoxp3⁻ Effector T Cells. *The Journal of Immunology*, 185(9): 5003–5010.
 236. Fang, R., Ismail, N., Shelite, T., & Walker, D. H. (2009). CD4⁺ CD25⁺ Foxp3⁻ T-regulatory cells produce both gamma interferon and interleukin-10 during acute severe murine spotted fever rickettsiosis. *Infection and Immunity*, 77(9): 3838–3849.
 237. Ramsdell, F. (2003). Foxp3 and natural regulatory T cells: Key to a cell lineage? *Immunity*, 19(2): 165–168.
 238. Yao, Y., Vent-Schmidt, J., McGeough, M. D., Wong, M., Hoffman, H. M., Steiner, T. S., & Levings, M. K. (2015). Tr1 Cells, but Not Foxp3 + Regulatory T Cells, Suppress NLRP3 Inflammasome Activation via an IL-10-Dependent Mechanism. *The Journal of Immunology*, 195(2): 488–497.
 239. Roncarolo, M.-G., & Gregori, S. (2008). Is FOXP3 a bona fide marker for human regulatory T cells? *European Journal of Immunology*, 38(4): 925–927.

240. Roederer, M., Nozzi, J.L., and Nason, M.C. (2011). SPICE: exploration and analysis of post-cytometric complex multivariate datasets. *Cytometry A* 79: 167–174.
241. Sakaguchi, S., Miyara, M., Costantino, C. M., & Hafler, D. A. (2010). FOXP3 + regulatory T cells in the human immune system. *Nature Reviews Immunology*, 10(7): 490–500.
242. Lim, T. S., Chew, V., Sieow, J. L., Goh, S., Yeong, J. P.-S., Soon, A. L., & Ricciardi-Castagnoli, P. (2016). PD-1 expression on dendritic cells suppresses CD8+ T cell function and antitumor immunity. *Oncoimmunology*, 5(3): e1085146.
243. Park, S.J., Namkoong, H., Doh, J., Choi, J.C., Yang, B.G., Park, Y., Chul Sung, Y. (2014). Negative role of inducible PD-1 on survival of activated dendritic cells. *J Leukoc Biol* 2014, 95(4): 621-9.
244. Krempsi, J., Karyampudi, L., Behrens, M.D., Erskine, C.L., Hartmann, L., Dong, H., Goode, E.L., Kalli, K.R., Knutson, K.L. (2011). Tumor-infiltrating programmed death receptor-1+ dendritic cells mediate immune suppression in ovarian cancer. *J Immunol*, 186: 6905-13.
245. Yao, S., Wang, S., Zhu, Y., Luo, L., Zhu, G., Flies, S., Xu, H., Ruff, W., Broadwater, M., Choi, I.H., et al. (2009). PD-1 on dendritic cells impedes innate immunity against bacterial infection. *Blood*, 113: 5811-8.
246. McCoy, K. D., and Le Gros, G. (1999). The role of CTLA-4 in the regulation of T cell immune responses. *Immunology and Cell Biology*, 77(1): 1–10.
247. Schmittel, A., Scheibenbogen, C., and Keilholz, U. (1995), Lipopolysaccharide Effectively Up-Regulates B7-1 (CD80) Expression and Costimulatory Function of Human Monocytes. *Scandinavian Journal of Immunology*, 42: 701-704.
248. Lim, W., Ma, W., Gee, K., Aucoin, S., Nandan, D., Diaz -Mítoma, F., Kozłowski, M. and Kumar, A. (2002). Distinct role of p38 and c-Jun N-terminal kinases in IL -10-dependent and IL -10-independent regulation of the costimulatory molecule B7.2 in lipopolysaccharide-stimulated human monocytic cells. *J. Immunol.*168: 1759.
249. Kehrl JH, Thevenin C, Rieckmann P, Fauci AS. (1991). Transforming growth factor-beta suppresses human B lymphocyte Ig production by inhibiting synthesis and the switch from the membrane form to the secreted form of Ig mRNA. *J Immunol*, 146: 4016–23.
250. Fujio, K., Okamura, T., Sumitomo, S., & Yamamoto, K. (2012). Regulatory T Cell-Mediated Control of Autoantibody-Induced Inflammation. *Frontiers in Immunology*, 3: 28.
251. Dagenais-Lussier, X., Loucif, H., Murira, A., Laulhé, X., Stäger, S., Lamarre, A., & van Grevenynghe, J. (2018). Sustained IFN-I expression during

- established persistent viral infection: A “bad seed” for protective immunity. *Viruses*, 10(1): 12.
252. Luckheeram, R. V., Zhou, R., Verma, A. D., and Xia, B. (2012). CD4+T cells: Differentiation and functions. *Clinical and Developmental Immunology*. 2012: 925135.
 253. Mohamadzadeh, M., Chen, L., and Schmaljohn, A. L. (2007). How Ebola and Marburg viruses battle the immune system. *Nature Reviews Immunology*. 7(7): 556–567.
 254. Mak, T. W., and Saunders, M. E. (2006). 17 - Cytokines and Cytokine Receptors BT - *The Immune Response* (pp. 463–516). Burlington: Academic Press.
 255. Li, S., Gowans, E. J., Chougnet, C., Plebanski, M., & Dittmer, U. (2008). Natural Regulatory T Cells and Persistent Viral Infection. *Journal of Virology*, 82(1): 21–30.
 256. Zhu, J., Yamane, H., and Paul, W. E. (2010). Differentiation of Effector CD4 T Cell Populations. *Annual Review of Immunology*. 28: 445–489.
 257. Kawai, T., and Akira, S. (2009). The roles of TLRs, RLRs and NLRs in pathogen recognition. *International Immunology*. 21(4): 317–337.
 258. Crotty, S. (2014). T follicular helper cell differentiation, function, and roles in disease. *Immunity*, 41(4): 529–542.
 259. Fazilleau, N., Mark, L., McHeyzer-Williams, L. J., & McHeyzer-Williams, M. G. (2009). Follicular Helper T Cells: Lineage and Location. *Immunity*, 30(3): 324–335.
 260. Sojka, D. K., Huang, Y.-H., & Fowell, D. J. (2008). Mechanisms of regulatory T-cell suppression – a diverse arsenal for a moving target. *Immunology*, 124(1): 13–22.
 261. Gebre, M., Nomburg, J. L., & Gewurz, B. E. (2018). CRISPR–Cas9 Genetic Analysis of Virus–Host Interactions. *Viruses*, 10(2): 55.
 262. Autissier, P., Soulas, C., Burdo, T. H., and Williams, K. C. (2010). Immunophenotyping of lymphocyte, monocyte and dendritic cell subsets in normal rhesus macaques by 12-color flow cytometry: Clarification on DC heterogeneity. *Journal of Immunological Methods*, 360(1-2): 119–128.
 263. Martins, K. A. O., Bavari, S., and Salazar, A. M. (2015). Vaccine adjuvant uses of poly-IC and derivatives. *Expert Review of Vaccines*. 14(3): 447–459.
 264. Longhi, M.P., Trumpfheller, C., Idoyaga, J., et al. (2009). Dendritic cells require a systemic type I interferon response to mature and induce CD4+ Th1 immunity with poly IC as adjuvant. *J Exp Med*, 206: 1589–602.
 265. Nagato, T., Lee, Y.R., Harabuchi, Y., et al. (2014). Combinatorial immunotherapy of polyinosinic-polycytidylic acid and blockade of

programmed death-ligand 1 induce effective CD8 T-cell responses against established tumors. *Clin Cancer Res*, 20: 1223-34.

266. Alsaab, H. O., Sau, S., Alzhrani, R., Tatiparti, K., Bhise, K., Kashaw, S. K., and Iyer, A. K. (2017). PD-1 and PD-L1 Checkpoint Signaling Inhibition for Cancer Immunotherapy: Mechanism, Combinations, and Clinical Outcome. *Frontiers in Pharmacology*, 8: 561.
267. Velcheti, V., Schalper, K. A., Carvajal, D. E., Anagnostou, V. K., Syrigos, K. N., Sznol, M., Herbst, R. S., Gettinger, S. N., Chen, L., Rimm, D. L. (2014). "Programmed death ligand-1 expression in non-small cell lung cancer". *Laboratory Investigation; A Journal of Technical Methods and Pathology*. 94 (1): 107–16.
268. Anderson, A. C., Joller, N., and Kuchroo, V. K. (2016). Lag-3, Tim-3, and TIGIT: Co-inhibitory Receptors with Specialized Functions in Immune Regulation. *Immunity*. 44(5): 989–1004.

Vita

Courtney Brooke Woolsey was born in Houston, TX on July 17, 1984. She graduated from La Porte High School (La Porte, TX) in 2002 and was awarded a Bachelor of Science degree from Texas A&M University (College Station, TX) in the fall of 2006. Prior to commencing graduate studies, she worked six years as a research associate under the direction of Dr. Johnny W. Peterson, developing countermeasures against inhalational anthrax. In 2012, she joined the laboratory of Dr. Thomas W. Geisbert to conduct her dissertation work. After completion of her graduate studies, she will continue her work at UTMB as a postdoctoral associate, investigating the pathogenesis of hemorrhagic fever viruses.

Permanent address: 1205 Ball Street, Galveston, Texas, 77550

This dissertation was typed by Courtney Woolsey.